

<https://www.ametsoc.org/ams/index.cfm/publications/journals/meteorological-monographs/ams-centennial-monograph/>

Chapter 17

100 Years of Research on Mesoscale Convective Systems

ROBERT A. HOUZE JR.

University of Washington, Seattle, and Pacific Northwest National Laboratory, Richland, Washington

ABSTRACT

When cumulonimbus clouds aggregate, developing into a single entity with precipitation covering a horizontal scale of hundreds of kilometers, they are called mesoscale convective systems (MCSs). They account for much of Earth's precipitation, generate severe weather events and flooding, produce prodigious cirriform anvil clouds, and affect the evolution of the larger-scale circulation. Understanding the inner workings of MCSs has resulted from developments in observational technology and modeling. Time–space conversion of ordinary surface and upper-air observations provided early insight into MCSs, but deeper understanding has followed field campaigns using increasingly sophisticated radars, better aircraft instrumentation, and an ever-widening range of satellite instruments, especially satellite-borne radars. High-resolution modeling and theoretical insights have shown that aggregated cumulonimbus clouds induce a mesoscale circulation consisting of air overturning on a scale larger than the scale of individual convective up- and downdrafts. These layers can be kilometers deep and decoupled from the boundary layer in elevated MCSs. Cooling in the lower troposphere and heating aloft characterize the stratiform regions of MCSs. As a result, long-lived MCSs with large stratiform regions have a top-heavy heating profile that generates potential vorticity in midlevels, thus influencing the larger-scale circulation within which the MCSs occur. Global satellite data show MCSs varying in structure, depending on the prevailing large-scale circulation and topography. These patterns are likely to change with global warming. In addition, environmental pollution affects MCS structure and dynamics subtly. Feedbacks of MCSs therefore need to be included or parameterized in climate models.

1. Introduction: Hints of mesoscale convection

When Huckleberry Finn told the story of floating down the Mississippi River on a raft, he said, “The fifth night below St. Louis we had a big storm after midnight, with a power of thunder and lightning, and the rain poured down in a solid sheet.” Before he wrote this story in 1884, Mark Twain had worked for some years on Mississippi River boats—long before scientific research on storms had gotten under way and revealed that *mesoscale convective systems* (MCSs) have a tendency to form just east of the Rocky Mountains in the afternoon or evening and propagate eastward and produce heavy rain over the Mississippi basin during nighttime. The keen observations of this experienced riverboat man presaged a century of research on the nature of convective storms over the central United States and elsewhere in the world. We have since learned that MCSs

are not confined to the U.S. Midwest, but actually are important elements of the global circulation and water cycle as well as one of the world’s most significant producers of extreme weather. We also know from satellites and radars that MCSs take on a variety of forms, depending on whether they occur over ocean or land, near mountains, over plains, in the paths of moist jets, or in a variety of other circumstances. This review chronicles what we have learned about these important atmospheric phenomena and how this knowledge has arisen from technological advances in meteorological observations over the last century.

In the nineteenth century, a few hints about mesoscale organization of convection also cropped up in the scientific community. By studying some of the very first cloud photography, the Scottish meteorologist Ralph Abercromby, in collaboration with the Swedish meteorologist Hugo Hildebrand Hildebrandsson ([Abercromby 1887; Hildebrandsson 1887](#)), identified the cloud form that is now generally recognized as cumulonimbus. Earlier,

Corresponding author: Robert A. Houze Jr., houze@uw.edu

Luke Howard (1865) had identified cumulus as a basic cloud type seen by eye from ground or ship. Upon studying his photographs, many taken by himself in his travels around the world, Abercromby thought that the term cumulonimbus was needed to identify the “mountainous cumulus which discharges rain in showers and thunderstorms” to separate this cloud type from “the cumulus of a fine day from the similar cloud of showery day.” It is perhaps less well known that these pioneers also identified the anvil clouds of cumulonimbus. Hildebrandsson described the upper part of the cloud as “towering up to colossal proportions as mountain ranges, or a gigantic mushroom, with a flat layer of ‘false cirrus’ around or on the top.” But, in this early age, without satellites, radar, or aircraft, it was hard for the extreme horizontal dimensions of these storms to be fully recognized.

As a result, these nineteenth-century literary and early scientific harbingers mostly did not comprehend the massive scale on which convective clouds can become organized. One exception appeared when, in 1883, at a meeting of the American Association for the Advancement of Science in Minneapolis, Minnesota, University of Iowa physicist Gustavus Hinrichs gave the first known description of the straight-line winds behind gust fronts, which are a common feature of MCSs moving across the plains states of the midwestern United States. He found that these gust fronts extended over tens to hundreds of kilometers.¹ He formally published his work in a two-part article in the long defunct *American Meteorological Journal* (Hinrichs 1888a,b). Another early study of note was that of W. J. Humphreys (1914), who worked with the nascent U.S. Weather Bureau under the title of Professor of Meteorological Physics. He speculated on the structure of a thunderstorm with a sketch indicating a period of heavy rain followed by lighter rain, but the essential horizontal and vertical scale and circulation characteristics of MCSs would not be fully recognized for another 30 years.

2. World War II and the amazing work of Hamilton and Archbold

Working in Nigeria during World War II, two Royal Air Force officers supporting wartime air operations developed an extensive manual on the meteorology of tropical western Africa (Hamilton and Archbold 1945). Based on pilot reports, balloon soundings, and surface meteorological data, they determined the mesoscale nature of convective storms characterized as spatially

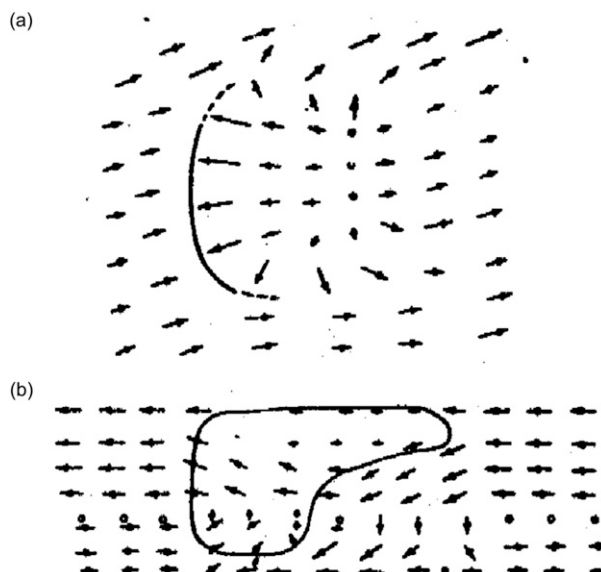


FIG. 17-1. (a) Surface wind and squall line, and (b) cloud outline and circulation in a vertical plane in a West African “disturbance line.” From [Hamilton and Archbold \(1945\)](#); © Royal Meteorological Society.

extensive convective “disturbance lines.” From the observed speed and duration of the events passing a point, it was apparent that the rainfall zones were $\sim 75\text{--}150\text{ km}$ in width. Synoptic analysis of surface station reports showed that the leading wind-shift lines were up to 1000 km in length and bowed outwardly in the direction of storm motion. These rudimentary observations indicated that the convection was organized on a spatial scale much larger than that of isolated convective clouds yet considerably smaller than synoptic scale; that is, the disturbance lines were the leading edges of mesoscale storms.

The early paper by [Hamilton and Archbold \(1945\)](#) also captured the essential character of the storm-scale overturning air motions within these mesoscale systems. [Figure 17-1a](#) shows the wind pattern at the ground as they deduced it from surface meteorological stations in West Africa, while [Fig. 17-1b](#) is an accompanying vertical section showing the cloud outline and system-relative air motions in a plane normal to the line. Hamilton and Archbold did not indicate the horizontal and vertical scales in these particular figures, but from their maps of specific events and statements in the text, we know that the wind-shift line and width of the circulation features normal to the line are mesoscale in horizontal extent. They did not have radar or other observations to show the embedded convective-scale structures. As we will see, much of the research on the mesoscale aspects of MCSs subsequent to the study of Hamilton and Archbold has employed information from radar, aircraft, satellite, and numerical models to

¹ He even introduced the use of the Spanish term *derecho*, which is now commonly used to describe certain long-lived windstorms.

provide details and variations on the theme composed of the cloud outline and circulation features illustrated in Fig. 17-1, but modern technology has not changed their fundamental conclusions. Nonetheless, details are important, and we have learned much more about the characteristics of MCSs and their role in the large-scale circulation of the atmosphere since the time of Hamilton and Archbold.

3. The emergence of mesometeorology and radar in the 1950s

Unfortunately, the study of Hamilton and Archbold that had laid such a clear foundation for understanding the mesoscale organization of atmospheric convection was barely noticed and largely forgotten after 1945—possibly as part of the general global societal chaos and reconfiguring of the scientific community after World War II. Research on convective storms in midlatitudes nevertheless was taking hold in the United States with the massive postwar Thunderstorm Project led by the University of Chicago professors [Byers and Braham \(1949\)](#). In what remains one of the largest and most innovative field projects in the history of meteorology, they deployed aircraft, radars, and radiosonde units left over from the war to observe storms in Ohio and Florida.² The Thunderstorm Project revealed the nature of the individual up- and downdrafts embedded in convective storms. The mesoscale characteristics of the convection observed in the Thunderstorm Project were harder to decipher because, unlike the tropical convection studied by Hamilton and Archbold, midlatitude convective processes were difficult to disentangle from other factors—especially frontal dynamics in Ohio and sea-breeze dynamics in Florida.

Polar-front theory had dominated midlatitude meteorological thought since the 1930s, and a first impulse of researchers was to apply frontal reasoning to large convective systems. It was widely recognized by this time by U.S. weather analysts that thunderstorms in midlatitudes lined up parallel to, but often ahead of, cold fronts and that these lines of storms extended over meridional distances of thousands of kilometers. An

example of applying frontal reasoning to these great lines of storms is the study of a case observed in the Thunderstorm Project by Chester [Newton \(1950\)](#), one of the greatest meteorologists of the era. He presented the cross-section analysis of Thunderstorm Project radiosonde data collected in Ohio in Fig. 17-2 in which he drew isotherms according to the rules of standard synoptic frontal analysis, with first-order discontinuities defining the boundaries of a frontal zone (indicated by heavy lines). Reliance on synoptic surface meteorological observations and polar-front thinking also led [Tepper \(1950\)](#) to try to explain the pressure rise accompanying the line of storms ahead of a front as the result of a gravity wave being triggered at the cold front and moving out ahead of the front. We now know that this pressure rise is mainly associated with the spreading downdraft cold pool of the storms, and that deep convective clouds breaking out by the release of instability in the warm sector air ahead of a cold front tend to arrange themselves in lines ahead of an approaching cold front for a variety of synoptic and mesoscale reasons that would have been difficult to decipher by standard synoptic analysis and frontal reasoning alone.

A paradigm shift in analysis methods occurred when Tetsuya (Ted) Fujita emigrated from post–World War II Japan and joined the Chicago School of Byers and Braham. In an innovative paper ([Fujita 1955](#)), he introduced the community to *mesometeorology* in which meteorological observations were painstakingly combined by space–time conversion to produce horizontal and vertical cross sections that revealed meteorological structures on subsynoptic scales. It was in this way that he showed that a line of thunderstorms along or ahead of a cold front was not a kind of front in the sense of polar-front thinking, but rather a lining up of convective entities organized individually on the mesoscale. In today’s lexicon, we would say that he identified the MCS as the building block of the prefrontal or frontal squall line. As Fujita put it, “The mesosynoptic disturbances greatly influence the situation as viewed on the regular synoptic scale, which is about 10 times the mesoscale, and make conventional [synoptic] analysis hopelessly difficult.”

[Figure 17-3](#) shows the conceptual model of an MCS as inferred by Fujita. An important feature of this conceptual model is the horizontal scale of the storm’s footprint, which was ~300 km. This model was thus comparable in scale and air motion characteristics to the tropical systems analyzed by [Hamilton and Archbold \(1945\)](#). Fujita’s detailed analysis of an example case in his 1955 paper showed that the line of storms occurring just ahead of a cold front consisted of a series of entities like that of the conceptual model rather than resembling a variety of polar front as implied by analyses such as that of

²The Thunderstorm Project used 22 freight cars full of instrumentation, including radiosondes and radars, plus numerous trucks and jeeps. In addition, 10 Northrup P-61C Black Widow aircraft, flown by “highly competent instrument pilots of the Air Force,” and gliders flown by pilots from the Soaring Society of America volunteered for aircraft operations. Although enormous in terms of platforms, the instruments used were generally of a primitive nature, thus limiting the success of the program. Nearly three decades went by before another massive effort was undertaken to understand convection.

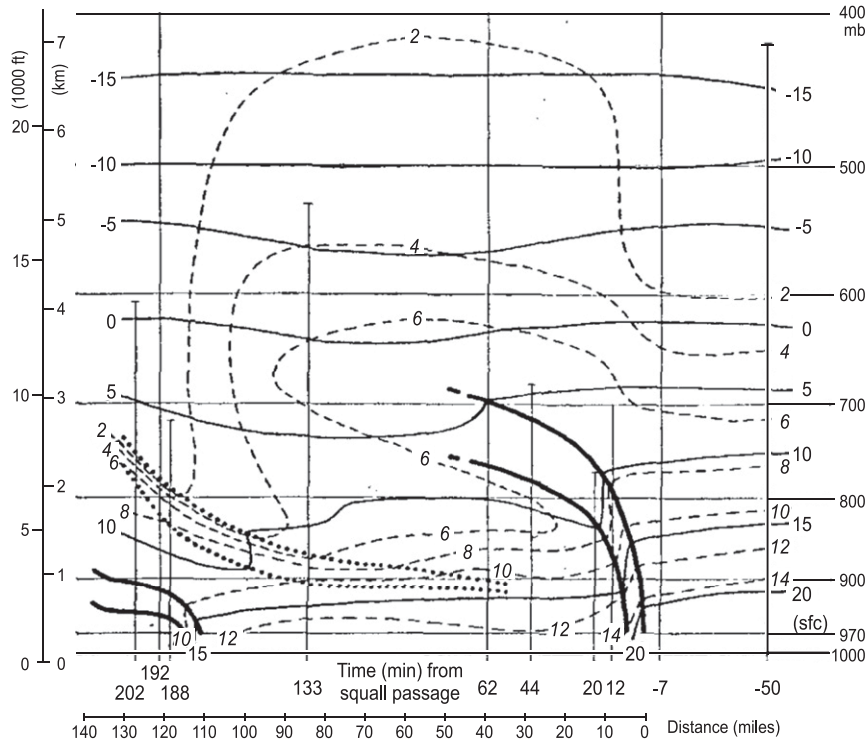


FIG. 17-2. Time cross section through squall line and cold front, Wilmington, OH, 0730–1135 eastern standard time (EST) 29 May 1947. Heavy lines show boundaries of squall-front and polar-front layers; heavy dotted lines show boundaries of subsidence inversion. Light solid lines show isotherms (0°C); light dashed lines show isolines of mixing ratio (g kg^{-1}). Below the cross section is the time of radiosonde observation before or after squall-line passage; distance scale is in miles. From [Newton \(1950\)](#).

Fig. 17-2. Because time series often capture mesoscale events better than scheduled observations, time–space conversion has remained an important method of mesometeorological analysis through the years; notable examples would be the highly referenced work of Fujita's protégé Roger Wakimoto (1982) and the more recent study of Adams-Selin and Johnson (2010).

4. The rise of radar meteorology

Even using his clever time–space conversions, Fujita could not reveal anything about the internal structures of MCSs on smaller scales because his mesometeorological methods did not benefit from targeted aircraft measurements like those in the Thunderstorm Project, or from radar, which was still emerging from its development in World War II to become one of the most important meteorological instruments of the last 100 years. One of the pioneers of radar meteorology was the relatively unheralded Herbert Ligda, who worked at the Massachusetts Institute of Technology, Texas A&M, and Stanford, but published relatively little in the formal literature. A remarkable finding of Ligda during his time

at Texas A&M was his discovery of the internal structure of the same types of MCSs described both by Hamilton and Archbold and by Fujita. [Figure 17-4](#) (from a Texas A&M project report) was published in the nonrefereed proceedings of a conference of glider pilots ([Ligda 1956](#)). It showed in schematic but amazingly precise form the details of the typical radar echo pattern of an MCS of the type analyzed by [Hamilton and Archbold \(1945\)](#) and [Fujita \(1955\)](#). Notable features were a narrow sharp line of weak echo (A) marking the gust front immediately ahead of a convective line (B), which was advancing with an eastward component of motion and consisted of numerous intense convective elements, each elongated northwest to southeast. The feature D was a trailing region of stratiform precipitation, separated from the line of convective cells by a zone of weak echo (C). [Houze et al. \(1990\)](#), still unaware of Ligda's early study hidden in nonstandard literature, arrived at an essentially similar conceptual model of the radar echo in an MCS of this type. Radar was thus beginning to show that an MCS, which had been determined by Hamilton, Archbold, and Fujita, to be of a horizontal scale of a few hundred kilometers,

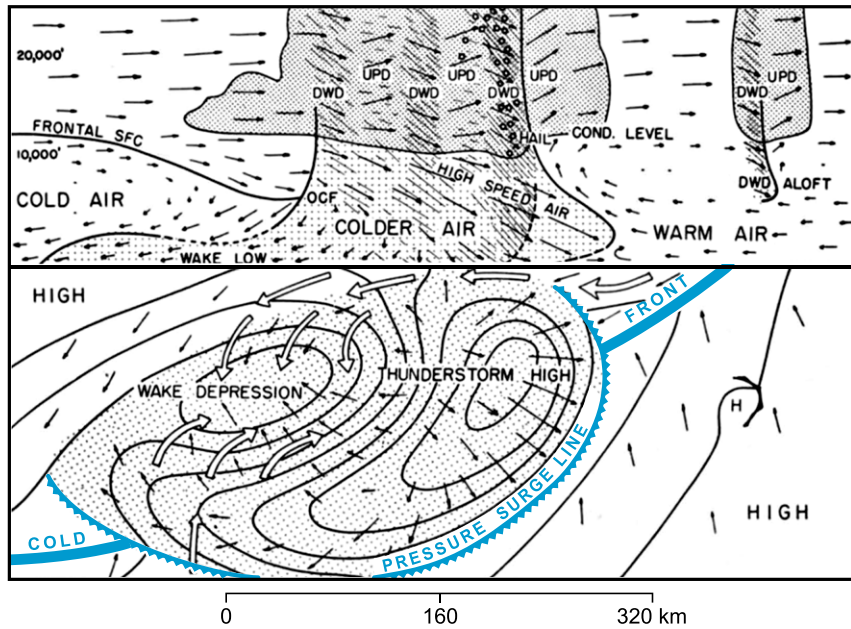


FIG. 17-3. Schematic section through a squall line. Adapted from Fujita (1955).

contained important substructures on a range of smaller scales, all of which have turned out to be important elements when considering the role of MCSs as weather producers and elements of larger-scale circulations.

At this point of the review, I would like to emphasize that MCSs are *not always in the form of lines of intense convective cells followed by a zone of stratiform precipitation*, as in the examples studies by Hamilton and Archbold, Newton, and Ligda. Such storms, often called *squall-line MCSs*, attract attention because they are dramatic—as they pass over, they are marked by a predictably ordered sequence of events: a sudden wind shift (called a “squall front” or “gust front”), followed by a short period of heavy rain or hail, and then a longer period of quasi-steady lighter stratiform rain. As such, this type of MCS is especially amenable to analysis and modeling—and great fun to analyze. However, MCSs of similar dimension can exhibit a variety of more complex patterns of convective cells and stratiform rain. Tropical studies carried out long after Hamilton and Archbold’s (1945) work have shown both squall-line and non-squall-line MCSs (Leary and Houze 1979b; Houze and Betts 1981; LeMone et al. 1998; Kingsmill and Houze 1999; Yamada et al. 2010; Barnes and Houze 2016). In midlatitudes, Houze et al. (1990) noted that non-squall-line MCS were seen in about one-third of the major springtime rainstorms in Oklahoma.

Much of the radar-based work on the convective-stratiform patterns of MCS precipitation has been over the central United States, which raises a cautionary

concern because this region of the world is unique so that the MCSs in this region are likely not universally representative of MCSs around the world. The MCSs in the United States are affected by significant geographic factors that affect the forms taken by the convective storms. The Rocky Mountains to the west, the mountains of Mexico to the southwest, and the Gulf of Mexico to the south are the most important of these geographical features. Combined with the semipermanent Atlantic subtropical anticyclone, these geographical features favor a moist low-level jet that systematically feeds warm, moist air into MCSs in this region. The only other somewhat similar region on Earth is Argentina where the South American low-level jet emanating from Amazonia and guided by the Andes to the west feeds MCSs in that region. Rasmussen and Houze (2011) found that MCSs in subtropical South America take on forms very similar to those over the central United States. In general, however, MCSs are a global phenomenon, and while the evolution and forms of MCSs seen over the central United States and subtropical South America may be useful for forecasting in these particular regions, some of the characteristics of MCSs seen in these regions may not apply universally over the globe.

With this geographical caveat in mind, we note some milestones of radar-based studies of MCS structure over the United States. Although the convective cells in MCSs are not always arranged in lines, such lines of convection are nevertheless of special interest to

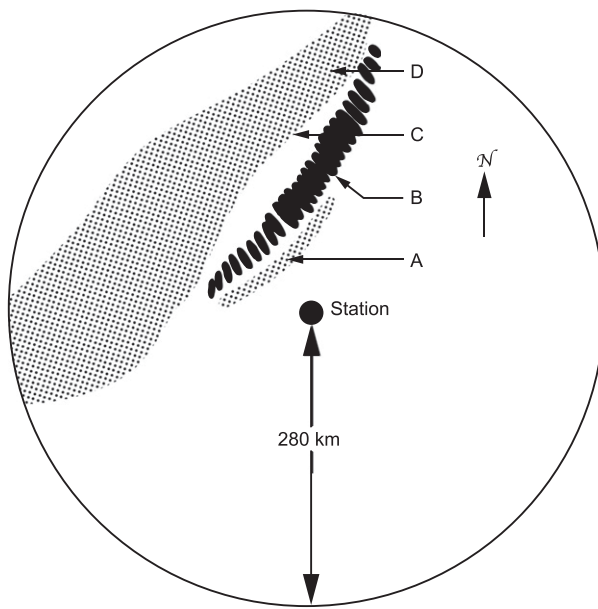


FIG. 17-4. Schematic structure of surface precipitation features seen in early meteorological radar data. Adapted from Ligda (1956).

forecasters. Bluestein and Jain (1985) found that over the central United States, lines of deep convective cells form in four ways, but they did not consider the relation of the cells to stratiform precipitation in MCSs. Houze et al. (1990) examined the convective–stratiform configurations of the precipitation in MCSs over Oklahoma. The example from their study in Fig. 17-5a has leading-line/trailing-stratiform structure of the type described by Ligda (1956). Houze et al. (1990) called this form “symmetric.” However, the radar echoes in Fig. 17-5b were said to be of an “asymmetric” form in which the stronger convective cells were on the equatorward end of the line and the stratiform region was trailing the poleward portion of the line. Skamarock et al. (1994) found the asymmetric structure to be favored by the action of the Coriolis force acting on the time scale of the MCS, which probably accounts for this asymmetric structure not appearing (at least to this author’s knowledge) in the tropics. Loehrer and Johnson (1995) and Parker and Johnson (2000) further examined the symmetric and asymmetric paradigms in midlatitude continental MCSs over the region east of the Rocky Mountains in the United States. They found that the most common life cycle scenario was an initial line of convective cells developing a stratiform region, first in a symmetric juxtaposition with the line and then evolving into an asymmetric form, as evidently the Coriolis force had longer to act. The second most common evolution had the only stratiform precipitation forming on the

northeast end of the convective line, as old cells weakened and new ones formed on the southwest end of the line.³ Also analyzing radar data over the central United States, Jirak et al. (2003) found that MCSs evolving from linearly arranged convective cells were longer-lived, more severe, and more effective at producing precipitation than MCSs that developed from areally arranged convection. That result is probably very specific to the United States. Schumacher and Johnson (2005) and Peters and Schumacher (2015, 2016) have distinguished additional variations on the convective–stratiform structures of MCSs, especially in flood-producing MCSs. However, the structures and circulations these authors identified remain entangled with midlatitude frontal activity that also strongly influences convection over the region east of the Rocky Mountains.

5. The 1960s–early 80s: The beginning of the satellite era

Ground-based radar studies, such as those described above, are intrinsically regional in scope. The global significance of MCSs and their convective–stratiform structures has followed from developments in satellite meteorology, which allows global analysis of the frequency of occurrence of MCSs of various types. This opportunity arose with the launch of the first weather satellite in 1960 (Anderson 2010). One of the first things to be noticed was that cirrus shields in regions of deep convection were mesoscale in extent. Martin and Karst (1969) and Martin and Suomi (1972), using digitally enhanced visible images, were able to track “cloud clusters” that lasted for 3–6 days. These clusters were regions of high cloud that were 3000–7000 km in horizontal scale, that is, they were nearly synoptic-scale features. However, these early investigators also noted bright cores within these cloud shields that lasted 1–4 h, moved slower than the clusters, and sometimes were in the form of bands. These bright cores were evidently the active convective entities that we would now identify as MCSs. Another important early satellite study was that of Frank (1970), who found that cloud clusters over the tropical Atlantic were systematically associated with the troughs of synoptic-scale easterly waves. However, this study did not address the subsynoptic substructure of the cloud clusters.

Visible satellite imagery is limited to daytime and is largely nonquantitative. The first clear identification of MCSs in satellite data arose from the use of infrared

³This behavior is similar to the rainbands in tropical cyclones (Hence and Houze 2008; Houze 2010; Didlake and Houze 2013).

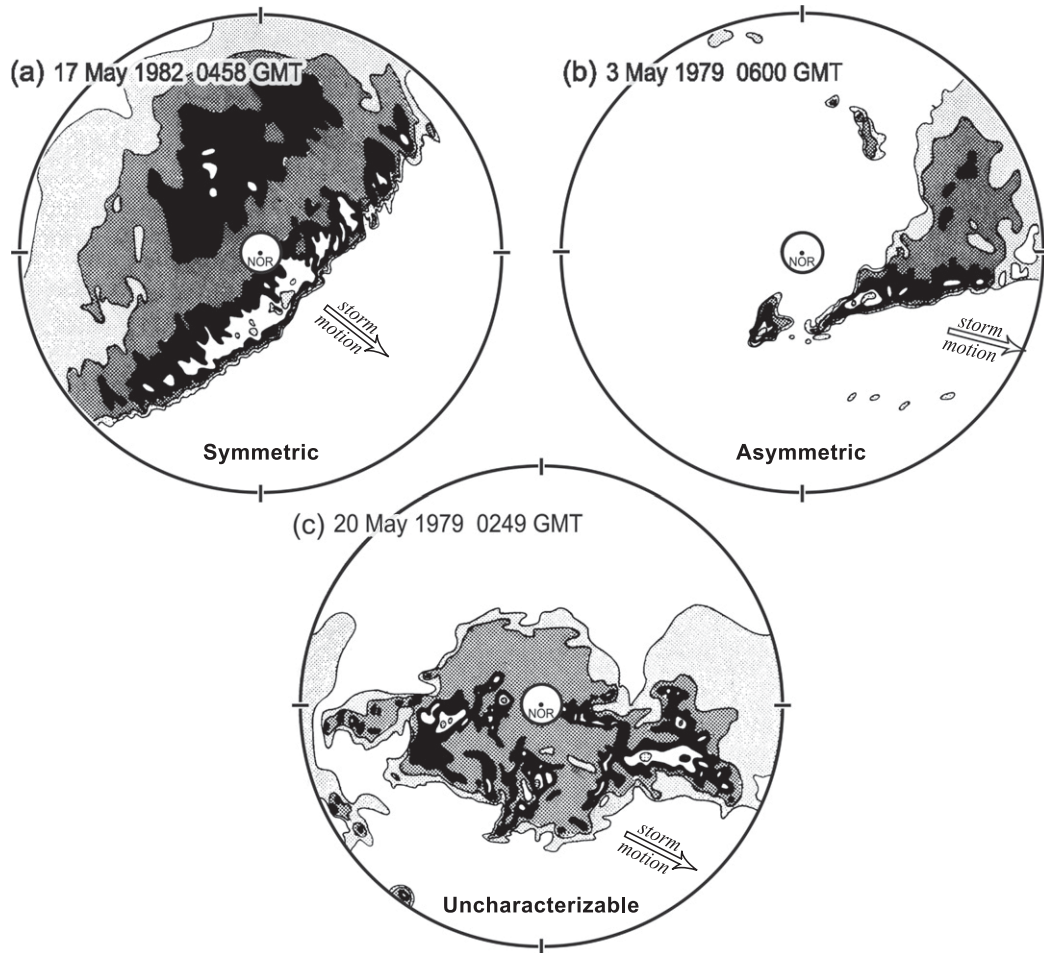


FIG. 17-5. Examples of radar data from the rain areas of midlatitude MCSs. Low elevation reflectivity patterns from the National Severe Storms Laboratory radar located at Norman (NOR), OK, are indicated by shading levels corresponding to 20–24 dBZ (light gray), 25–34 dBZ (dark gray), 35–44 dBZ (black), 45–54 dBZ (white), 55–64 dBZ (light gray), and >65 dBZ (dark gray). Range rings are at 20, 200, and 240 km. Registration marks on outermost ring are at 90-azimuth intervals (north toward top of figure). From [Houze et al. \(1990\)](#).

imagers on satellites, which provide an indication of cloud-top temperature. Using early infrared imagery, [Maddox \(1980\)](#) identified what he called *mesoscale convective complexes* (MCCs). These entities are defined as large, circular, cold cloud tops whose infrared brightness temperatures are lower than -32°C over an area $>100\,000\,\text{km}^2$ (radius of 178 km) and lower than -52°C over an embedded area $>50\,000\,\text{km}^2$. The peculiar choices of thresholds of -32° and -52°C arose from the fact that the work was done using photographic operational satellite products that used these particular isotherm values, as can be seen in the illustration of an MCC in Maddox's classic paper ([Fig. 17-6](#)).

An ensuing series of papers (synthesized by [Laing and Fritsch 1997](#)) showed where MCCs identified in this way occur around the world. However, we now know that MCCs are an extreme form of mesoscale

convection. Many deep convective systems bearing a large amount of precipitation and high-impact weather have horizontal scales in which precipitation covers areas $\sim 100\text{--}500\,\text{km}$ in horizontal scale without satisfying the strong cold cloud-top criteria of [Maddox \(1980\)](#), and the term MCS is commonly used (including in this review) to encompass this broader population of mesoscale entities of which MCCs are an extreme subset. [Anderson and Arritt \(1998\)](#) also pursued this type of analysis. They provided a catalog of information on the seasonal and diurnal frequency of MCCs as well as of MCSs of similar intensity but whose upper cloud shields were not circular but elongated.

Visible and infrared imagery were just the beginning of the impact of satellites on the study of MCSs. As we will see in later sections of this review, the late

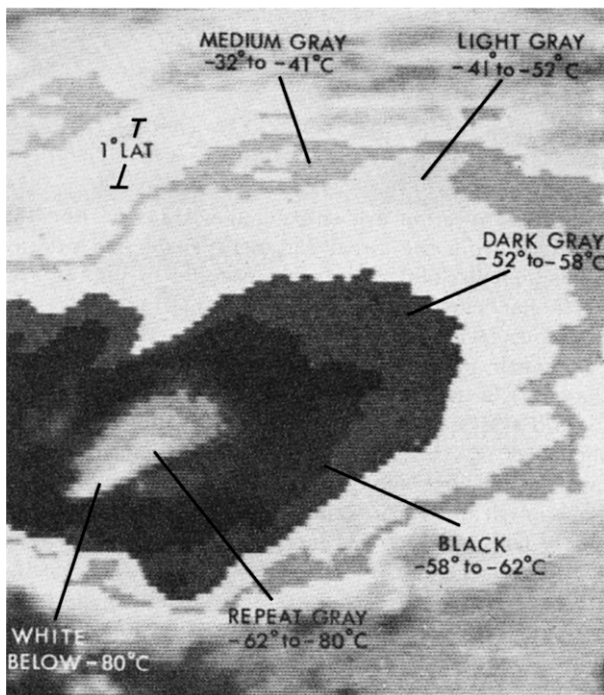


FIG. 17-6. Infrared image showing temperature ranges corresponding to the various gray shades. From Maddox (1980).

1990s and 2000s saw the introduction of radars on satellites, which further revolutionized understanding of MCSs and their global importance. But first we need to note the importance of the grand field experiments in the tropics.

6. The 1970s: The far-reaching impact of GATE

By the 1970s, Lorenz's (1963) work on predictability had led to the idea that prediction of global weather up to two weeks in advance could be accomplished if convection in the tropics could be better parameterized. This grand hypothesis required a grand experiment to achieve better understanding of the interaction of convective and synoptic scales of motion in the tropics, and an ambitious international field project was organized. That project was the 1974 Global Atmospheric Research Program Atlantic Tropical Experiment (GATE; Kuettner and Parker 1976), carried out over the eastern tropical Atlantic Ocean, off the western coast of Africa.

GATE was designed to reveal simultaneously properties on scales ranging from convective up- and down-drafts of the type documented in the Thunderstorm Project to the synoptic-scale motions of near-equatorial easterly waves that control the occurrence of convection in this part of the tropics. A massive effort was required to document the large-scale environment by a shipborne

sounding network, the convective structures by radars on ships, mesoscale air motions and in-cloud properties sampled by aircraft, and a variety of radiation and boundary layer flux measurements. The Thunderstorm Project in the late 1940s had shown the effectiveness of deploying such special observations in an organized community effort. In the decades following the Thunderstorm Project, instrumented aircraft had further proved themselves by flying into hurricanes (Dorst 2007), and some small field programs involving radars and/or aircraft in the tropical Pacific (Zipser 1969), the Caribbean (Holland 1970), and the Atlantic (Shupiatsky et al. 1976a,b) had been successful. GATE brought such fieldwork to an absolutely massive scale. Gathered in the eastern tropical Atlantic were the atmospheric research resources of 20 nations, deploying 12 large research aircraft, and 40 research ships (www.ametsoc.org/sloan/gate). Four of the ships hosted a network of three-dimensionally scanning weather radars making and recording quantitative reflectivity data over a 4-month period (Hudlow 1979) while soundings were launched from 14 ships surrounding the area of radar observations (Thompson et al. 1979). By this time, geosynchronous weather satellites were in orbit, providing the evolving cloud context within which the measurements were made. The coordinated soundings, radars, aircraft and satellite measurements in GATE led to a new appreciation of MCSs.

Ironically, the experiment design of GATE was founded on the conceptual model of convective–synoptic interaction being between convective updrafts and synoptic-scale motions, as expressed by Yanai et al. (1973) and Arakawa and Schubert (1974). In this view, mesoscale convection was not considered part of the interaction. However, the shipborne radar network showed that both squall-line and nonsquall MCSs were major components of the cloud population observed in the GATE observational array (Houze and Betts 1981), and the extensive multiscale observational array of GATE laid a foundation for research on MCSs that continues to this day. GATE studies produced fundamental knowledge of the thermodynamics, precipitation mechanisms, air motions, microphysical processes, dynamics, life cycle stages, heating processes, and relationship to larger scales of motion. While knowledge of each of these aspects of MCSs arose out of GATE studies or work inspired by GATE, it has advanced in concert with technological developments in radar, modeling, satellite remote sensing, and additional field programs—lesser in scope than GATE but more specifically targeted, with more sophisticated instruments, and including midlatitude venues. The next topics of this paper will therefore begin with GATE as the starting point and

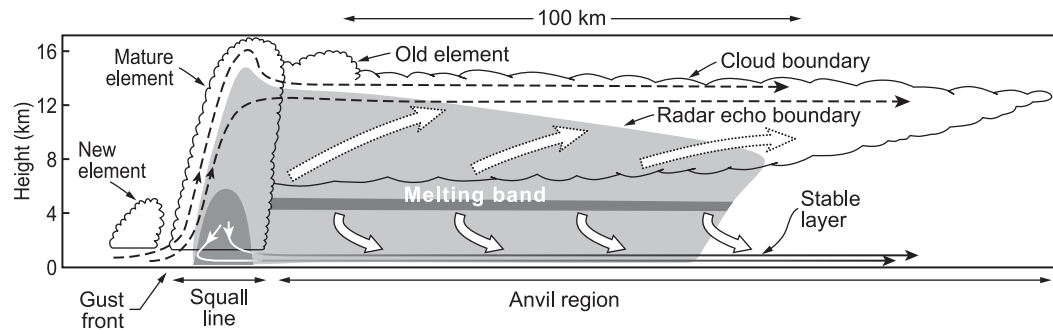


FIG. 17-7. Schematic cross section through a squall-line system observed over the eastern tropical Atlantic Ocean. Streamlines show flow relative to squall line. Thin dashed streamlines show convective updraft circulation. Thin solid streamlines show convective-scale downdraft circulation associated with mature squall-line element, and wide, dashed arrows show mesoscale downdraft below the base of the anvil cloud. Wide, dashed arrows show mesoscale ascent in the anvil. Dark shading shows strong radar echo in the melting band and in the heavy precipitation zone of the mature squall-line element. Light shading shows weaker radar echoes. Scalloped line indicates visible cloud boundaries. Adapted from [Houze \(1977\)](#) by [Houze and Betts \(1981\)](#).

then discuss how knowledge of the topic has been refined since that time.

7. Precipitation in MCSs: The universality of the convective–stratiform paradigm

A major result of GATE was the finding based on the four shipborne quantitative radars that the precipitation consisted of two primary components, convective and stratiform. Prior to GATE, there was no recognition that any tropical precipitation was stratiform. Each of the GATE radars was operated in a tilt-sequence mode in which the antenna rotated 360° in azimuth at a series of elevation angles. The three-dimensional echo coverage obtained continuously in this way showed that when MCSs passed over a ship, short periods of heavier precipitation had radar echoes in the form of vertically oriented cores, but that some 40% of the precipitation was of a more moderate nature and was characterized on radar by a horizontally oriented layer of maximum reflectivity just below the 0°C level ([Houze 1977](#); [Leary and Houze 1979a](#); [Cheng and Houze 1979](#)). The schematic in Fig. 17-7 illustrates the “bright band” produced by melting of large ice particles, which was a clear indication that a large proportion of the rain was stratiform in nature; that is, the vertical air motions were generally not strong enough to support vertical advection of precipitation particles. Instead, ice particles were systematically drifting downward and turning into light-to-moderate rain over very large areas. Figure 17-8 illustrates how the horizontally integrated rainfall (sometimes called volumetric rain) from the MCS begins as convective and then develops a stratiform component that over time becomes equivalent in magnitude to the convective component. Following [Houze \(2014\)](#),

precipitation is stratiform if the mean vertical air motion in a cloud is much smaller than the fall velocities of ice particles, so that ice particles are drifting downward, melting, and falling out as rain over a broad area. One way that stratiform precipitation forms is when active updrafts in a region of convection weaken and the precipitation particles aloft slowly fall out ([Houze 1997](#)). This process is how the stratiform regions of MCSs arise and is discussed further in [section 13](#). Oceanic MCSs of the type seen in GATE have now also been seen over the west Pacific ([Petersen et al. 1999](#); [Houze et al. 2000](#)), the Maritime Continent region ([Houze et al. 1981](#)), and the central Indian Ocean ([Barnes and Houze 2014, 2016](#)).

GATE studies included studies not only of oceanic MCSs but also studies of MCSs over the African continent ([Fortune 1980](#); [Payne and McGarry 1977](#)). These continental African MCSs have been documented in detail in a variety of studies (e.g., [Fink and Reiner 2003](#); [Schumacher and Houze 2006](#); [Futyan and Del Genio 2007](#); [Cetrone and Houze 2011](#); [Powell et al. 2012](#)), which show well-defined convective and stratiform behavior mainly of the leading-line/trailing-stratiform type.

GATE thus launched a direction of research on MCSs in the tropics that has paralleled studies of the structures of MCSs in the midlatitude region of the United States east of the Rocky Mountains, as was discussed in [section 3](#). Unlike the findings from the midlatitude studies, fronts and other baroclinic effects did not affect MCS structures in the tropics. The common denominator appearing from both the midlatitude and tropical studies was upscale growth of a region of deep convection so that the rain covered an area of mesoscale extent, and the existence of a mesoscale region of stratiform precipitation occurring in association with the deep convection.

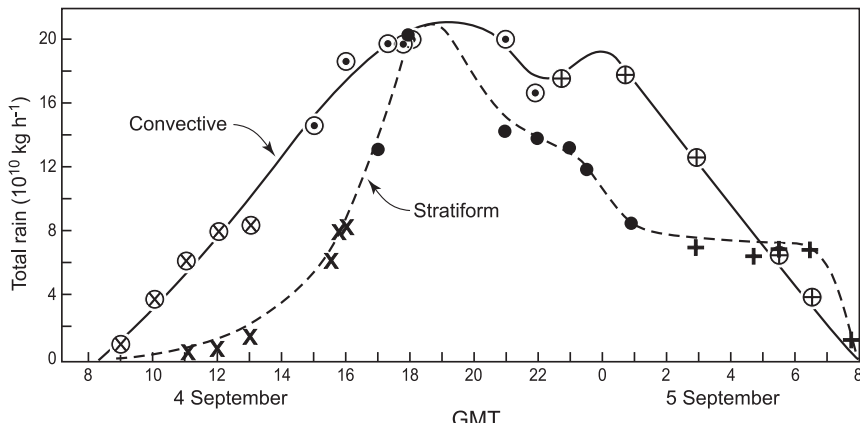


FIG. 17-8. Total rain integrated over the convective (circled points) and stratiform regions of a squall-line MCS located over the eastern tropical Atlantic Ocean. The data were obtained by three shipborne radars. The three types of symbols indicate different methods used for combining the information from the three radars. From Houze (1977).

This convective–stratiform behavior was thus being documented over disparate parts of the globe, and always the MCSs exhibited precipitation distinctly subdivided into convective and stratiform regions. The development of satellite-borne radar has provided a way to link the nature of MCSs over the globe. The Tropical Rainfall Measuring Mission (TRMM) satellite launched in 1997 provided the first radar observations of the three-dimensional structure of precipitation from space (between 35°N and 35°S). TRMM orbited until 2014, but in that year the Global Precipitation Measurement (GPM) satellite began providing similar radar measurements (between 65°N and 65°S). U.S. and Japanese teams responsible for processing the TRMM and GPM radar data have routinely separated the radar echoes into stratiform, convective, and “other” categories. The convective–stratiform separation algorithm used on the TRMM radar data (Awaka et al. 1997) was based both on brightband detection and on the horizontal texture analysis of Houze (1973), Churchill and Houze (1984), and Steiner et al. (1995). Mapping of TRMM radar data (Schumacher and Houze 2003) showed that ~30%–70% of tropical rainfall was stratiform, with lower fractions over land and higher fractions over the oceans (Fig. 17-9). The “other” components of the TRMM radar echo patterns accounted for only a small proportion of the

total rain over the low latitudes (Houze et al. 2015). Because the only source of stratiform rain in the tropics is primarily if not exclusively that occurring in MCSs, the large fractions in Fig. 17-9 showed that the latent heating in the tropics is substantially influenced by MCSs (see further discussions of TRMM in sections 16 and 17, below.)

8. Scales of air motions and thermodynamical processes within an MCS

Another paradigm-shifting result of GATE was the realization that two types of downdrafts occur in MCSs (Zipser 1977; Houze 1977). As indicated in Fig. 17-7, one type of downdraft is highly local and occurs in connection with the locally intense convective precipitation; it is forced by the weight of hydrometeors and can be locally strong. The denser air from aloft forms a density current with a leading edge called the “gust front.” The other type occurs in the stratiform precipitation areas and is less intense but more widespread; it is driven primarily by evaporation of falling hydrometeors, as first demonstrated by Brown (1979), but also by sublimation and melting of ice particles falling beneath the meso-scale stratiform cloud of the MCS (e.g., Braun and Houze 1997). The difference between convective and

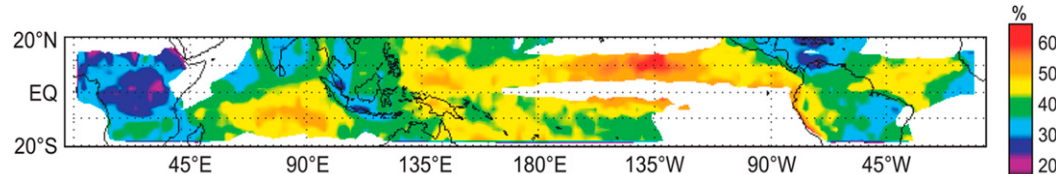


FIG. 17-9. Stratiform rain fraction obtained from TRMM precipitation radar data. From Schumacher and Houze (2003).

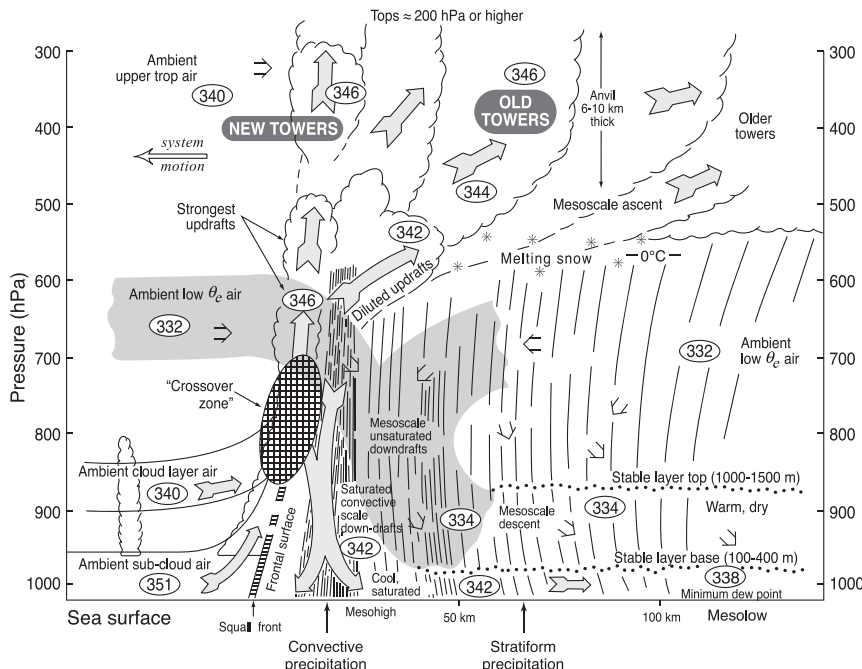


FIG. 17-10. Conceptual model of a tropical oceanic squall line with trailing-stratiform precipitation. All flow is relative to the squall line, which was moving from right to left. Numbers in ellipses are typical values of equivalent potential temperature (K). Adapted from Zipser (1977).

mesoscale downdrafts in an MCS was elaborated in the GATE study of Zipser (1977), which showed how both types of downdraft transport air of lower equivalent potential temperature (θ_e) downward, with the convective downdraft generally penetrating all the way to the surface (Fig. 17-10). Sometimes a mesoscale downdraft that has formed in the stratiform region extends downward and merges with the convective downdraft.

The updraft motions in an MCS also occur on two scales. This result was substantiated with the maturing of Doppler radar technology in the 1980s. One of the early dual-Doppler studies of MCSs was the Convection Profonde Tropicale 1981 field program carried out with two Doppler radars in West Africa (Sommeria and Testud 1984). Dual-Doppler synthesis by Roux (1988) of the wind field in the convective region of an MCS showed that cells of upward motion on the scale of a few kilometers and corresponding to reflectivity cells of similar dimension were superimposed on a broader region of sloping ascent over the downdraft density current at lower levels (Fig. 17-11). A similar dual-Doppler experiment in the 1985 Oklahoma-Kansas Preliminary Regional Experiment for Stormscale Operational and Research Meteorology (STORM)-Central (PRE-STORM; Cunning 1986) led to the conceptual model in Fig. 17-12, which describes a squall-line MCS. The Doppler radar syntheses showed that a

general, mesoscale flow of air originating in the lower troposphere ascends through the convective region, where stronger local updrafts are superimposed, and into the stratiform region where the air is still generally buoyant with respect to the large-scale environment but

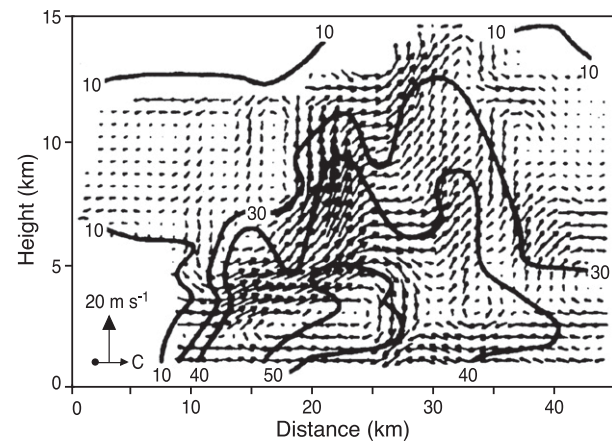


FIG. 17-11. Airflow pattern inferred by multiple-Doppler radar synthesis in the convective region of a tropical squall-line system observed by dual-Doppler radar in Ivory Coast, West Africa, on 23 Jun 1981. System is moving from right to left. Vertical arrow indicates scale of airflow vectors. Horizontal arrow C shows velocity of individual convective cells. Airflow vectors are computed relative to the cells. Contours show radar reflectivity (dBZ). From Roux (1988).

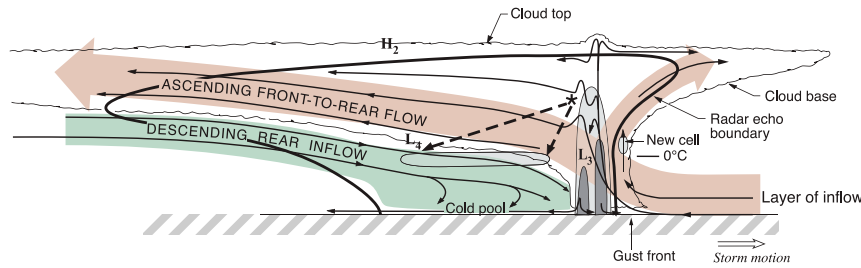


FIG. 17-12. Conceptual model of the kinematic, microphysical, and radar echo structure of a convective line with trailing-stratiform precipitation viewed in a vertical cross section oriented perpendicular to the convective line (and generally parallel to its motion). Medium and dark shading indicate intermediate and strong radar reflectivities. Adapted from Houze et al. (1989).

without the strong intense convective cells seen in the convective region.

In the stratiform region, the general ascending mesoscale flow lies over the layer of general descent of the mesoscale downdraft, which is drawn in from the mid-levels of the environment and is driven downward diabatically by sublimation, melting, and evaporation of precipitation. In the case of a squall-line MCS of the type conceptualized in Fig. 17-12, the midlevel inflow feeding the mesoscale downdraft was dubbed the “rear-inflow jet” by Smull and Houze (1987), who showed that this inflow is a ubiquitous feature of squall-line MCSs and may be intensified if the environmental shear favors strong flow relative to the storm in midlevels. As shown in Fig. 17-12, the stratiform region downdraft of a squall-line MCS flows horizontally toward the convective region, where the precipitation-driven downdrafts of convective cells dominate in the low levels. Doppler radar has shown that the mesoscale downdraft of the stratiform region of a squall-line MCS sometimes merges with the convective downdrafts in the leading line of convection and that these mergers can produce strong effects, with the gust front surging forward and triggering new convection in the form of a “bow echo.” An example of a bow echo is shown in Fig. 17-13a from Davis et al. (2004) and Jorgensen et al. (2004). Doppler radar observations showed strong midlevel flow toward the back edge of the curved convective line. In Fig. 17-13b, a vertical cross section through the bow echo portion of the line shows the descending rear inflow from the stratiform region of an MCS penetrating into the convective region, where it combined with the convective-scale downdraft and pushed the gust front forward, underneath the main updraft cell. These bow echo events are a major forecasting concern, as they are often associated with violent, damaging surface winds.

The broad, mesoscale overturning of the MCS is a major mechanism for vertical mixing of the atmosphere. Because it enters from midlevels, the mesoscale

downdraft transports a large amount of midtropospheric low- θ_e air to lower levels, while the generally ascending mesoscale flow brings high- θ_e air from low levels to the upper troposphere. This mesoscale overturning is often thought of as a two-dimensional process as it occurs in the squall-line type of MCS. However, Doppler radar observations have shown that the mesoscale overturning actually occurs in a variety of three-dimensional configurations. In the 1980s, Doppler radar was implemented on aircraft to observe the winds in tropical cyclones (Marks and Houze 1983), and by the 1990s airborne Doppler was a proven technology, with dual beams allowing for dual-Doppler synthesis of the airflow in convection. The second major tropical oceanic field campaign was the Tropical Ocean and Global Atmosphere Coupled Ocean–Atmosphere Response Experiment (TOGA COARE; Webster and Lukas 1992; Godfrey et al. 1998), and it capitalized on airborne Doppler radar technology. From 25 flights around the stratiform regions of MCSs, Kingsmill and Houze (1999) compiled statistics on the characteristics of the mesoscale airflow and found that midlevel inflow consistently entered from above and descended to below the 0°C level (Fig. 17-14), but that this inflow entered from a wide variety of directions, as indicated schematically in Fig. 17-15a. The midlevel inflow in Fig. 17-15a is completely consistent with the squall-line configuration of Fig. 17-12 but the observations show a more general result because the inflow can come from any direction, and Kingsmill and Houze (1999) found the midlevel inflow direction to be determined by the large-scale environmental wind direction.

From another set of 25 flights in TOGA COARE, Kingsmill and Houze (1999) determined statistics of the ascending flow entering the convection regions of fully developed MCSs (Fig. 17-16). The low-level flow came from various directions relative to the MCS, but in all cases it was coming from a layer that could be as deep as 4.5 km, implying that the convection was drawing in a layer of air much deeper than the boundary layer and

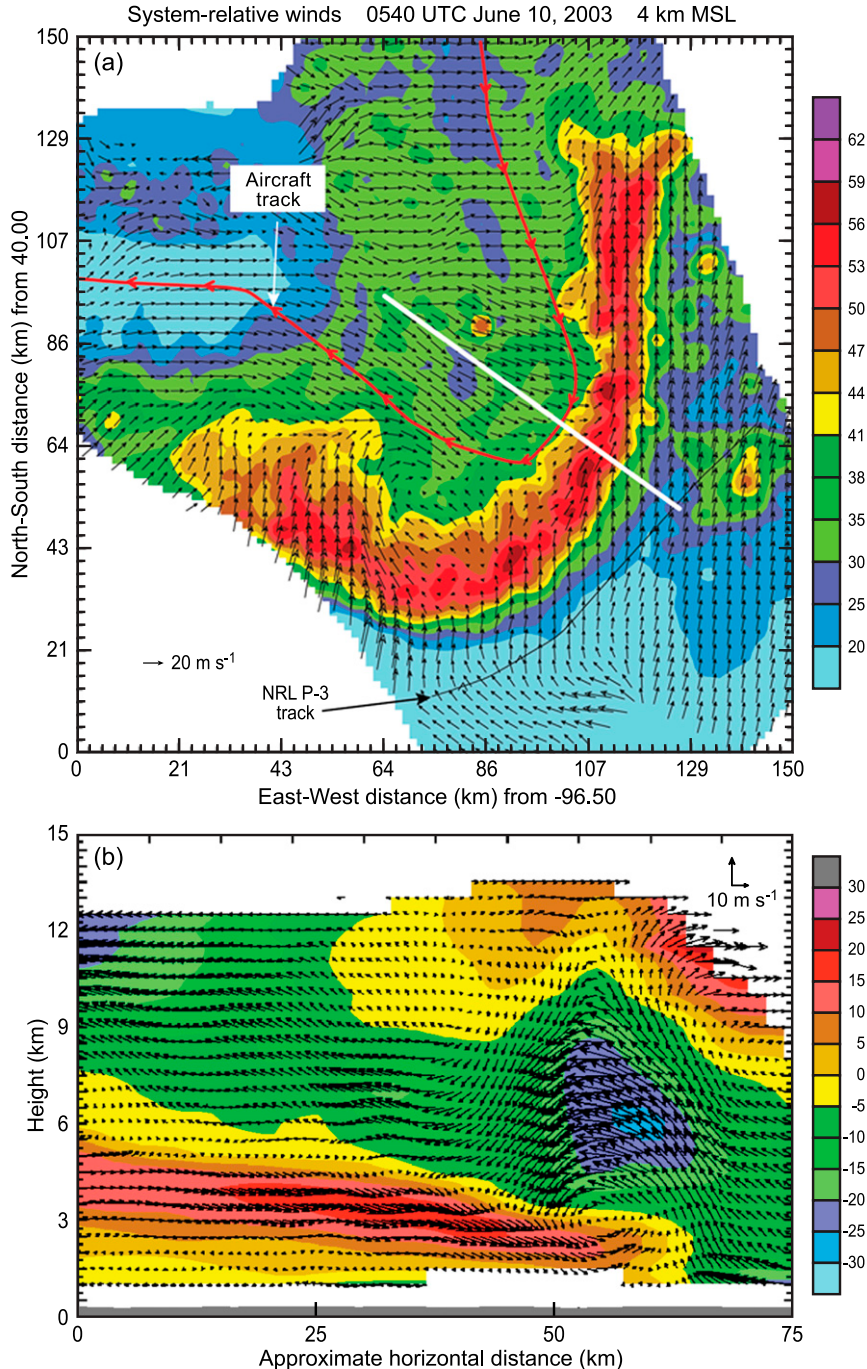


FIG. 17-13. (a) System-relative winds at the 4-km level derived from airborne Doppler radar data within a bow echo on 10 Jun 2003. Aircraft tracks are superimposed. Reflectivity in dBZ is in color. (b) Vertical cross section along the white line in (a) of Doppler-derived storm-relative flow in the plane of the cross section. Negative velocities (yellow, green, and blue colors) recede from the convective line while positive velocities (brown, red, and magenta colors) approach the line. The vector scale [shown in the upper right of (b)] is vertically stretched to match the aspect ratio of the plot. The panels are adapted from Davis et al. (2004) and Jorgensen et al. (2004), respectively, by Houze (2014).

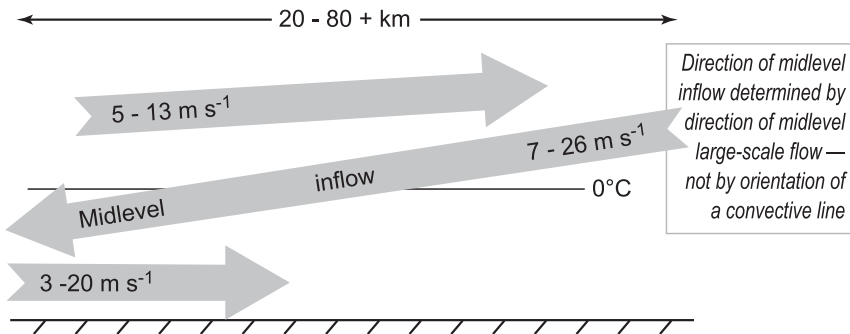


FIG. 17-14. Schematic of airflow in the stratiform regions of an MCS over the western tropical Pacific as observed by airborne Doppler radar in TOGA COARE. The numbers indicate the observed ranges of values of the horizontal relative wind velocity and the horizontal scale of the midlevel inflow. Based on figures and tables of [Kingsmill and Houze \(1999\)](#); © Royal Meteorological Society.

that, as such, the mature MCS is not simply a collection of deep but weakly entraining deep convective towers arising from the boundary layer, as is often assumed in parameterization schemes. In addition, as indicated in Fig. 17-16, the lower-tropospheric layer of air entering the MCS's convective region usually has a negative vertical gradient of θ_e . As noted by Houze (2014, chapter 9),

When this layer of potentially unstable air rises and saturates, the air becomes absolutely buoyantly unstable. Doppler radar observations show that despite its absolute instability, the inflow layer maintains a coherent structure as a sloping front to rear ascent. Evidently, the release of the instability is not rapid enough or deep enough to destroy the basic layer structure.

The term moist absolutely unstable layer (MAUL) has been used to describe such layers (Bryan and Fritsch 2000). Extremely high-resolution modeling reveals that within the layer of generally rising air, the buoyant elements overturn in rolls aligned along the shear (Bryan and Fritsch

2003), consistent with radar data, which show that the cells in convective zones of MCSs are often elongated, as in the early study of Ligda (Fig. 17-4) and later documented in the Oklahoma study of Houze et al. (1990).

The overturning in MCSs in the form of a circulation of a horizontal scale of the entire system and in the form of deep layers of air is a clear departure from the view that deep convection consists entirely of buoyant plumes arising from the planetary boundary layer. That view has traditionally dominated convective parameterization schemes. However, recent studies are finally considering how to parameterize layered MCS circulations into climate models (e.g., Moncrieff et al. 2017).

9. Wind shear in the environment in relation to the structure of MCSs

Over the summer season of GATE, it became apparent that two types of MCSs occurred within the oceanic data array. These became known as squall-line

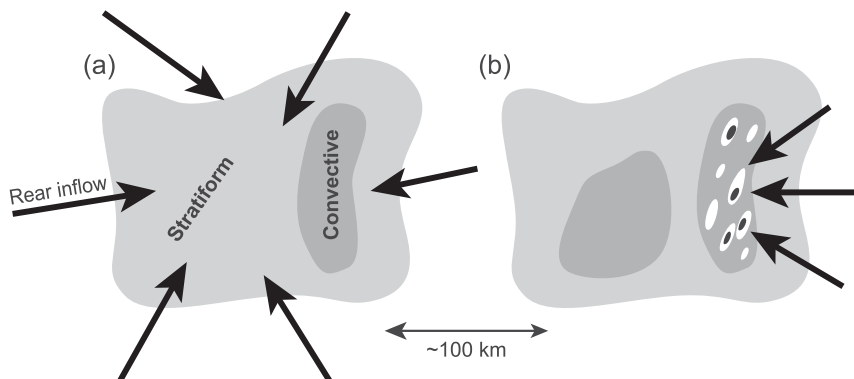


FIG. 17-15. (b) Idealization of a horizontal map of radar reflectivity (a) divided into convective and stratiform regions. Light gray represents the lowest reflectivity. Arrows in (a) show possible midlevel inflow directions. Arrows in (b) show possible low-level inflow directions. Adapted from [Houze \(1997\)](#).

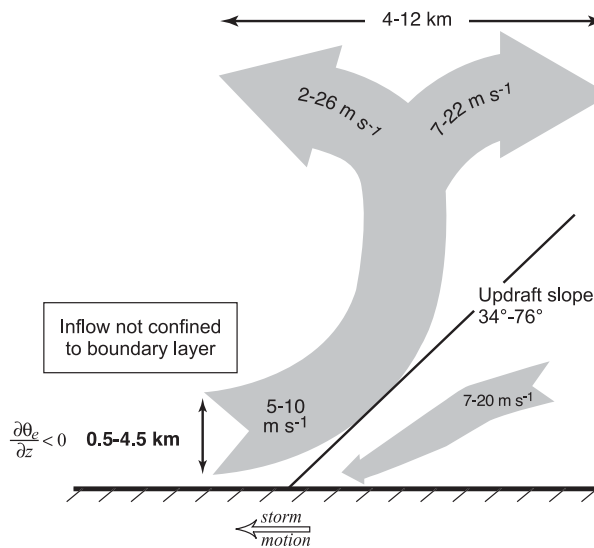


FIG. 17-16. Schematic of airflow in the convective regions of an MCS over the western tropical Pacific as observed by airborne Doppler radar in TOGA COARE. The numbers (from bottom to top) indicate the observed ranges of values of the depth of the inflow layer, horizontal relative velocity of inflow and outflow air currents, the slope of the updraft (angle measured relative to the ocean surface), horizontal relative outflow velocities, and the width of the divergent region aloft. The horizontal directional differences of the low-level updraft inflow and midlevel downdraft inflow were often significantly different from 180°. Based on figures and tables of [Kingsmill and Houze \(1999\)](#); © Royal Meteorological Society.

systems ([Houze 1977](#); [Zipser 1977](#)) and nonsquall events ([Leary and Houze 1979b](#)). [Houze and Betts \(1981\)](#) described the GATE observations of these two types of systems. The squall-line MCSs moved faster than other MCSs and featured a leading line of deep convective clouds followed by a broad region of stratiform precipitation, the latter accounting for ~40% of the rain from the MCS. The squall-line form of MCS has received much attention, largely because of its relationship to the large-scale environmental shear. The propagating line is usually somewhat curved convexly in the direction of system motion and generally normal to the lower-tropospheric wind shear, so that the relative wind is toward the line at low levels, switching to a front-to-rear direction aloft. Prior to GATE, [Moncrieff and Miller \(1976\)](#) and [Moncrieff \(1978\)](#) had begun to show from vorticity consideration how the overturning in a convective line should be organized into deep overturning layers, as shown by the colored shading in [Fig. 17-12](#). These papers indicated specifically that the overturning was related to the wind shear ahead of the line. The work of Moncrieff and Miller was highly influenced by the earlier work of [Browning and Ludlam \(1962\)](#), who showed that the overturning in a convective storm, regardless of scale, should consist of such overturning layers.

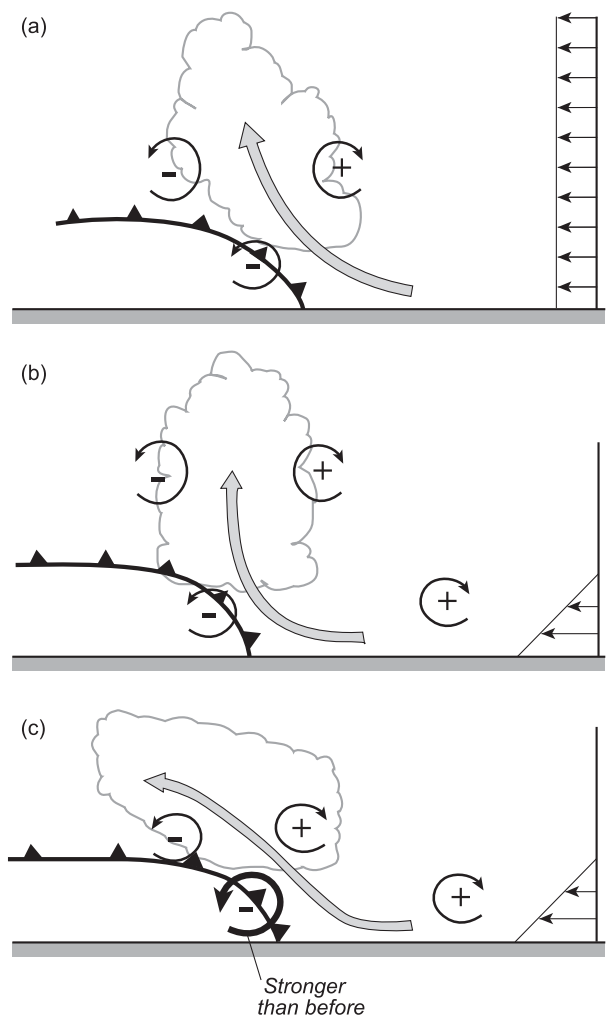


FIG. 17-17. Heuristic diagram indicating horizontal vorticity (+ and -) in the vicinity of a long-lived line of multicell storms. Profile of horizontal wind component normal to the line is shown on the right of each panel. Frontal symbol marks outflow boundary. (a) Case in which there is no wind shear normal to the line in the environment. (b) Early stage of line development in case of low-level shear ahead of the gust front. (c) Late stage of line development in case of low-level shear ahead of the gust front. Adapted from [Rotunno et al. \(1988\)](#), [Weisman \(1992\)](#), and [Weisman and Rotunno \(2004\)](#).

Moncrieff and Miller's insights are not restricted to tropical convection. Squall-line MCSs occur at all latitudes and over both land and ocean. The relationship to shear is always that indicated in these early papers.

After GATE, questions remained about how the convective cells embedded in the upward branch of the overturning layer of a squall-line MCS relate to the environment shear. In a highly influential paper, [Rotunno et al. \(1988\)](#) described how the line forming in an environment of shear like that considered in the Moncrieff and Miller papers first becomes erect.

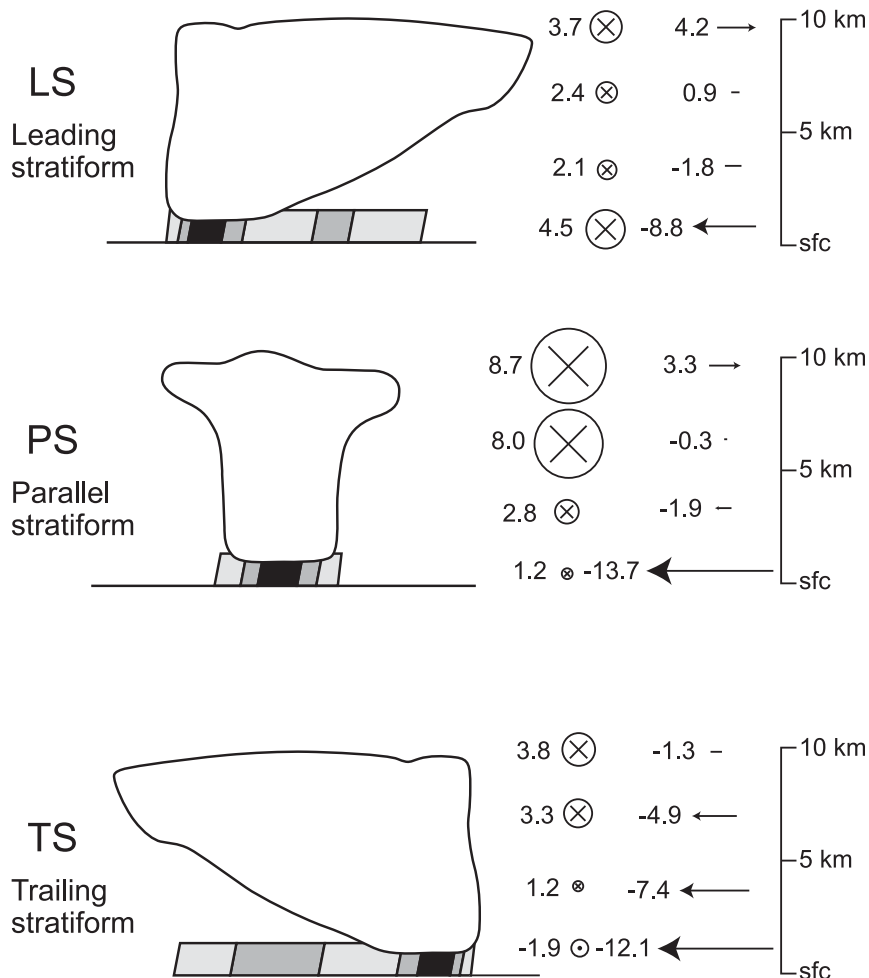


FIG. 17-18. Vertical profiles of layer-mean storm-relative pre-MCS winds for MCSs containing lines of convection. Wind vectors depicted as line-parallel (\otimes) and line-perpendicular (\rightarrow) components (m s^{-1}). Layers depicted are 0–1, 2–4, 5–8, and 9–10 km. Typical base scan radar reflectivity patterns (shading) and hypothetical cloud outlines are drawn schematically for reference. MCS leading edges are to the right. From [Parker and Johnson \(2000\)](#).

The ideas in this paper have become known as the Rotunno–Klemp–Weisman (RKW) theory, and [Weisman \(1992\)](#) and [Weisman and Rotunno \(2004\)](#) have published extensions and updates. The basic notion of RKW theory is that the convective cells in the line become erect in response to a balance of horizontal vorticity associated with the updrafts' positive buoyancy and the convective downdrafts' negative buoyancy (Figs. 17-17a,b). As the line ages, and the stratiform region grows, additional vorticity associated with the stratiform region's mesoscale downdraft leads to the convection becoming tilted rearward (Fig. 17-17c). When the mesoscale downdraft emanating from the stratiform region becomes extremely intense, its vorticity can push the cold pool boundary and vorticity balance illustrated in Fig. 17-17 far ahead of the main line in the form of a bow echo like the example in Fig. 17-13.

Again, it is important to note that squall-line MCSs are a subset of all MCSs, and when the environmental shear is different from that of the Moncrieff–Miller paradigm, very different arrangements and interactions of the convective and stratiform portions of MCSs can occur. In many situations the convective cells in an MCS are not even arranged in a line (Houze et al. 1990). Bluestein and Jain (1985) and Parker and Johnson (2000) have examined cases exhibiting line structure of deep convection over the United States and have found a variety of patterns, all systematically related to environmental shear. Parker and Johnson (2000) found that the tropospheric shear determined whether the precipitating cloud deck of an MCS formed ahead of, along, or behind a line of convection (Fig. 17-18). LeMone et al. (1998) examined lines of convection over the western tropical Pacific, and

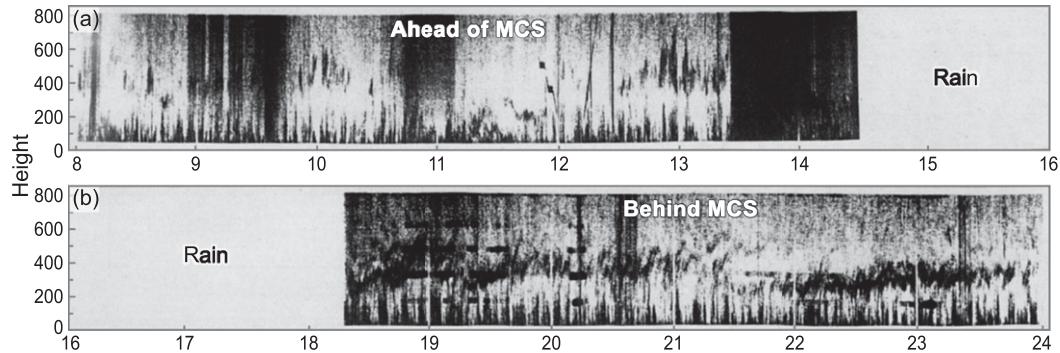


FIG. 17-19. Data obtained during GATE from an acoustic sounder on board the ship *Oceanographer* from 0800 to 0000 UTC on 4 Sep 1974. Black echoes extending from top to bottom of chart are from precipitation. Rectangular echoes at 1150–1200, 1845–1940 and 2015 UTC are from tethered balloon instruments flown from the *Oceanographer*. Spikey echoes emanating from bottom of chart are from turbulent plumes. Intermittent echoes between 300- and 600-m levels prior to 1325 are cloud echoes. The continuous layer of echo after 1815 is from a stable layer. From Houze (1977).

Johnson et al. (2005) documented lines over the South China Sea. Both studies showed several patterns of convective–stratiform organization that bore systematic but complex relationships to the environmental shear. Some lines were parallel to shear, while others were perpendicular. In an especially interesting variant of MCS structure over the tropical Indian Ocean examined by Yamada et al. (2010), the environment had low-level westerlies and upper-level easterlies, and convective and stratiform regions that separated over time by moving in opposite directions, with the stratiform regions moving systematically westward and ingesting eastward-moving deep convection.

Robe and Emanuel (2001) carried out idealized simulation of clouds in a radiative convective equilibrium setting. They provide some insight into how convective lines form in relation to both low-level and midlevel shear. For example, they find that if the low-level shear becomes too large, lines may rotate away from the direction orthogonal to the shear. Nevertheless, Johnson et al. (2005) note that while some of forms of convective line organization are understandable via conventional reasoning, many remain puzzling and in need of further study.

Despite all of these variations of line structure and horizontal patterns of the convective and stratiform components of MCSs, similarities remain in the precipitation-forming mechanisms. When Barnes and Houze (2014, 2016) analyzed, simulated, and compared squall and nonsquall MCSs over the tropical Indian Ocean, they found similar kinematic and microphysical processes to be operating in both types of MCSs.

10. Boundary layer and cold pools below MCSs

One of the results of GATE was the realization that MCSs over tropical oceans completely alter the character

of the planetary boundary layer. One of the innovative instruments deployed in GATE was a shipborne vertically pointing acoustic sounder. This instrument, analogous to radar, received reflections of emitted sound waves from irregularities in the lowest 800 m of the boundary layer (Mandics and Hall 1976; Gaynor and Mandics 1978). Clear-air convective plumes, small convective clouds, and stable layers were the primary identifiable echoes. Figure 17-19a (from Houze 1977) shows the structure of the undisturbed boundary layer ahead of the MCS. The vertically oriented spikes of high acoustic reflectivity seen emanating from the sea surface are clear-air turbulent plumes. The echo spikes with bases at about 300 m appearing intermittently above the layer containing the surface-based plumes are low-level small non-precipitating cumulus clouds. During the rainy period no signal was obtained. Figure 19b shows the boundary layer structure in the wake of the MCS. The stable layer capping the cool downdraft air that had entered the boundary layer was marked by the continuous, dark, undulating streak of echo between 200 and 400 m. As this cold air moved over the warm ocean, turbulent mixing was stronger than that ahead of the MCS, and the pattern of plume echoes seen immediately after 1820 was, therefore, denser than before the squall. Soundings obtained in the cold pool were consistent with the acoustic sounder data, and calculations of surface fluxes corroborated the increased turbulence. Bulk flux calculations for MCS wake conditions over tropical oceans readily show that latent heat fluxes dominate in cold pools over tropical oceans. Using soundings and flux measurements obtained aboard the GATE ships, Johnson and Nicholls (1983) mapped the boundary layer structure throughout the cold pool region of one of the tropical oceanic MCSs observed in GATE. Figure 17-20 shows the mapped latent heat flux.

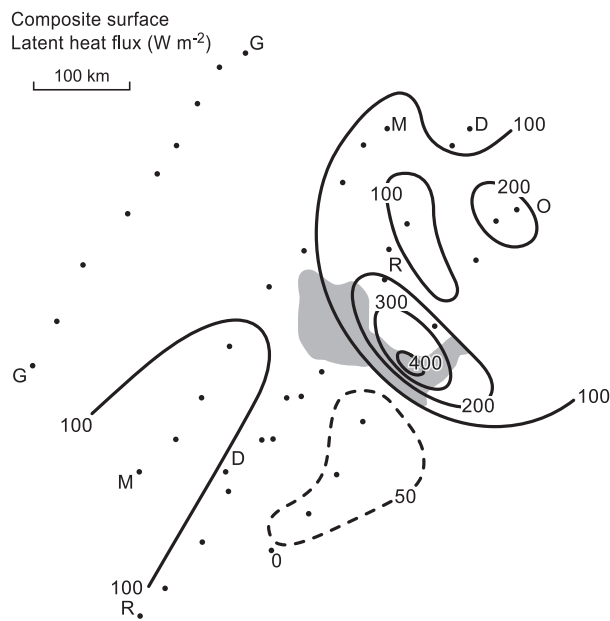


FIG. 17-20. Composite surface sensible heat flux (W m^{-2}) beneath an MCS observed in GATE. Dots indicate hourly positions of ships *Gilliss* (G), *Meteor* (M), *Dallas* (D), *Researcher* (R), and *Oceanographer* (O). Composite stability atop the mixed-layer inversion (m s^{-2}). From [Johnson and Nicholls \(1983\)](#).

Tethered balloon data taken from GATE ships during convective system passages were consistent with the surface fluxes ([Barnes and Garstang 1982](#)).

Cold pools from MCSs, as seen in GATE, have a major impact on the boundary layer in ocean regions where MCSs are frequent. Using the GATE acoustic sounder measurements, [Gaynor and Mandics \(1978\)](#) estimated that 30% of the area over the ocean in the eastern Atlantic intertropical convergence zone is occupied by cold pools at any given time, and because of their large areal coverage, MCSs account for a large proportion of that cold pool area. Over the western tropical Pacific, shipboard measurements of fluxes analyzed by [Young et al. \(1995\)](#) and [Saxen and Rutledge \(1998\)](#) showed increased fluxes similar to those seen in GATE during the passage and in the wakes of MCSs. The latent flux increases were mainly due to increased wind speed while the sensible heat fluxes were also affected by both wind and the temperature drop in the cold pools. Examining fluxes measured on moorings over the tropical Pacific, [Esbensen and McPhaden \(1996\)](#) found that the cold pools of MCSs enhanced surface fluxes by 10%–30%, depending on wind conditions.

One of the important effects of convective downdraft cold pools is that they act as density currents and trigger new convection at their leading edges. In this sense, the cold pools can be thought of as a medium of communication between existing and future convection. Capturing

cold pool formation and interaction is thus a key to representing accurately whole populations of convection. In the Dynamics of the Madden-Julian Oscillation (MJO) (DYNAMO) field experiment over the central tropical Indian Ocean, [Feng et al. \(2015\)](#) have shown the characteristics of a population of cold pools filling the boundary layer, colliding with each other, and triggering new convection. They found that the strongest new convection occurs at points of collision. Starting with a population of only a few small precipitating clouds, ever-larger new clouds form, with some eventually reaching MCS proportions with very large cold pools ([Rowe and Houze 2015](#)). From DYNAMO aircraft data, [Chen et al. \(2016\)](#) found that cold pools were deeper and stronger in MCSs during suppressed periods, when midlevel dry air surrounded the MCSs and prolonged the boundary layer recovery time.

The flux characteristics, formation, growth, and dissipation of MCS cold pools over land has been harder to determine because of the wide variety of land surface characteristics, and much remains to be determined. Unlike over oceans, where the latent heat flux dominates, over land, the surface sensible heat flux is important in modifying the cold pools. Modeling has produced a few insights, but no holistic understanding of MCS cold pools over land. [Grant and van den Heever \(2016\)](#) have performed model calculations indicating that both surface sensible heat flux and turbulent entrainment of environment air is important in MCS cold pool dissipation over land. Model results of [Gentine et al. \(2016\)](#) indicate that surface roughness is an important factor to consider in cold pool evolution, but their calculations do not necessarily apply to MCS cold pools. Simulations by [Drager and van den Heever \(2017\)](#) have shown that passage of MCS cold pools over wet patches of ground mitigates the cold pool dissipation.

11. Elevated MCSs

In midlatitude continental regions, boundary layer factors sometimes cease to be a consideration, as the layered overturning of an MCS is sometimes completely aloft, disconnected from the planetary boundary layer. [Trier and Parsons \(1993\)](#) noted this behavior in an MCC documented in PRE-STORM. [Marsham et al. \(2010\)](#) developed a conceptual model of such an “elevated MCS” (Fig. 17-21). In this model, the MCS overrides a layer of stable air, located on the cold side of a front or over a stable layer produced by nocturnal cooling of a land surface. Warm unstable air running over the top of the stable layer provides the layered ascent of the mature MCS lying atop the stable layer. The mesoscale downdraft emanating from midlevels lies under the

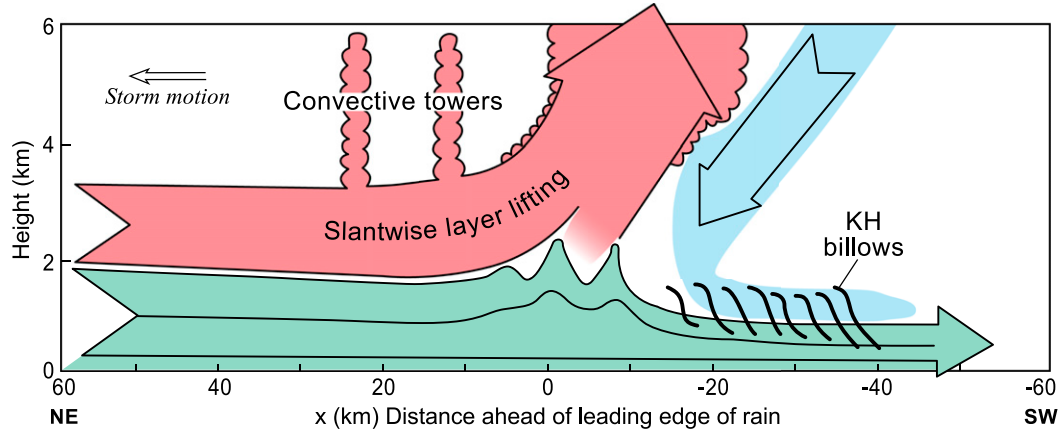


FIG. 17-21. Schematic of the structure of the various features of an elevated MCS. Arrows indicate system-relative flows. Adapted from [Marsham et al. \(2011\)](#).

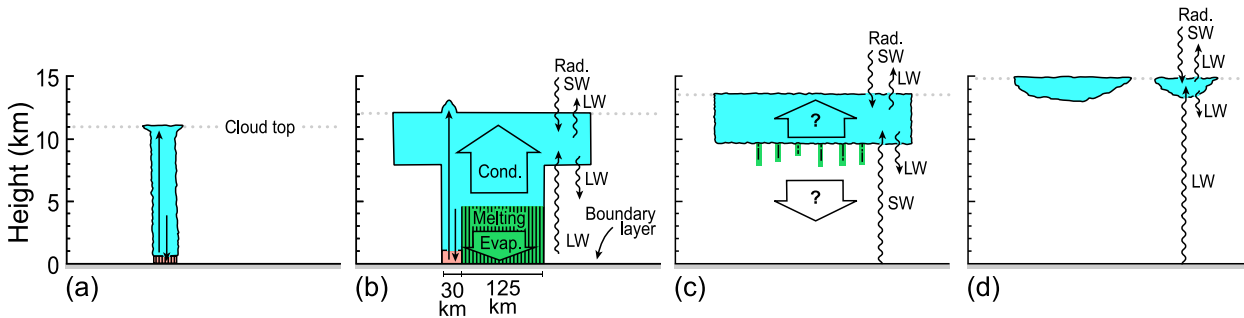
mesoscale ascent, as in Fig. 17-12, but may remain atop the stable layer, as depicted in Fig. 17-21. Also indicated in the conceptual model is a perturbation of the stable layer underneath the MCS. The updraft layer of the MCS rises over this bump in the stable layer, which is thought to be due to a gravity wave or bore propagating through the stable layer. In a model simulation, [Parker \(2008\)](#) obtained an MCS initiated before nocturnal cooling produced the stable layer, and the MCS subsequently became elevated above the stable layer. The perturbations of a stable layer, associated with a front or strong nocturnal cooling over land, may also trigger new convection that may evolve into an elevated MCS (e.g., [Parker 2008](#)), and the downdrafts of a developing MCS triggered aloft may penetrate to the surface and change an elevated MCS into an ordinary MCS ([Marsham et al. 2011](#)). These various scenarios led to a field project in 2015 called the Plains Elevated Convection at Night (PECAN), which aimed to study elevated deep convection in its various forms, with an emphasis on nighttime conditions when stable layers are most pronounced ([Geerts et al. 2017](#)).

The occurrence of elevated MCSs in connection with fronts is sufficiently common in midlatitude continental regimes that it led [Fritsch and Forbes \(2001\)](#) to identify them as a special category of MCS, which they called “Type-1,” in contrast to “Type-2” MCSs that occur in more barotropic environments, such as the tropics. [Wilson and Roberts \(2006\)](#) estimated that about half of the MCSs over the central United States are elevated. Other regions of the world such as the Pampas of Argentina, which has MCSs similar to those in the central United States ([Rasmussen and Houze 2011](#)), likely have similar occurrences of elevated MCSs. The existence of elevated MCSs poses a complex forecast problem and a particular complication for projecting climate change.

Global models that are used to project long-term changes in the general circulation and climate still depend on parameterization of deep convection, and existing parameterization schemes assume deep convection to be rooted in the planetary boundary layer. The existence of elevated mature MCSs like that illustrated in Fig. 17-21 and the further complication of deep convection being initiated above stable layers implies the inability of existing parameterizations to represent elevated forms of deep convection. Clearly radical changes in parameterization methods will be needed for global models used for climate projections over long time periods, or advances in computing power will need to allow such models to run with sufficiently fine grid spacing for MCSs to be fully resolved as they are in “cloud resolving models,” which are presently being run regionally over modestly long climatic periods (e.g., [Prein et al. 2015](#); [Yang et al. 2017](#); and others).

12. Canonical life cycle of an MCS, modes of heating, and potential vorticity generation

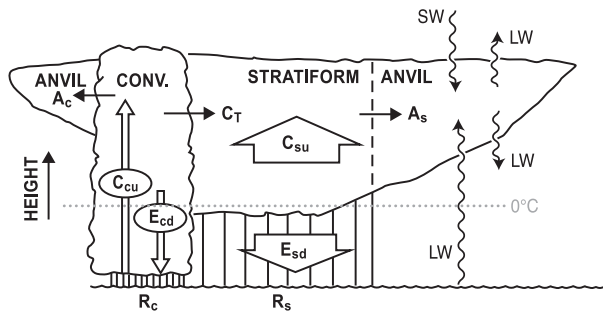
One of the significant results of GATE was the recognition that MCSs undergo a canonical life cycle, which is illustrated schematically in Fig. 17-22. This life cycle has been confirmed and elaborated by subsequent field campaigns using satellite imagery and radars on ships, aircraft, islands, and continental landmasses. Figure 17-22a shows a single “cell” of deep convection at this early stage, but in reality, a group of such “cells” occurring in close proximity is an essential feature for the system to reach mesoscale proportions. The group is often in the form of a line, but the cells may be grouped in other patterns. Note in Fig. 17-8 how the precipitation is almost completely convective in the early hours of the MCS. Over time, the initial cells weaken while new ones

FIG. 17-22. MCS in successive stages of development. Adapted from [Houze \(1982\)](#).

form. As the older cells weaken, their vertical motions no longer support vertical advection of hydrometeors, and the precipitating ice particles aloft generally drift downward through the environment of weakened mean upward motion (Fig. 17-22b). They melt as they fall below the 0°C level and turn into rain. The raining layer is dominated by downward motion where the drops are falling through a layer of subsaturated air and evaporating at rates calculated by [Brown \(1979\)](#). This period when both active convection and stratiform precipitation are present characterizes the mature stage of an MCS. In Fig. 17-8 the mature stage would be the period \sim 1700–2300 UTC. After the mature stage, the convective and stratiform portions of the MCS decline together. Figures 17-22c and 17-22d illustrate this period of decline, which can last well beyond the time when precipitation is reaching Earth's surface. The remaining ice cloud aloft can last tens of hours. An important detail in Fig. 17-22 is that the cloud top continues to rise. Turbulent motions in the stratiform cloud layer cause the top to rise as the cloud layer entrains dry air from above. The mixing is strongest at night when radiative cooling in the upper portion of the cloud layer is actively destabilizing the layer. The high thin cloud layer left aloft remains for long periods of time and has climatological implications for radiative transfer in the upper troposphere ([Hartmann 2016](#)).

The heating of the atmosphere by an MCS over its lifetime is a combination of latent and radiative heating. The latent and radiative heating are interrelated through the water budget of the MCS. The fallout of rainwater from the MCS is proportional to the net latent heat released into the atmosphere by the MCS, and the ice cloud aloft affects radiative transfer in the upper troposphere. Furthermore, the MCS dynamics and physics affect the distribution of both latent and radiative heating by the system. GATE and subsequent field studies led [Houze \(1982\)](#) to realize that the distribution of the latent heating with height differs between the convective and stratiform portions of an MCS. The

latent heating is related to the water budget of the MCS. Figure 17-23 illustrates the bulk water budget over the area and lifetime of an MCS. The bulk components of the water budget are shown as if they were combined into one convective region, one associated stratiform region, and anvil clouds associated with both the convective and stratiform regions. The variables represent the disposition of condensed water mass, which is interrelated by water budget equations ([Houze et al. 1980](#)). The net heating in the convective region is dominated by condensation and sublimation of vapor in the convective updrafts (C_{cu}), which must account for all of the convective rain (R_c), as well as the condensate transferred from the convective to the stratiform region (C_T) and rain reevaporated in the convective downdraft (E_{cd}). Freezing of supercooled water in the convective updrafts further increases heating in the upper part of the convective cells ([Zipser 2003](#)). The heating profile in the convective region tends to be positive throughout the troposphere (Fig. 17-24). Sometimes the maximum is somewhat below the middle troposphere and sometimes somewhat higher, but generally not in the upper troposphere ([Houze 1989](#)). The net heating and cooling processes in the stratiform region are dominated aloft

FIG. 17-23. Schematic vertical cross section of an idealized MCS with convective region (CONV.), associated stratiform precipitation region and nonprecipitating cirriform anvil. Longwave (LW) and shortwave (SW) radiation are shown. Symbols are defined in text. Adapted from [Houze et al. \(1980\)](#).

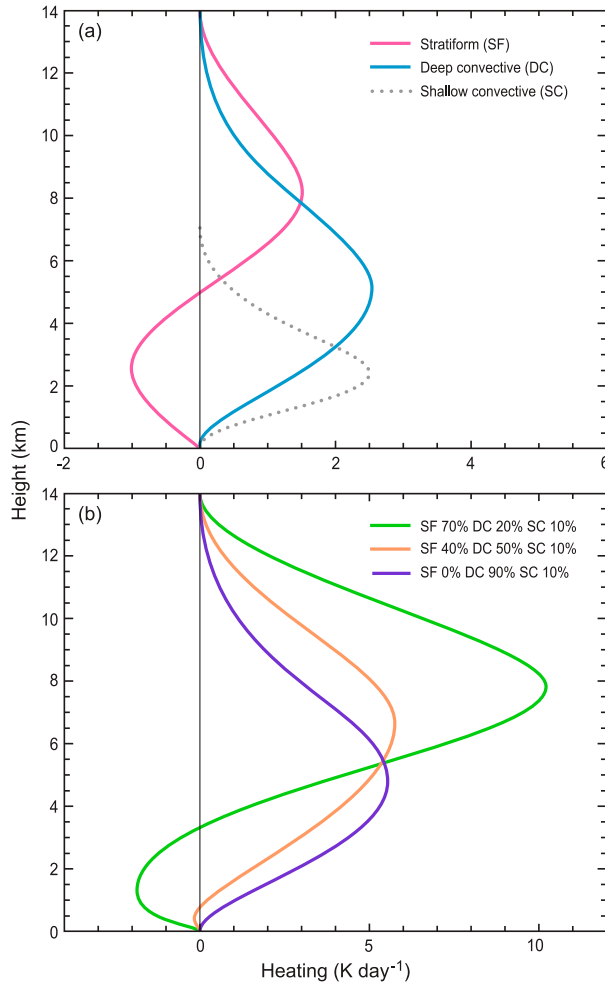


FIG. 17-24. (a) Idealized stratiform, deep convective, and shallow convective latent heating profiles. The x axis is meant to be non-dimensional until a precipitation amount is specified. (b) Total latent heating profiles for 0%, 40%, and 70% stratiform rain fractions, assuming 3.5 m yr^{-1} rain accumulation. Adapted from Schumacher et al. (2004).

by sublimation of vapor onto ice particles (C_{su}) in the weakly buoyant stratiform updraft region at upper levels and evaporation (E_{sd}) of stratiform precipitation particles in the mesoscale downdraft occupying the lower part of the troposphere. In addition to the evaporation, cooling by melting occurs in a $\sim 0.5\text{-km-thick}$ layer just below the 0°C level in the stratiform zone (Leary and Houze 1979a). As a result of these processes, the latent heating profile is positive at upper levels and negative at lower levels (Fig. 17-24a). In addition to the latent heating and cooling processes, convergence of radiative fluxes in the long-lived and extensive ice cloud “ anvils” of the MCS leads to further heating aloft, making the net heating profile “top heavy.” As shown in Fig. 17-24b, the larger the stratiform proportion of MCS rainfall, the

more the overall profile is “top heavy,” meaning that heating is more concentrated aloft than would be the case if all the precipitation were occurring in convective towers. The top-heaviness of heating profiles associated with MCSs was first pointed out by Houze (1982), and Hartmann et al. (1984) showed that the general circulation of the tropics was substantially impacted by the top-heaviness of MCS heating. Schumacher and Houze (2003) used data from the TRMM satellite radar to show that across the tropics rainfall from convection ranges between $\sim 20\%$ and 70% stratiform, implying that as a result of MCSs heating profiles across the tropics tend to be top-heavy. The stratiform rain fraction tends to be higher over the oceans (see section 17). Similar stratiform proportions occur in connection with midlatitude MCSs.

The top-heaviness of the heating profile of an MCS has important dynamical implications. The quasi-balanced flow of the large-scale circulation of the atmosphere is in a constant state of adjustment to the potential vorticity (PV) field. When diabatic processes occur, potential vorticity is not conserved, but rather it is affected by spatial gradients of the heating. In particular, the time rate of change of potential vorticity is directly proportional to the vertical gradient of heating. Thus, as can be inferred from Fig. 17-24, the more top-heavy the MCS heating profile, the stronger the feedback to the large-scale. This feedback is sometimes felt locally in the form of a “mesoscale convective vortex (MCV),” identified and named by Bartels and Maddox (1991) and illustrated schematically in Fig. 17-25 for a case analyzed by Fritsch et al. (1994). Raymond and Jiang (1990) pointed out how the environment shear profile typical of certain MCSs can interact with the potential vorticity anomaly associated with the heating profile to prolong the lifetime of the MCS. The importance of the MCV associated with the potential vorticity anomaly to the duration and precipitation productivity of MCSs has been shown by Trier and Davis (2002) and Schumacher et al. (2013). On seasonal time and space scales, it has been found that more realistic structures of the mean Walker cell (Hartmann et al. 1984) and El Niño–Southern Oscillation (Schumacher et al. 2004) are obtained in simple climate models if it is assumed that the net effect of convection on the large-scale circulation has an imprint of the top-heavy stratiform heating of MCSs.

13. Microphysics and the connection between convective and stratiform precipitation of MCSs

Although GATE was massive in terms of the number of observational platforms brought to bear on tropical

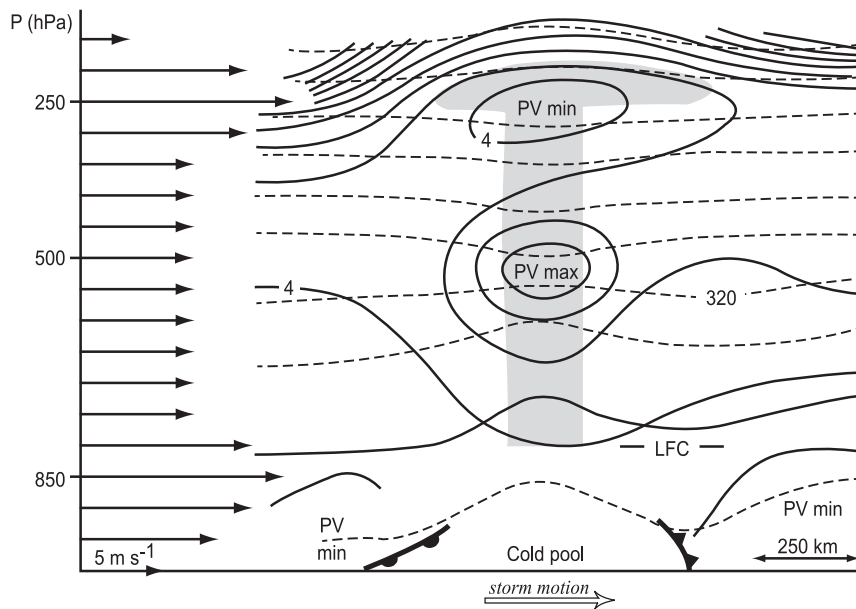


FIG. 17-25. Conceptual diagram of the structure and development mechanism of a midlevel PV maximum associated with an MCS—based on a case study. Thin arrows along the ordinate indicate the vertical profile of the environmental wind. Frontal symbols indicate outflow boundaries. Dashed lines are potential temperature (5-K intervals) and solid lines are PV (in intervals of $2 \times 10^{-7} \text{ m}^2 \text{ s}^{-1} \text{ K kg}^{-1}$). The system is propagating left to right at about $5\text{--}8 \text{ m s}^{-1}$ and is being overtaken by air of high equivalent potential temperature in the low-level jet. Air overtaking the vortex ascends isentropic surfaces, reaches its level of free convection (LFC), and thereby initiates deep convection. Shading indicates cloud. Adapted from Fritsch et al. (1994).

convection, instrumentation on those platforms as well as numerical modeling were limited in sophistication at that point in time, and analysts had to rely on inference more than is the case today. The only particle-scale microphysical measurements obtained were raindrop-size distributions detected by ship-based electromechanical disdrometers (Austin and Geotis 1979) and by a foil impactor on a DC-6 aircraft (Cunning and Sax 1977). Nevertheless, on the basis of this primitive information on drop-size distributions measured below the melting layer of the stratiform regions of several MCSs observed in GATE, Leary and Houze (1979a) inferred aspects of the ice-phase microphysics of the stratiform regions of MCSs in GATE. Combining the drop-size measurements with quantitative radar reflectivity patterns and sounding data, they concluded that the ice particles just above the melting layer in the stratiform region were most likely rimed aggregates and/or graupel (Fig. 17-26). These inferences have been generally confirmed as technology has improved (Barnes and Houze 2014).

Just 5 years after GATE, another field campaign of the Global Atmospheric Research Program was the Monsoon Experiment (MONEX) in which MCSs similar to those seen in GATE were investigated over the Bay of Bengal by some of the first flights of an

instrumented National Oceanic and Atmospheric Administration P-3D aircraft, on which some of the earliest optical Particle Measuring System probes were mounted to obtain shadow-gram images of ice particles through a wide range of altitudes (i.e., temperatures) in the deep layer of stratiform cloud above the melting layer. Most particle images were of indiscernible shape but occasionally displayed certain crystal habits and structures. Houze and Churchill (1987) determined the frequency of occurrence of identifiable ice particle types seen at different flight-level temperatures (Fig. 17-27). They found that the frequencies were consistent with ice particles growing by vapor deposition in a cloud in which vertical air motions were weak enough for the particles to be growing by vapor deposition and aggregating while drifting downward toward the melting level. The most frequent particle types at each level were consistent with the pattern of ice particle growth, development, and fallout in a stratiform cloud of weak upward air motion. In addition, the occurrence of nearly round particles just above the 0°C level would be consistent with riming producing some graupel or other rimed particles just above the melting layer, as suggested by Fig. 17-26.

In the 1980s and 1990s, intensive observations of MCSs turned to midlatitudes, and Doppler radar was beginning

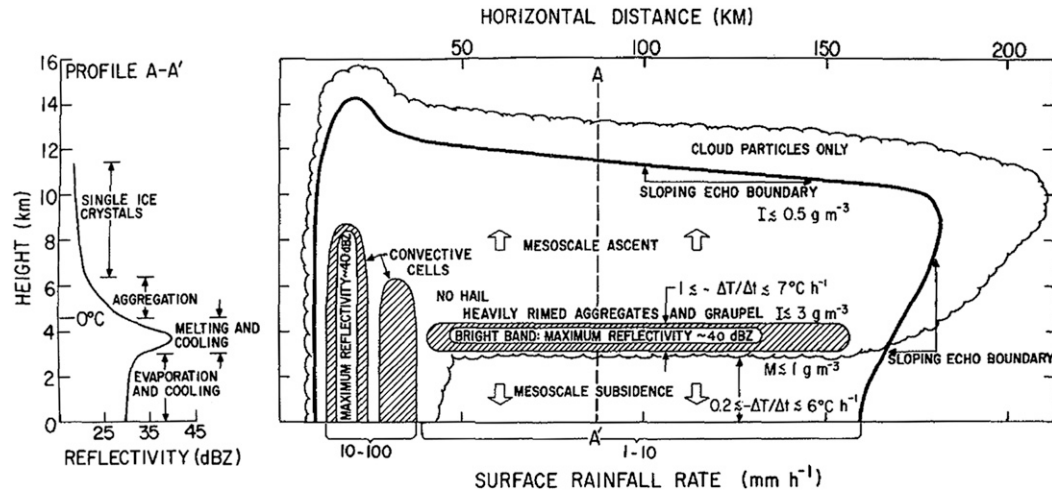


FIG. 17-26. Schematic vertical cross section and vertical profile of radar reflectivity (along dashed line A–A' in the cross section) in horizontally uniform precipitation associated with an anvil cloud. The anvil cloud occurs to the rear of intense convective cells moving from right to left in the figure. The dark solid line is the contour of minimum detectable radar echo, lighter solid lines and shading indicate contours of higher reflectivity, and the scalloped line indicates the cloud boundary. From [Leary and Houze \(1979a\)](#).

to be used in research on precipitation cloud systems. The 1985 PRE-STORM program was one of the first large field campaigns to employ multiple research Doppler radars. Working with data from an MCS over Kansas, [Braun and Houze \(1995\)](#) retrieved the patterns of freezing and melting in the MCS by applying thermodynamic and bulk microphysical equations to the air motion field synthesized from dual-Doppler radar observations. They found that the melting in the stratiform region was occurring in a thin horizontal layer ~ 200 km in breadth, while the freezing was in a vertical column corresponding to the intense active convective cells of the MCS (Fig. 17-28). As noted in [section 12](#), the cooling due to melting in mid- to low levels of the stratiform region and the column of freezing in the upper parts of convective cells both contribute to the top-heavy heating profile of the MCS.

In 2011–12 another technological advance led to a significant increase in the observational knowledge of the microphysical processes in the convective and stratiform regions of MCSs, when dual-polarization S-band Doppler radar measurements were made during a nearly 4-month period over the equatorial Indian Ocean to study the MJO ([Madden and Julian 1971, 1972](#)) in the DYNAMO field experiment ([Yoneyama et al. 2013](#)).⁴ MCSs similar to

those seen in GATE and MONEX occur in that tropical oceanic region, and [Barnes and Houze \(2014\)](#) analyzed statistics of the radial velocity and microphysical particle type retrieved from the dual-polarization radar data. They composited the patterns of identified particle types in relation to the mesoscale flow patterns in both convective and stratiform regions for data obtained in two DYNAMO MCSs. The composite for the stratiform region (Fig. 17-29a) validated the general pattern of microphysics in the stratiform region that had been suggested in GATE and MONEX (cf. [Figs. 17-26 and 17-27](#)) in that rimed particles occurred intermittently just above the melting layer at the base of a deep layer of snow. [Barnes and Houze \(2016\)](#) carried this work further by assimilating Doppler radar velocities observed in two DYNAMO MCSs into a cloud-resolving model and found that the same general layering of microphysical processes was found in both observations and simulations, although the model results varied substantially with the particular choice of microphysics parameterization. The model results generally showed deposition everywhere above the 0°C level, aggregation at and above the 0°C level, melting at and below the 0°C level, and intermittent riming near the 0°C level, consistent with the GATE and MONEX results seen in [Figs. 17-26 and 17-27](#).

[Barnes and Houze \(2014, 2016\)](#) also composited the dual-polarization radar results for convective regions of DYNAMO MCSs (Fig. 17-29b). The convective regions had a vertical column of graupel, extending a few kilometers above the 0°C level and signifying the occurrence

⁴ DYNAMO was part of a multiagency program and was also known by the names Cooperative Indian Ocean Experiment on Intraseasonal Variability in the Year 2011 (CINDY) and ARM Program MJO Investigation Experiment (AMIE), which are explained by [Yoneyama et al. \(2013\)](#).

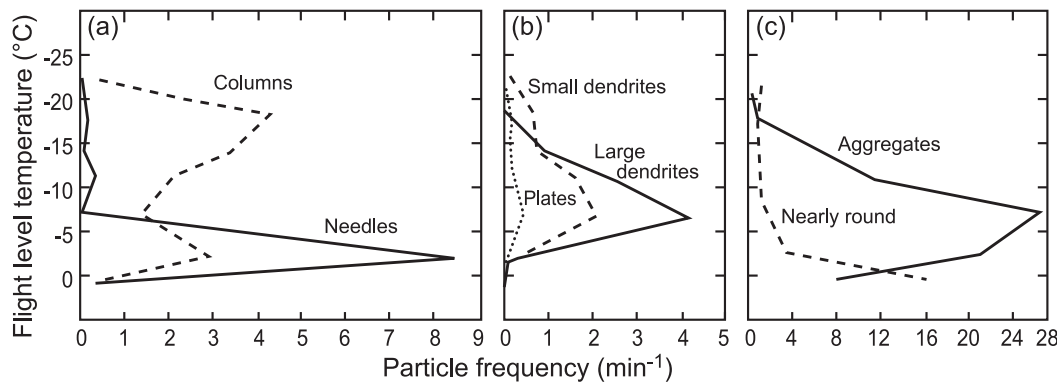


FIG. 17-27. Ice-particle data obtained on aircraft flights through nimbostratus in tropical MCSs over the Bay of Bengal. Plots show relative frequency of observation of ice particles of a particular type per minute of in-cloud flight time as a function of flight-level temperature. From Houze and Churchill (1987).

of freezing associated with riming in that zone—consistent with Fig. 17-28. The composite also shows wet (i.e., melting) aggregates just below the 0°C level, consistent with the pattern of melting below the column of freezing in Fig. 17-28. A composite similar to those in Fig. 17-29 has not yet been compiled for midlatitude MCSs, but based on the fact that continental convective updrafts are generally stronger than those over oceans (Zipser and LeMone 1980; LeMone and Zipser 1980), we would expect the signal of graupel (and hail) and associated freezing to be stronger over continental regions, except perhaps for the Amazon environment, which has some maritime-like characteristics.

It has also been apparent since the time of GATE that the microphysical processes in the convective and stratiform regions of an MCS are not independent but instead closely related. The term C_T in Fig. 17-23 represents condensate generated in the convective region that later becomes part of the precipitating stratiform cloud. That figure, however, does not indicate the process by which condensate initiated in convective cells becomes part of the stratiform region. Results from GATE hinted at the process when Leary and Houze (1979b) described the evolution of radar echo structure in an MCS. They found that over time an area of active convective echoes became stratiform while new convective elements formed in the near vicinity of the now-stratiform cells. As this process repeated, an increasingly large portion of the MCS radar echo became stratiform. Figure 17-30 illustrates the process schematically. Note how ice particle 1 generated in an active cell eventually falls out and melts in the stratiform region partially formed by its parent cell. From this schematic it is evident that the term C_T in Fig. 17-23 does not represent a spatial advection so much as a temporal transformation that occurs while the ice particles are falling out. It is also

important to note that the buoyant elements rising in active convective towers expand as they rise, as illustrated schematically in Fig. 17-31. Yuter and Houze (1995) dubbed these elements “particle fountains.” Ice hydrometeors suspended in the updraft therefore fall out over an ever-expanding area as the buoyant element approaches its maximum level of ascent. As more and more such widened elements arrive aloft and convective towers weaken, a mesoscale region of the mid-to-upper troposphere becomes filled with old, weakly buoyant elements depositing ice particles. Thus, a stratiform region forms from the remains of old and weakened but still buoyant convective elements.

Note that the process in Fig. 17-30 requires no shear of the environment. Thus, in principle, an MCS with convective and stratiform regions can develop without shear. However, MCSs often form in the presence of environmental shear, which affects the arrangement of the convective and stratiform components of the MCS. A common and oft-studied form of MCS is the leading-line/trailing-stratiform squall line (Fig. 17-12)

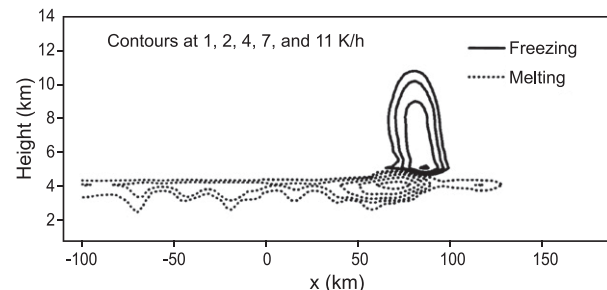


FIG. 17-28. Melting and freezing rates retrieved from dual-Doppler radar data for a squall-line MCS with its leading edge at about 100 km on the horizontal axis. From Braun and Houze (1995); © Royal Meteorological Society.

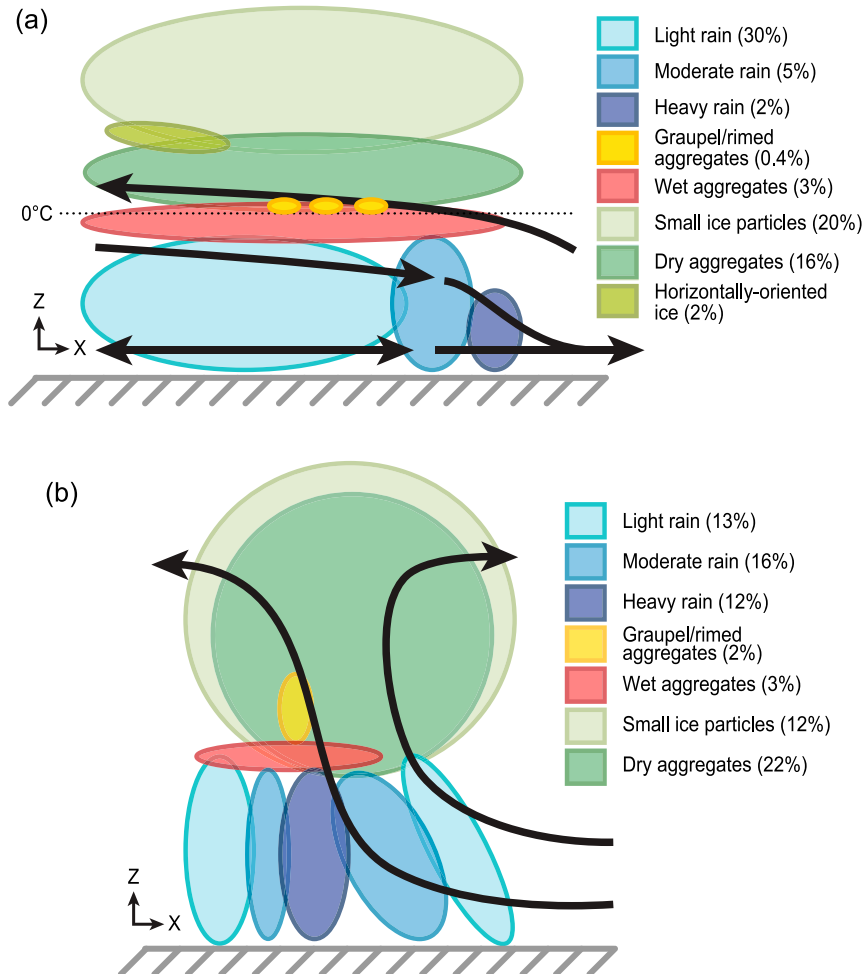


FIG. 17-29. Schematics showing the location of hydrometeor types in an MCS over the tropical ocean relative to (a) the layered airflow crossing the stratiform region, and (b) the layer of upward slantwise motion entering in the convective region. The percentages in the color bar indicate the average areal coverage of each particle type. From Barnes and Houze (2014).

in which the particle fountain elements are systematically advected rearward in the front-to-rear ascending flow. Thus, the widened elements of weak buoyancy and slowly falling ice particles are systematically moved rearward of the leading line where they form the upper part of the stratiform region, as illustrated in Fig. 17-32.

14. Modeling of individual MCSs

At the time of GATE, “cloud resolving” or “convection permitting” models of the type that are ubiquitous today were in their infancy, so only very primitive numerical modeling of convective clouds was part of GATE research (e.g., Simpson and van Helvoort 1980). Rapid development of models in the 1980s–90s, however, quickly led to many simulations of MCSs. Almost all such modeling has

been focused on the type of MCS that has a leading-line and trailing-stratiform region (e.g., Fovell and Ogura 1988; Lafore and Moncrieff 1989; Skamarock et al. 1994). One exception is the study of Barnes and Houze (2016). They successfully ran and compared simulations of both squall and nonsquall MCSs observed in DYNAMO in which the air motions in convective and stratiform regions were assimilated into the model. Results were consistent with the observational results of Kingsmill and Houze (1999) (Figs. 17-14 and 17-16) in that tropical oceanic nonsquall MCSs consistently have a midlevel downward-sloping flow below the melting level in the stratiform region and a deep upward sloping flow in the convective region.

An example of a simulation of an MCS of the leading-line/trailing-stratiform type, provided to the author by Professor Robert Fovell, is shown in Fig. 17-33. It exhibits

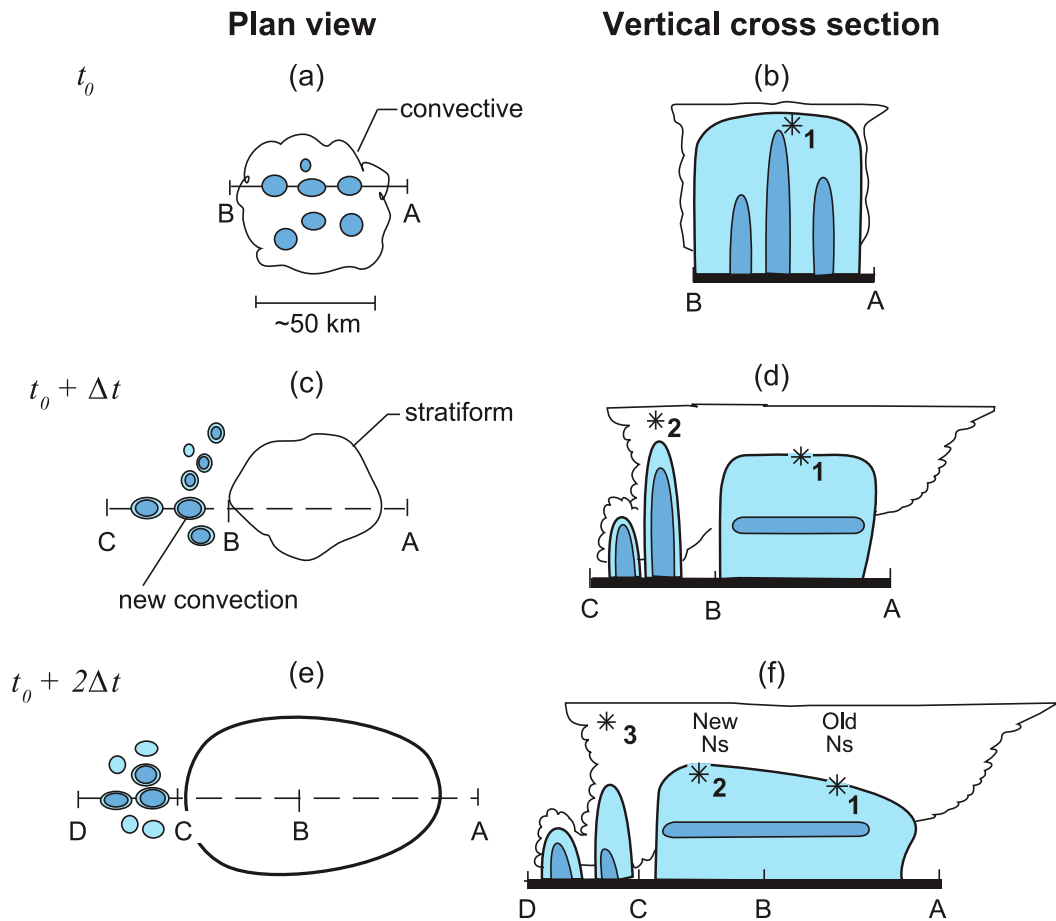


FIG. 17-30. Conceptual model of the development of nimbostratus associated with deep convection. Horizontal radar echo pattern at Earth's surface with two levels of intensity at three successive times: (a) t_o , (c) $t_o + \Delta t$, and (e) $t_o + 2\Delta t$. (b), (d), (f) As in (a), (c), and (e), but for the corresponding vertical cross sections. A sketch of the visible cloud boundary has been added to the vertical cross sections. Asterisks trace the fallout of three ice particles. From Houze (2014).

the main features of the MCS: A vertical tower of high reflectivity is centered in the convective zone at ~ 340 km on the horizontal axis; behind the convective zone is the stratiform region with a bright band at the melting level. The negative values of the horizontal wind field show the front-to-rear flow ascending from low levels ahead of the storm, through the convective zone, and into the stratiform region. The consistency with the conceptual model in Fig. 17-12 is evident. The positive values show the midlevel flow entering from the rear of the storm, descending to the surface below the melting level, and feeding into the bulbous head of the gust front in the convective zone. The exact characteristics of the model's radar reflectivity field depend on the microphysical parameterization and radar simulator used in the calculations. Effort directed toward determining the most accurate representation of the cloud and precipitation fields of MCSs continues to be an active area of research (e.g.,

[Morrison et al. 2009](#); [Powell et al. 2012](#); [Van Weverberg et al. 2013](#); [Barnes and Houze 2016](#); and others).

The ability to simulate MCSs accurately is important diagnostically because some features of MCSs are almost impossible to observe. For example, one of the most important properties of an MCS is its thermal structure. Yet the thermal properties of an MCS are nearly impossible to measure directly, especially in stratiform regions where temperature perturbations are small but important. Temperature may be retrieved from dual-Doppler radar observations, but such measurements are seldom available and that methodology is fraught with assumptions and far from precise. Accurate model simulations are at present the best indicators of MCS thermal structure. The simulation in Fig. 17-33 shows how the upper portion of the stratiform region is filled with weakly buoyant air previously located in the convection zone, as suggested by Figs. 17-31 and 17-32.

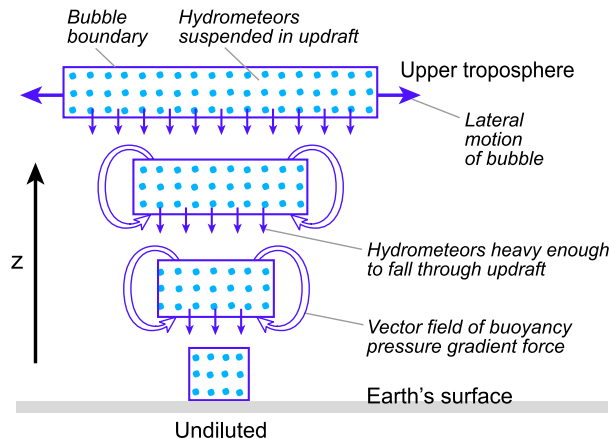


FIG. 17-31. Conceptual model of a buoyant updraft element. Dots indicate hydrometeors suspended by updraft, downward-pointing arrows indicate particles heavy enough to fall through updraft, and horizontal arrows indicate lateral spreading of bubble. Open arrows represent the vector field of the buoyancy pressure-gradient force. From Yuter and Houze (1995).

15. Dynamical interpretations

The ability to model MCSs fairly accurately should help us to understand MCSs on a theoretical basis. Nevertheless, such basic questions as, “Why do MCSs exist?” or “Why do they have a preferred scale of a few hundred kilometers?” have yet to be fully answered. A reason for this state of poor understanding is that MCSs

do not lend themselves easily to fluid dynamical explanations as do, for example, baroclinic instability waves. At horizontal scales of a few hundred kilometers, MCSs occur near the boundary between two-dimensional balanced flow and three-dimensional turbulent flow (Tulloch and Smith 2006). Theoretically accounting for MCSs in this scale range is especially complicated because MCSs are not simply fluid dynamical entities. Thermodynamics, cloud microphysics, turbulence, and probably radiative transfer complicate theoretical explanations accounting for the existence of MCSs in the atmosphere. For example, the horizontal scale of an MCS is affected strongly by ice-phase cloud microphysics. Because an MCS is composed of the aggregate of convective and stratiform regions of the system, its horizontal area coverage depends in part on the fallout trajectories of ice particles (Fig. 17-30). The maximum horizontal extent reached by an MCS also depends on it having a continual supply of moisture to supply the formation of new convective elements while old ones weaken and become part of the stratiform region of the MCS, and a host of topographic and radiative factors impact the moisture supply.

Despite these obstacles, progress has been made on some aspects of dynamical understanding of MCSs. More or less contemporaneously with GATE, but not as part of the GATE scientific activity, Moncrieff and Miller (1976) had been considering the question of what

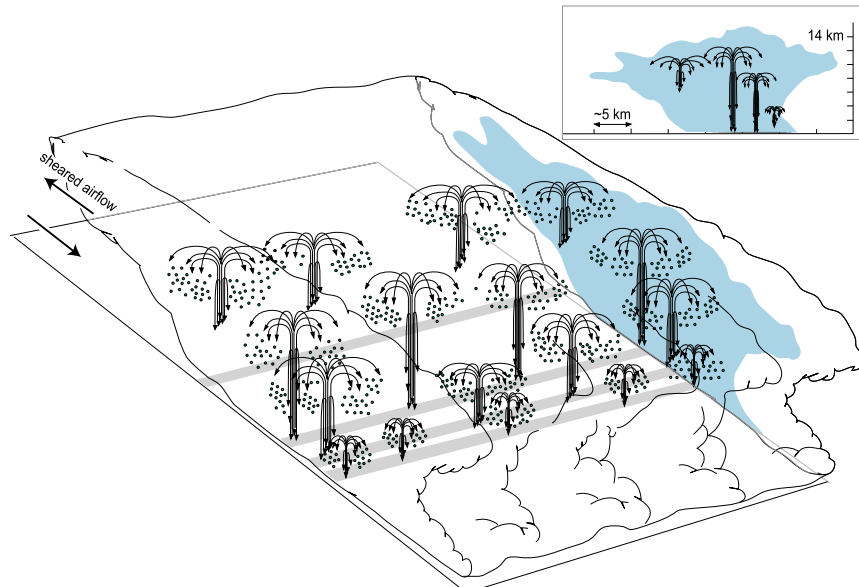


FIG. 17-32. Conceptual model of an ensemble of particle fountains in a multicellular MCS. Shaded area represents radar reflectivity along a cross section normal to the convective region. Cloud boundary is indicated by the scalloped outline. Inset shows approximate scales and arrangement of the largest particle fountains relative to the radar echo. From Yuter and Houze (1995).

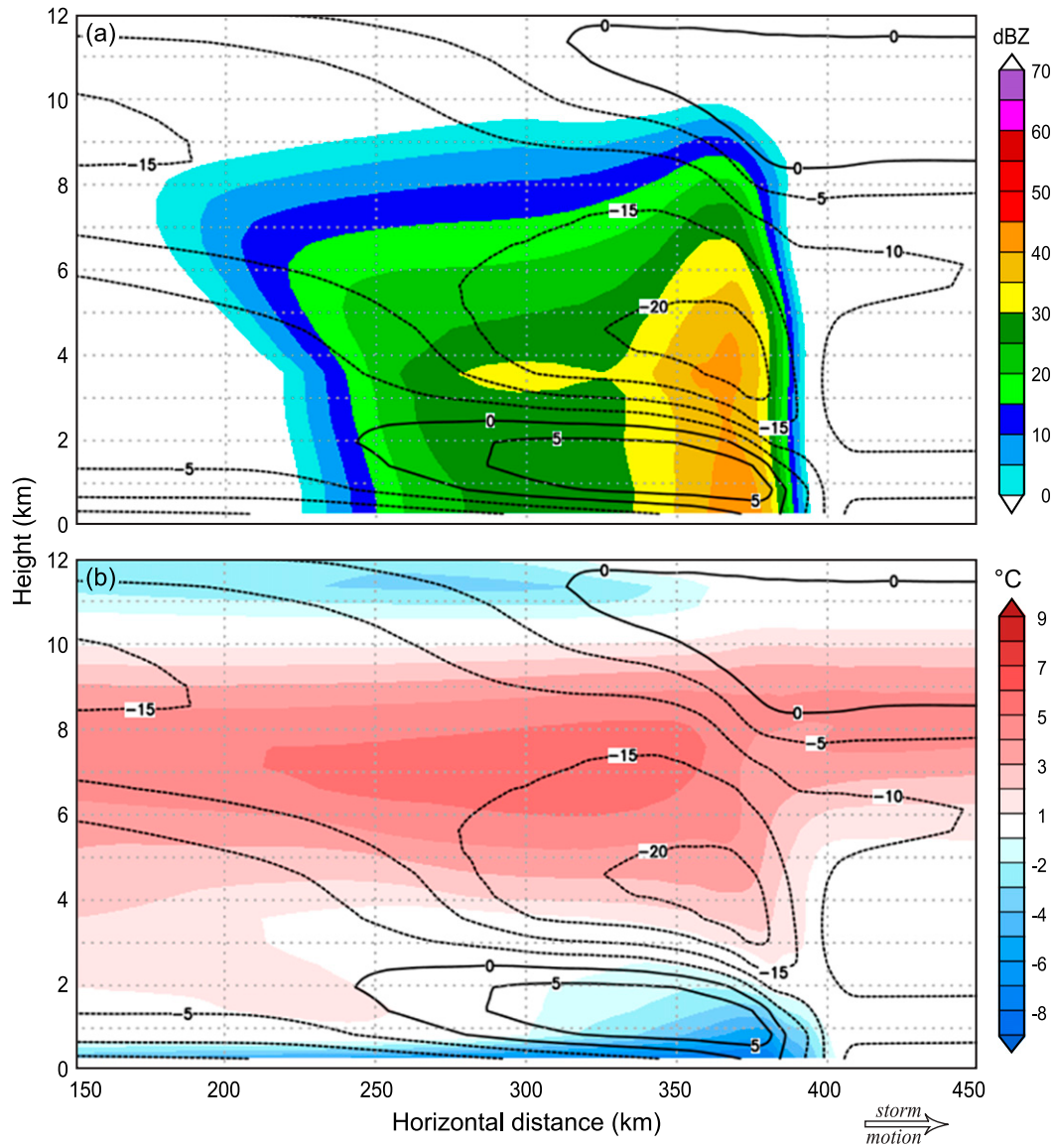


FIG. 17-33. Results of a 3D simulation of a squall-line MCS initiated with a line thermal (with random perturbations) and periodic along-line boundaries. The initial sounding is moderately sheared, and the microphysics scheme is that of Thompson et al. (2008). The domain is 800 km (cross line) \times 80 km (along line) \times 20 km deep. Horizontal resolution is 2 km. The images are averaged over a 3.5-h period (between simulation hours 4.5 and 8), and the x - z images are also averaged along the line. (a) Radar reflectivity (color) and wind component ($m s^{-1}$, negative right to left) in the plane of the cross section relative to the storm. (b) Potential temperature (color) and same relative wind component as in (a). Provided to the author by R. Fovell.

factors determine the mesoscale circulation of an MCS, which they realized needed to be viewed as layered overturning rather than as convection in the form of bubbles of buoyant air rising from the boundary layer. A series of papers by Moncrieff and colleagues [Moncrieff and Miller 1976; Moncrieff 1978, 1981; Thorpe et al. 1982; Crook and Moncrieff 1988; Moncrieff 1992; Moncrieff et al. 2017; see also Cotton and Anthes (1989, 497–505) and Houze (2014, chapter 9)

for synopses of the Moncrieff work] have quantified this view for the case of an idealized steady-state two-dimensional MCS. A key assumption of the theory is that the storm may be characterized by a prescribed decrease in hydrostatic pressure across the updraft at midlevels. If the large-scale environment is sheared as well as unstably stratified, air must flow through the storm along a unique set of streamlines. The geometry of the streamlines is deduced from conservation of

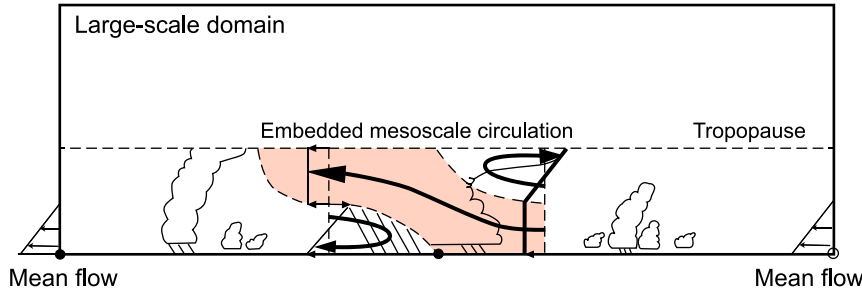


FIG. 17-34. Schematic diagram showing the airflow relative to a 2D, steady-state MCS in a large-scale environment of given wind shear and potentially instability. The streamlines are those required by conservation of mass, momentum, entropy, and vorticity. Adapted from Moncrieff (1992); © Royal Meteorological Society.

entropy, mass, momentum, and vorticity along streamlines. Similar reasoning is employed to determine the streamlines of the downdraft fed by midlevel inflow on the rear side of the storm. For a typical environment of strong low-level shear, the updraft consists of a layer ascending on a slantwise path through the storm (Fig. 17-34). The mathematical basis of the Moncrieff theory is summarized in Houze (2014, chapter 9). Models of MCSs generally confirm the layered overturning model of Moncrieff (Fig. 17-35).

Because the Moncrieff theory is for steady-state conditions and prescribed environmental shear and stability, it provides no explanation for why the layer inflow and ascent initially develops in an MCS. Explanations that have been offered usually involve gravity wave thinking. Such thinking traces all the way back to Hamilton and Archbold's (1945) groundbreaking study (section 2). They posited that the disturbance lines of West Africa were an atmospheric manifestation of a gravity wave. In their words, the "disturbance line" behaved as a traveling disturbance that "shifts the various air particles while they are under its influence, somewhat after the manner of a wave at sea." Regarding factors controlling the movement of the system, they noted, "It is tempting to argue that the disturbance line must be carried along in the prevailing upper wind current, where the bulk of its cloud is." They "very tentatively" compared the motion of the disturbance line to that of a simple gravity wave in a channel of stratified liquid and concluded that the motion of such a wave was not unlike that of the observed disturbance lines. Several decades passed before gravity wave thinking reemerged in relation to MCS dynamics. In the 1970s and 1980s, a flurry of papers were inspired by Charney and Eliassen's (1964) concept of "conditional instability of the second kind" (CISK) to describe an hypothesized cooperative interaction in which friction-layer convergence drives deep convection and associated heating to strengthen and/or

perpetuate a warm core cyclone. Applying this idea to gravity waves, Lindzen (1974) dubbed the interaction of wave dynamics and convective clouds "Wave-CISK" on the basis that the convergence and upward motion in the circulation of an inviscid mesoscale or larger-scale wave (rather than frictional convergence) can maintain a deep convective heat source, which in turn strengthens or maintains the wave. Raymond (1984) applied Wave-CISK to try to study the scale of wave response to an imposed heating profile. The resulting dispersion relation did not definitively determine a wave response that would correspond to MCSs because the results are sensitive to the details of the parameterization of the heating. However, the calculations show that under environment wind and thermodynamic stratification characteristic of squall lines, a dominant growing mode appears that has the layer-lifting structure seen in real squall-line MCSs (Fig. 17-36).

Schmidt and Cotton (1990) and Pandya and Durran (1996) took another analytic approach based on gravity wave thinking to explain the layer overturning in an MCS. These studies ran nonlinear high-resolution models to simulate the realistic detailed behavior of an MCS consisting of a squall line and trailing-stratiform region. Pandya and Durran (1996) averaged the diabatic heating field in the region of the simulated convective line over a 2-h period (Fig. 17-37a). Then they input the averaged heating field into the model and let an initially undisturbed field respond. The result yielded the horizontal wind field shown in Fig. 17-37b. They noted that this field is consistent with Moncrieff's steady-state model, and they showed theoretically that the layered overturning in Fig. 17-37b is a gravity wave response to the mean heating in the convective line. This result indicates that the deep-layer inflow occurs after the convective cells have "organized," that is, clustered into one mesoscale group that constitutes a quasi-steady heat source. Layers of inflow are then drawn up and down

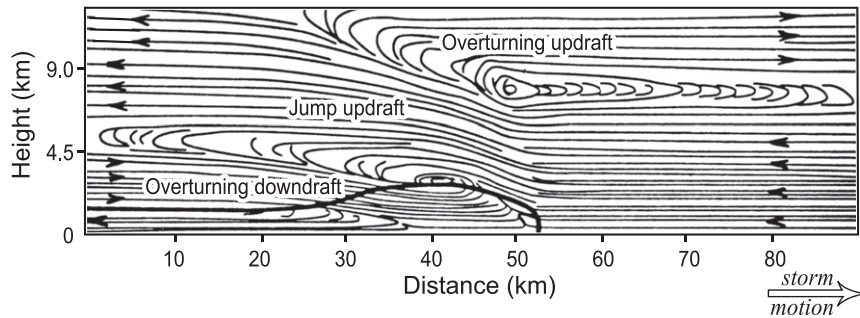


FIG. 17-35. Time averaged numerical model simulation of a squall line with trailing-stratiform precipitation. (a) Simulated radar reflectivity (in intervals of 5 dBZ). (b) Streamlines of system-relative airflow. (c) Equivalent potential temperature (intervals of 3 K). Bold solid contour outlines cold pool (region of negative potential temperature perturbation). Adapted from [Fovell and Ogura \(1988\)](#).

through the system as a gravity wave response to the heating, as in Fig. 17-34. Thus, it is seen that the meso-scale circulation is not the sum of convective elements but rather develops over time as a broader circulation induced by the aggregated heating in the region of grouped convection.

16. Relationship of MCSs to synoptic-scale and larger circulations

a. MCSs in equatorial waves and the MJO

In the years just preceding GATE, visible and infrared satellite imagery were showing that high clouds atop deep convection in the tropics bore a systematic relationship to synoptic-scale easterly waves in the tropics, over both the Atlantic and Pacific ([Frank 1970; Chang](#)

[1970; Chang et al. 1970; Reed and Recker 1971](#)). GATE showed the relationship of MCSs (“cloud clusters” in the terminology of that time) in relation to tropical easterly waves of African origin ([Payne and McGarry 1977](#)). Studies of satellite imagery of tropical convection continued into the 1980s. [Nakazawa \(1988\)](#) found that deep convective clouds seen in satellite imagery over the tropical western Pacific moved with propagating motion systems on multiple scales in a kind of interference pattern. These early satellite studies did not, however, by themselves isolate the specific importance of MCSs in the relationship of convection to the larger-scale envelopes of waves in other tropical disturbances.

In the tropics, the upward air motion and associated heating processes in synoptic- and larger-scale waves are highly concentrated within MCSs and other convective

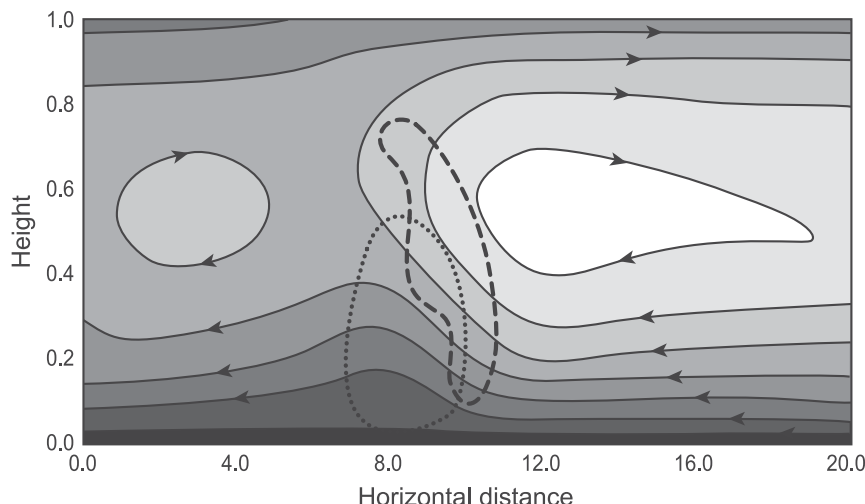


FIG. 17-36. Streamlines for an MCS simulated by making a Wave-CISK assumption to represent the latent heating. The dashed and dotted contours outline regions of updraft and downdraft, respectively. From [Raymond \(1984\)](#).

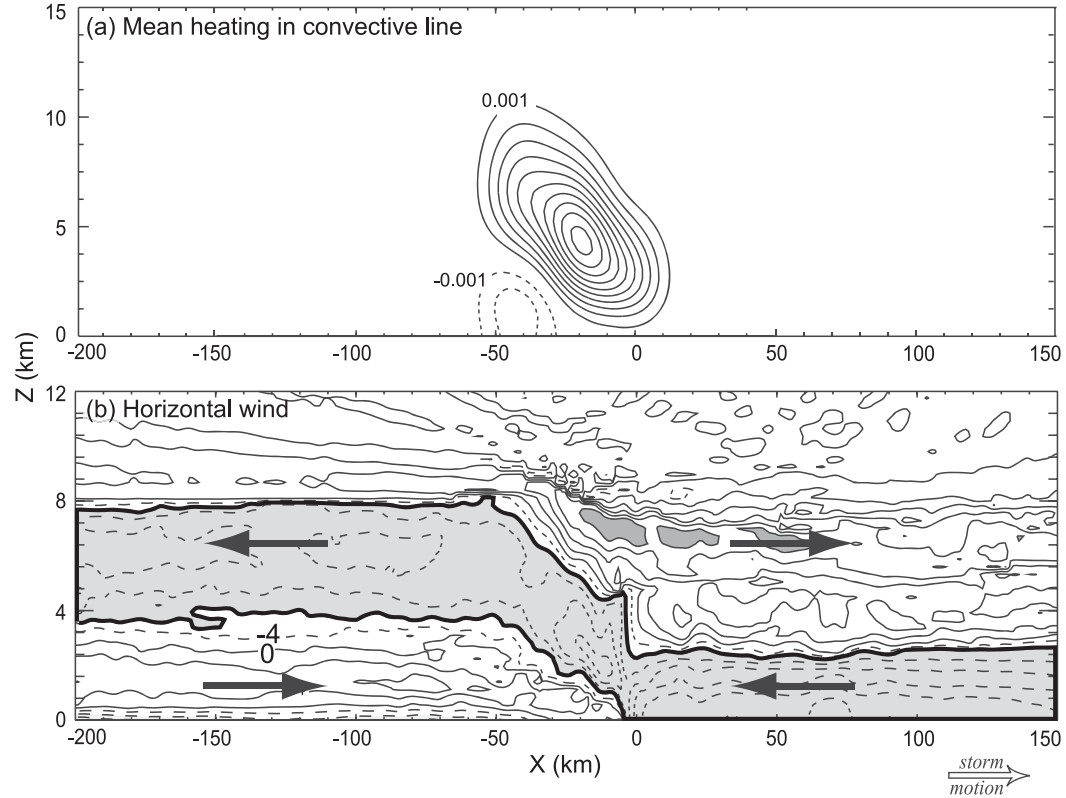


FIG. 17-37. 2D model simulation results for a leading-line/trailing-stratiform squall-line MCS. (a) Time-mean thermal forcing due to the leading convective line alone. Contour interval is 0.001 K s^{-1} . (b) Horizontal velocity at time = 6 h generated by the thermal forcing in (a). Horizontal velocity contours are at intervals of 4 m s^{-1} . Arrows indicate direction of the horizontal flow. Cold pool forward boundary is at $X = 0$. Bold contour and shading emphasize layer inflow constituting the layer ascent of air originating ahead of the storm and rising through it. Adapted from Pandya and Durran (1996).

clouds. After the GATE and MONEX campaigns in the tropics, it was becoming apparent that the heating processes occurring in MCSs are top-heavy as a result of cooling by melting and evaporation at lower levels (section 12), and that this top-heavy heating was significantly influencing the feedback of MCSs to the larger-scale circulation (Houze 1982, 1989; Hartmann et al. 1984; Schumacher et al. 2004). Within an equatorial wave or other large-scale circulation feature numerous convective cloud entities occur. The vertical profile of net vertical air motion (and hence heating) in a sector of a near-equatorial large-scale wave thus depends on the mix of clouds of different types and sizes in that sector. For this reason, Mapes et al. (2006) pointed out that a tropical large-scale wave (synoptic and larger) must have a varying population of convective clouds (“building blocks”) to account for the net upward air motion in any wave sector. They hypothesized that the population varies across a wave as indicated in Fig. 17-38. Figure 17-38a shows building blocks that are mostly shallow convection. That population is followed in

Fig. 17-38b by an ensemble of building blocks of different sizes and depths, with some of the blocks being MCSs with large stratiform components. A third population in Fig. 17-38c is dominated by a large proportion of MCSs. Observations in DYNAMO were consistent with this building-block idea as synoptic-scale waves repeatedly passed over the observational network during the four months of the campaign. Figure 17-39a (from Zuluaga and Houze 2013) composites reanalysis data temporally centered on the maximum precipitation of a DYNAMO wave event. The large-scale convergence was initially concentrated in low levels, extended through a deep layer near and just after the time of maximum rainfall, and was finally concentrated aloft with divergence in lower levels. Figure 17-39b shows that the precipitating cloud population (determined by radar) exhibited a behavior consistent with the building-block hypothesis. Four categories of radar echoes were compiled statistically relative to the wave. In the early stages of the wave passage, shallow isolated convective cells reached their maximum occurrence. As time went

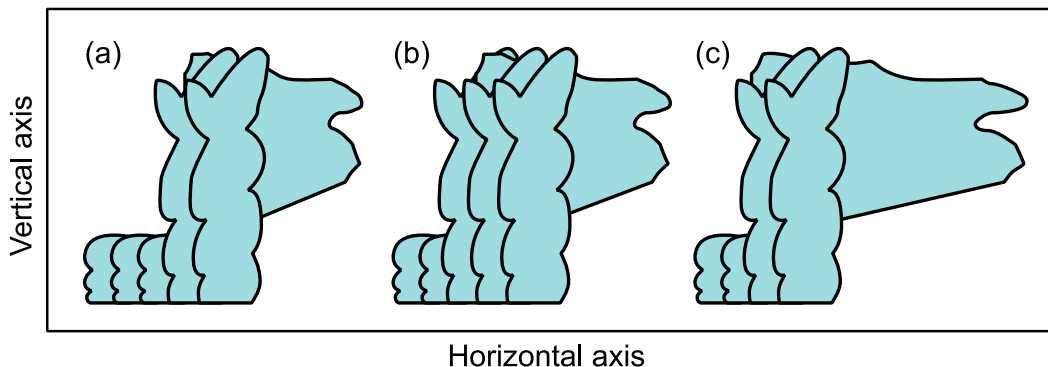


FIG. 17-38. Depiction of three of cloud populations, made up of (a) shallow convection, (b) deep convection, and (c) stratiform elements. In (a) the fraction of shallow convection is highest in the left-hand population. In (b) the fraction of deep convective elements is highest. In (c) the fraction of stratiform elements is greatest. Adapted from Mapes et al. (2006).

on and the convective population changed, the maximum frequency of deep but relatively isolated convective cells occurred. Just before the peak rainfall, the convective elements that were both deep and wide achieved maximum frequency of occurrence, indicating that the convection elements were systematically increasing in scale to mesoscale proportions. These elements were indicating the presence of developing MCSs. Finally, in the later time period, echoes with broad stratiform precipitation areas dominated, indicative of a large presence of mature MCSs. The cloud population was thus in sync with the large-scale vertical motion in Fig. 17-39a. The shallow cloud population in the early stages corresponding to the convergence and upward motions was concentrated in the low troposphere. The population in middle stages was dominated by deep and wide convective elements of growing MCSs, when the upward motion extended through a deep layer. The late stages had a predominance of broad stratiform echo consistent with the wave's upward motion aloft and downward motion in the lower troposphere.

Thus, the vertical motion in the composite synoptic-scale wave, like that in a gravity wave (Fig. 17-36), is similar to the layer lifting in an individual MCS but on a larger scale. Such similarity also occurs on scales larger than gravity waves and synoptic-scale waves, namely the MJO (Moncrieff 2004; Moncrieff et al. 2017). Figure 17-40 shows layered overturning in the MJO, qualitatively similar to an MCS but on a scale of thousands of kilometers. The vertical motions of the MJO are again related to the populations of convective clouds in the different sectors of the large-scale disturbance. Barnes and Houze (2013) used a statistical analysis of TRMM Precipitation Radar (PR) data to show how the precipitating cloud population changes with the stage of the MJO. Figure 17-41 compares the frequencies of

occurrence of two types of radar echoes seen by the TRMM PR over the central Indian Ocean. An isolated shallow echo is an echo covering no more than $2 \text{ km} \times 5 \text{ km}$ pixels and having tops at least 1 km below the 0°C level and may be thought of as showers of "warm rain." A broad stratiform region is a contiguous stratiform echo covering $>30000 \text{ km}^2$. From Fig. 17-41, it can be seen that the active phase of the MJO has maximum frequency of precipitation from the broad stratiform regions of MCSs and the lowest frequency of shallow isolated precipitating convective clouds. Using the TRMM latent heating product, Barnes and Houze (2016) determined the latent heating profiles associated with different categories of radar echoes as a function of MJO phase. Barnes et al. (2015) found that the top-heavy heating profile associated with the stratiform regions of MCSs was by far the most pronounced during the active phase of the MJO (Fig. 17-42). Virts and Houze (2015) showed that during the MJO active periods lightning decreases as MCSs increasingly dominate the cloud population.

b. MCSs in relation to midlatitude baroclinic waves and low-level jets

Since the 1980s, tropical studies of MCSs in relation to the larger-scale circulation were proceeding largely in parallel with similar studies of midlatitude MCSs. Studying continental convection over the central United States, Maddox (1983) published a landmark observational paper showing that MCCs occurred systematically ahead of synoptic-scale baroclinic troughs in the westertlies (Fig. 17-43). Yang et al. (2017) have confirmed this behavior in a modeling study verified by satellite and radar data. They showed that MCSs in free-running cloud-resolving simulations over two warm seasons systematically formed ahead of large-scale troughs in the

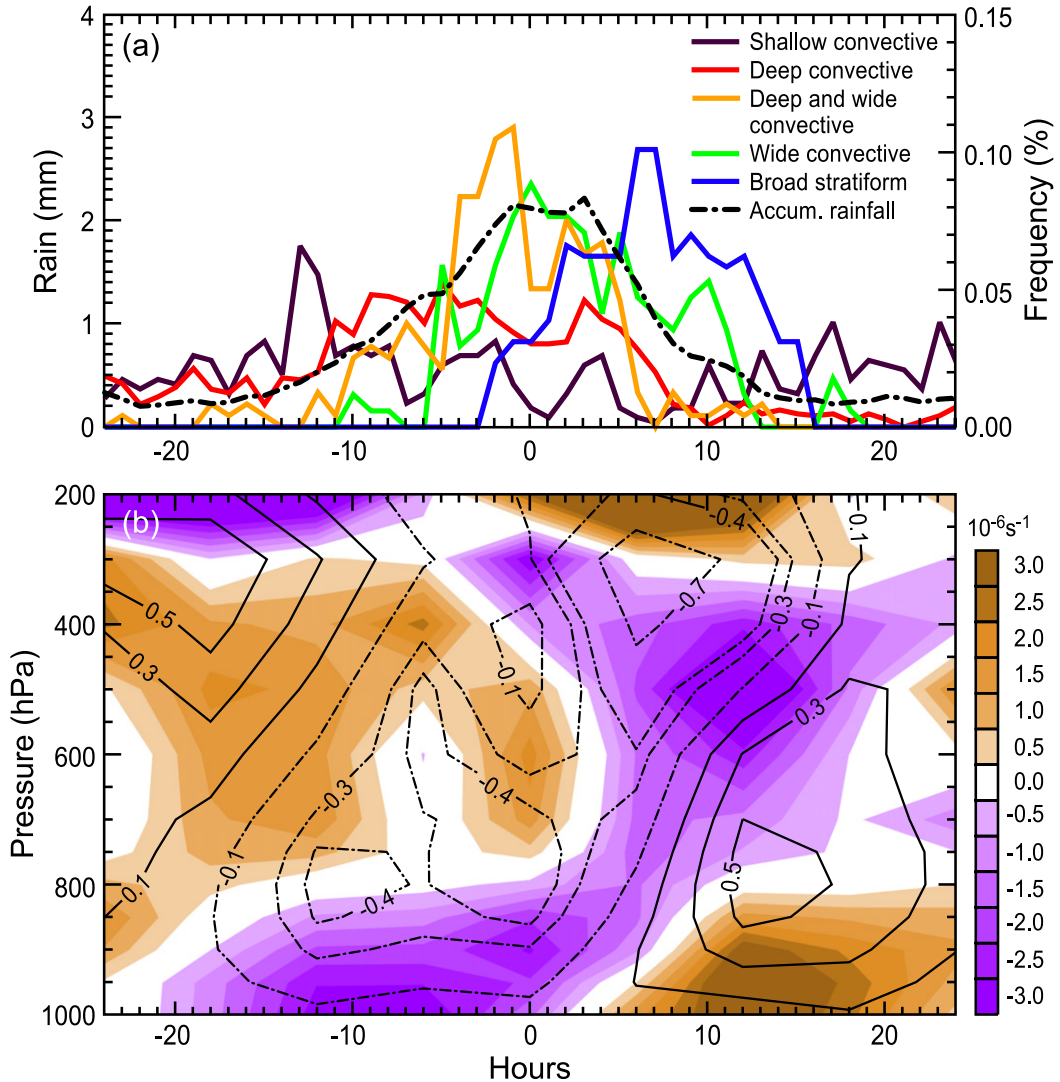


FIG. 17-39. (a) Composite time–height sections of divergence (shading, 10^{-6} s^{-1}) and anomalies of vertical velocity (contours, $10^{-3} \text{ hPa s}^{-1}$; solid lines indicate positive values) calculated from reanalysis data composed around the time of maximum in rain accumulation seen by the National Center for Atmospheric Research S-Pol Ka radar located on Addu Atoll on the equator in the central Indian Ocean during DYNAMO. (b) Composite of the frequency of occurrence of different types (color coded) of radar echo structure before (negative time) and after (positive time). The right y axis is for the colored-coded frequency curves. The rainfall accumulation amounts shown on the left y axis is the composite computed by centering each of the 11 rain episodes of DYNAMO on the time of the maximum of its running-mean curve. From [Zuluaga and Houze \(2013\)](#).

westerlies (Fig. 17-44). Trier and Parsons (1993) noted how a trough moving over the Rocky Mountains and into the Great Plains area strengthens the climatological southerly low-level jet that feeds moisture into MCSs forming over the central United States (Fig. 17-45). A similar behavior occurs in South America, where the South American low-level jet (SALLJ) flows southward along the eastern edge of the Andes from the moist Amazon region to feed MCSs in the region centered on Argentina (Nogués-Paegle and Mo 1997; Douglas et al.

1998; Saulo et al. 2000; Marengo et al. 2004; Vera et al. 2006; Salio et al. 2007; Rasmussen and Houze 2016). As shown by Bonner (1968), these low-level jets are stronger at night, which gives nocturnal preference for MCSs over the central United States (as noted by Huckleberry Finn, see introduction). Dai et al. (1999) showed how the diurnal and semidiurnal processes favor large-scale convergence over the Rockies during the day and over the plains to the east at night. These processes assure that the enhanced jet associated with an approaching trough has its

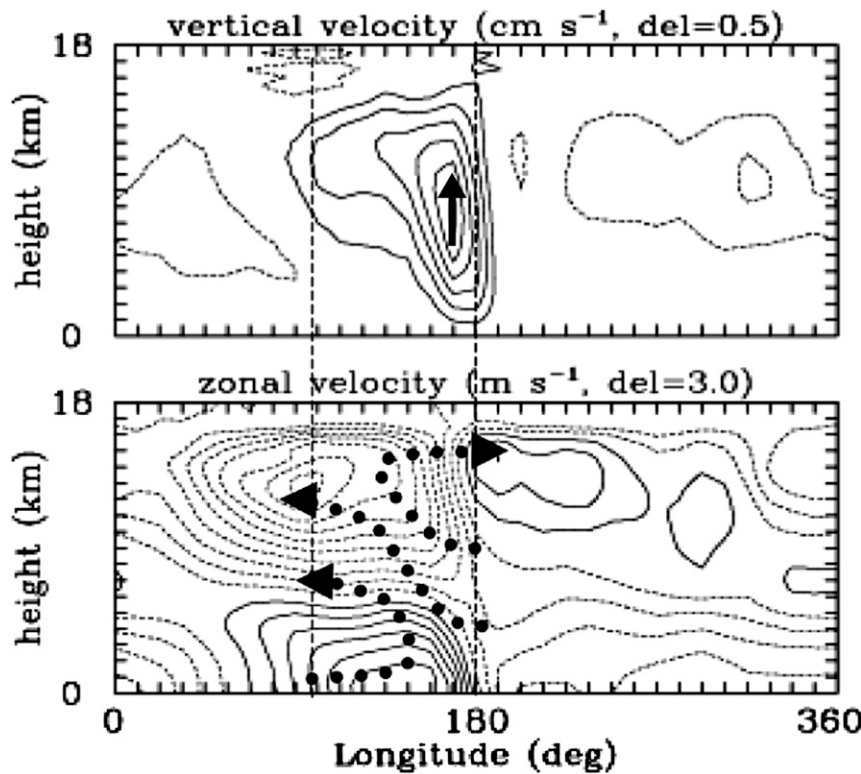


FIG. 17-40. Vertical structure of the MJO system. Primary airflow branches are sketched. All quantities are 20-day averages and relative to the traveling system. From Moncrieff (2004).

maximum effect on MCSs at night in the central United States. Data from the U.S. radar network show that MCSs developing from diurnally triggered convection over the Rockies and propagating eastward maximize at night over the central United States (Carbone et al. 2002), in conjunction with the nocturnal maximum of the low-level jet in that region. Feng et al. (2016) found that an increase in MCS activity over the central United States has been accompanied by strengthening of the low-level jet and its moisture transport over the past 30–40 years.

In an early modeling study, Stensrud (1996) found that the persistent occurrence of parameterized deep convection feeds back in a way that strengthens the parent trough. The modeling study of Yang et al. (2017) suggests that the mechanism by which the longer-lived MCSs strengthen the trough is the top-heavy heating profile resulting from the large stratiform regions of long-lived MCSs (section 12).

17. Global distribution of mesoscale convection: Variability and impacts on the global circulation

At the time of GATE, in the mid-1970s, satellite meteorology was still in its infancy. For the next 2–3

decades, satellite studies relative to MCSs (e.g., Laing and Fritsch 1997) were limited to two-dimensional visible and infrared imagery. Fritsch et al. (1986) used these images to show that MCCs, as identified by Maddox (1980, see section 5) account for about 50% of warm season rainfall over the central United States. The first use of passive microwave sensors on satellites in the 1980s added the ability to detect precipitation from space (Wilheit 1986). By combining infrared brightness and passive microwave data from different satellites, Yuan and Houze (2010) used infrared and passive microwave imagery to define and identify a mature MCS by multisensor satellite analysis. They used the fact that an MCS has both a large cold cloud shield (minimum brightness temperature <220) and a large rain area ($>2000 \text{ km}^2$ in passive microwave rain detection), with the additional criterion that the large cold cloud shield contain some intense rain, also identified by passive microwave data. MCSs so defined accounted for 56% of tropical rainfall over the years of the Yuan and Houze study. This objective method is consistent with others, who have, on the one hand, used large cold cloud shields to distinguish MCSs (e.g., Maddox 1980) or, on the other hand, considered an MCS to be a cumulonimbus system that has become large enough to support a contiguous

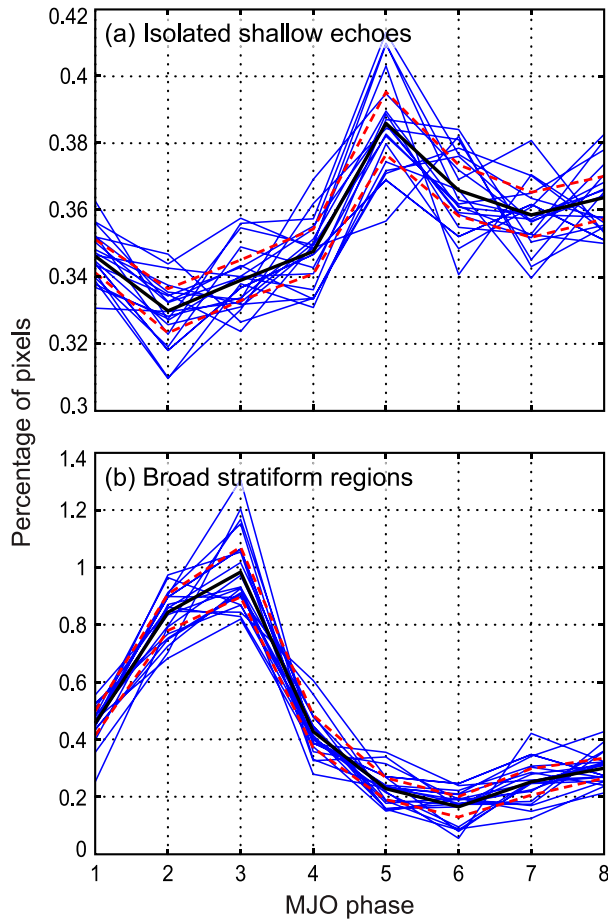


FIG. 17-41. Frequency of occurrence of different types of radar echoes seen by the TRMM PR over the central Indian Ocean: Total frequency of (a) isolated shallow echoes and (b) broad stratiform regions. The frequency is defined as the number of TRMM PR pixels in the central Indian Ocean that contain an isolated shallow echo normalized by the total number of TRMM PR pixels detected in the central Indian Ocean, which include both echo-covered and echo-free pixels. The frequency is reported as a percent. The blue lines show the frequency-phase series for the 20 realizations, the black line is the mean of the realizations, and the dashed red lines are 99% confidence intervals of the mean and are calculated using the Student's *t* statistic. In the central Indian Ocean the indices for the active and suppressed phases of the MJO are 3 and 6, respectively. From Barnes and Houze (2013).

rain area of mesoscale dimension (e.g., Mohr and Zipser 1996; Nesbitt et al. 2000). Using this objective method, Yuan and Houze (2010) were able to show the variability of MCS occurrence across the tropics (Fig. 17-46). The patterns of frequency of occurrence of MCSs differ from land to ocean and by size of MCS. In general, the largest ones occur over oceans and smaller ones concentrate over land.

In late 1997, the launch of the TRMM satellite provided the first Precipitation Radar (the Ku-band TRMM PR) in space. In 2006, the launch of *CloudSat* provided

the first satellite-borne cloud radar (W band). With these radars in orbit, it became possible to observe the three-dimensional structures of cloud systems around the entire globe. Yuan et al. (2011) used the *CloudSat* radar data to analyze the internal microphysical characteristics of the large anvil clouds of MCSs. However, *CloudSat*'s radar is highly attenuated in precipitation, and for determining MCS characteristics it is crucial to observe the three-dimensional structure of radar echoes to distinguish convective and stratiform portions of MCSs. TRMM PR with its Ku-band radar has been the basis of determining the internal structures of precipitating convective systems from space. Although Ku band suffers from attenuation, effective methods for correcting the attenuation have been applied to the TRMM PR data, and they have been a most effective way to characterize convective precipitation systems in low latitudes. Figure 17-47 is an example of the TRMM PR data in an MCS located over the tropical west Pacific. In this example, the echo between ~ 70 and 200 km on the horizontal axis has a bright band and is clearly stratiform, while the deep vertical column of echo centered at ~ 210 km is obviously convective. The National Aeronautics and Space Administration (NASA) and Japan Aerospace Exploration Agency (JAXA) routinely apply an algorithm that uses the three-dimensional echo structure to classify all of the TRMM PR echoes as convective, stratiform, or other (Awaka et al. 1997). The “other” category is only a tiny fraction of all the echoes seen by TRMM (Schumacher and Houze 2003; Funk et al. 2013).

Using only the TRMM radar echoes identified as convective, Liu and Zipser (2013) analyzed the frequency of occurrence of convective features that were mesoscale in horizontal dimension (contiguous convective echo covering $>1000\text{ km}^2$). Such echoes are almost certainly indicating the existence of MCSs. Figure 17-48a shows the frequency of such echoes that were roughly circular in shape, while Fig. 17-48b shows where the elongated (“linear”) mesoscale convective echoes occur. This mapping led to several important conclusions that show how MCS characteristics vary regionally. Figures 17-48a and 17-48b both show that mesoscale convective echoes tend to be larger over land. However, using radar data from the GPM satellite, Liu and Zipser (2015) have shown that the precipitation areas are overall bigger over oceans (Fig. 17-49). Combined with Liu and Zipser’s (2013) finding that the convective echo features are smaller over ocean, we may therefore infer that the stratiform regions of MCSs are larger over the tropical oceans than over tropical landmasses. Liu and Zipser (2013) also reported that the mesoscale convection is less deep over the oceans, especially in

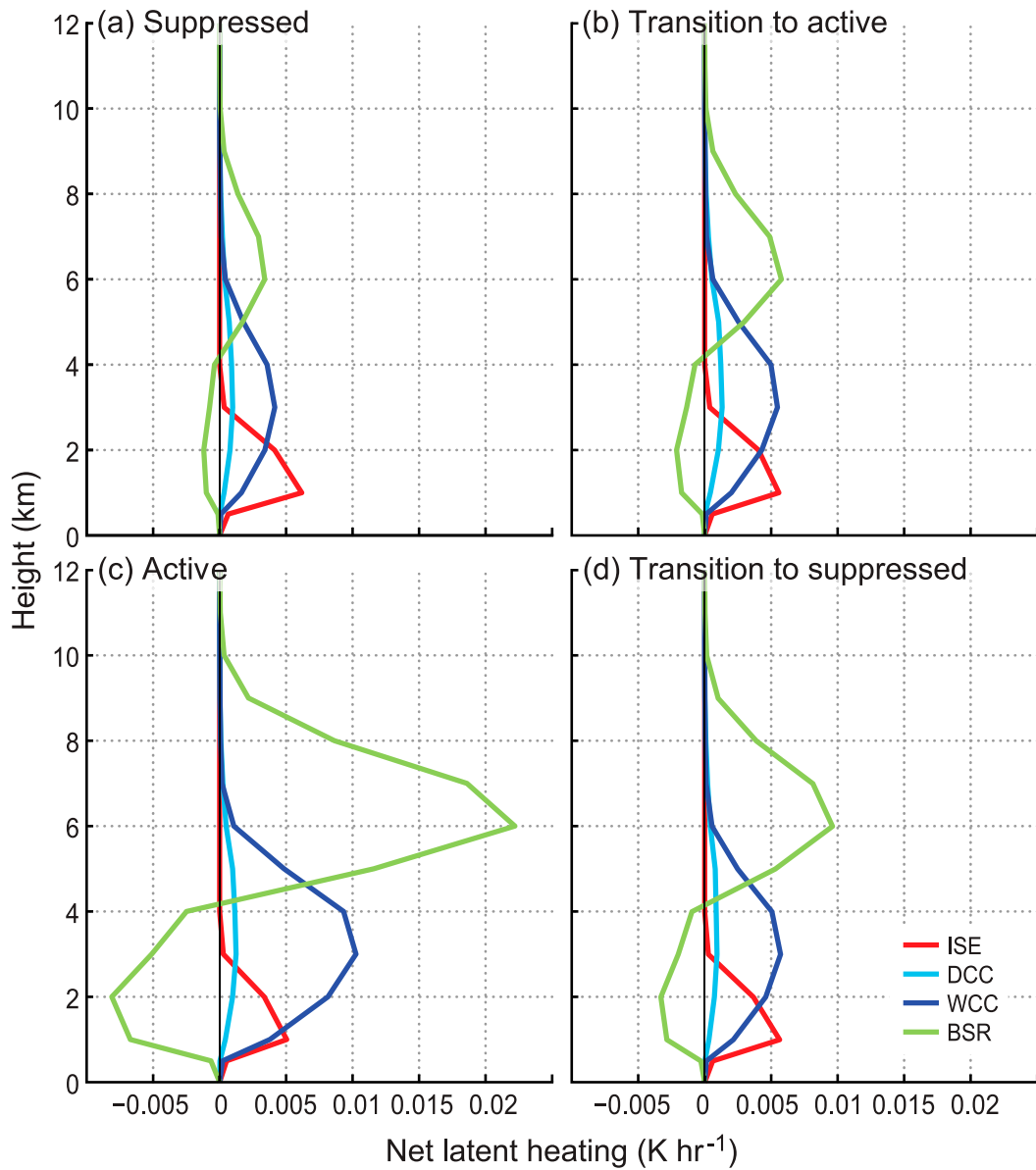


FIG. 17-42. Net heating from isolated shallow convective elements (red), deep convective cores (cyan), wide convective cores (dark blue), and broad stratiform regions (green) as seen by the TRMM radar during different stages of the MJO over the central Indian Ocean. Net heating is normalized by the total number of pixels sensed by the TRMM PR. From Barnes et al. (2015).

the intertropical convergence zone of the east Pacific, and as indicated in Fig. 17-48b oceanic regions at low latitudes have a higher fraction of linear mesoscale convective entities than over land. Their results also show orientations of linear systems being controlled by factors such as warm ocean currents and fronts.

Making further use of the three-dimensional radar echo fields provided by the TRMM PR, Houze et al. (2015) defined four categories of radar echoes: isolated shallow echo (ISE) is the same type of isolated warm-rain

shower echo as that analyzed by Barnes and Houze (2013) in Fig. 17-41, the deep convective core (DCC) is a three-dimensional echo object consisting entirely of echo >40 dBZ extending to >10 km in maximum height, a wide convective core (WCC) is a three-dimensional echo object consisting entirely of echo >40 dBZ and covering 1000 km² in horizontal dimension, and a broad stratiform region (BSR) is a contiguous stratiform echo covering >50 000 km². While these characteristics do not alone define an MCS, an MCS

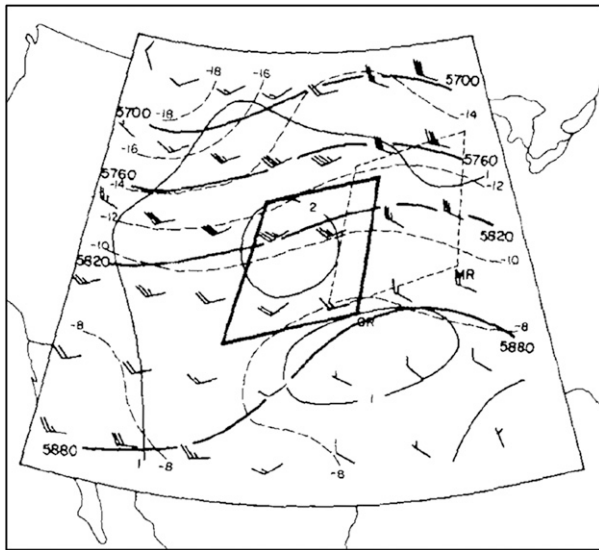


FIG. 17-43. Analysis of the 500-hPa level prior to MCC development. Heights (m) are heavy solid contours, isotherms ($^{\circ}\text{C}$) are dashed, and mixing ratio (g kg^{-1}) is indicated by light solid contours. Winds (full barb = 5 m s^{-1}) are plotted at every other grid point and the dark arrow shows the axis of maximum winds. The crosshatched region indicates terrain elevations above the 500-hPa level. From [Maddox \(1983\)](#).

would normally contain a WCC. Indeed from results such as [Pandya and Durran \(1996\)](#), it is essential that intense convection must be grouped together to induce a mesoscale circulation of the type that characterizes an MCS (see [section 15](#)). Thus, a WCC is a proxy for a developing MCS. A BSR, on the other hand, would be found in an especially robust MCS and is a proxy for a mature MCS. Therefore, mapping the frequency of occurrence of WCCs and BSRs around the globe informs us as to the variability in location and occurrence of MCSs that appear to be in developing and mature stages. The definition of the DCC does not have an areal coverage requirement and thus does not necessarily indicate the presence of an MCS although such deep convection often precedes MCS development. The thresholds of 10 km , 1000 km^2 , and 50000 km^2 given in the definitions above are extreme and are referred to as “strong” thresholds. The same echo-object categories can be redefined with thresholds relaxed to “moderate” values of 8 km , 800 km^2 , and 30000 km^2 , respectively. The strong thresholds tend to give better depictions over land, while the moderate thresholds better characterize oceanic convection. However, [Houze et al. \(2015\)](#) applied both thresholds over the entire band of TRMM PR observations in low latitudes.

[Figure 17-50](#) contains analyses of the frequency of occurrence of the four categories defined by [Houze et al. \(2015\)](#) for the austral summer season. The warm oceans

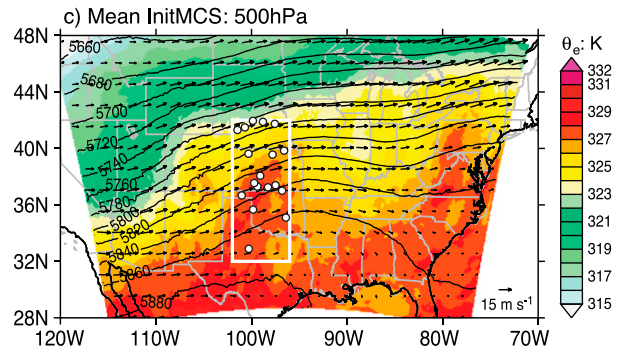


FIG. 17-44. Results of a cloud-resolving model run for two warm seasons. The fields are composites of the mean geopotential height (m, contour lines), wind (vector), and equivalent potential temperature (K, color filled) at 500 hPa at 0–3 h before MCS initiation. The dots indicate the locations of MCS initiation. The box is the region in which MCS initiation was sought. From [Yang et al. \(2017\)](#).

host dense populations of shallow isolated cumulonimbi ([Fig. 17-50a](#)). The most frequent occurrence of ISEs is in trade wind zones, where deeper convection is suppressed. However, it is also apparent from comparing [Figs. 17-50a and 17-50d](#) that ISEs are populous in zones where WCCs occur, that is, where MCSs are most likely developing. It is thus possible that the self-aggregation process ([Wing and Emanuel 2014; Emanuel et al. 2014](#)) is operating to produce MCSs in these tropical oceanic regions. However, the land areas at low latitudes have almost no ISEs. So if the self-aggregation process operates over the land areas it must initiate with non-raining clouds or deeper precipitating convective elements. Comparison of [Figs. 17-50a and 17-50b](#) shows that the strong deep convective cores, where 40 dBZ echo extends above 10 km , occur almost exclusively over land, consistent with the findings of [Zipser et al. \(2006\)](#) and [Liu and Zipser \(2015\)](#), who have pointed out that these deepest and most intense cells do not correspond to where rainfall is maximum. For example, the DCCs defined by the 40 dBZ strong threshold do not occur over the Amazon region, which is where the South American rainfall is greatest, while they occur with high frequency over the relatively arid region of Argentina. However, if the thresholds for intensity and maximum height are relaxed to 30 dBZ and 8 km , respectively, DCCs are seen over the ocean and Amazon ([Fig. 17-50c](#)). In addition, wide convective cores, which are the convective areas of MCSs, generally occur at the locations of the moderate-threshold DCCs (cf. [Figs. 17-50c and 17-50d](#)). Thus, we see that MCSs do not require the presence of the very deepest and most intense convection. MCSs form prolifically in the regions of moderately intense convective cores. Note: [Fig. 17-50d](#) shows the

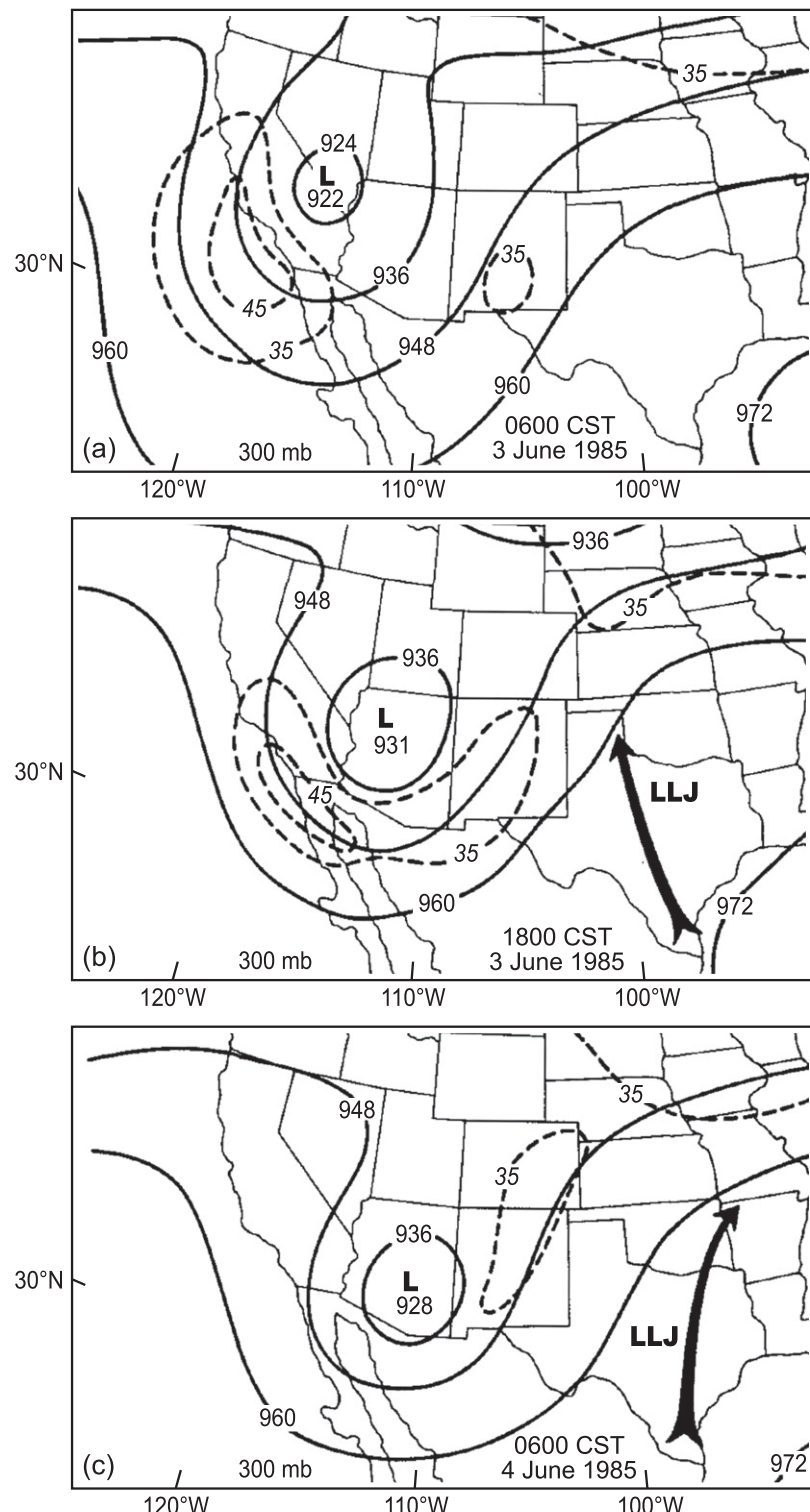


FIG. 17-45. Sequence of 300-hPa analyses with geopotential height contours (solid) analyzed in 12-dam intervals with the 35 and 45 m s⁻¹ isotachs (dashed) at (a) 0600 central standard time (CST) 3 Jun, (b) 1800 CST 3 Jun, and (c) 0600 CST 4 Jun 1985. The bold arrow schematically illustrates the approximate streamline of the low-level jet in (b) and (c). From [Trier and Parsons \(1993\)](#).

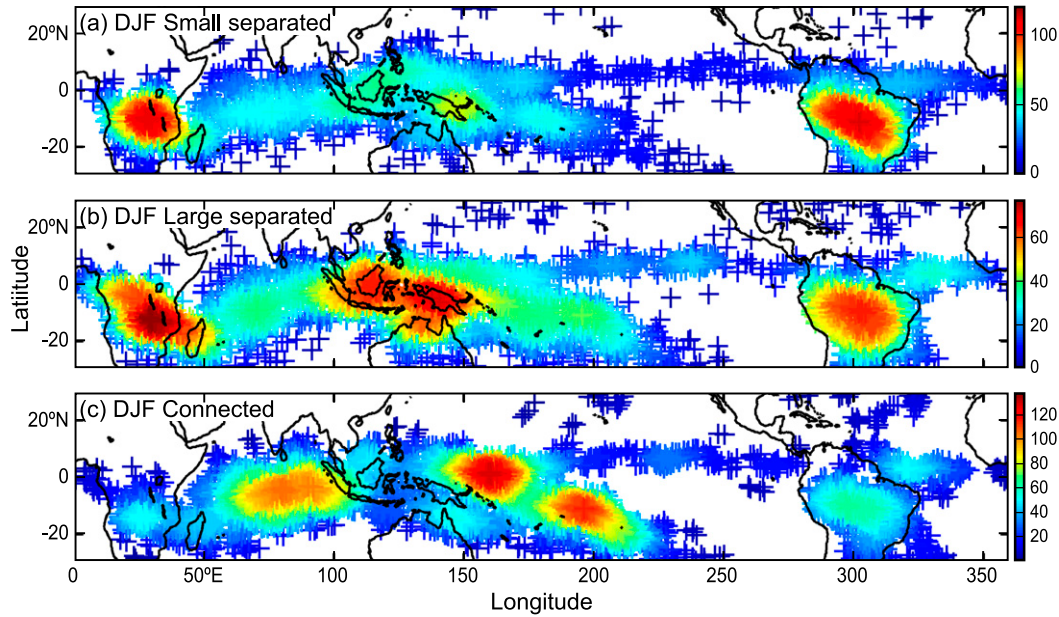


FIG. 17-46. Frequency of occurrence of (a) “small separated,” (b) “large separated,” and (c) “connected” tropical MCSs during the months December, January, and February, as shown by satellite infrared and passive microwave sensors on the NASA *Aqua* satellite. Small and large MCSs have anvil plus raining area $<10^4 \text{ km}^2$ and $>2.25 \times 10^4 \text{ km}^2$, respectively. Connected MCSs have separate infrared cloudtop signatures but share a rain area. From [Yuan and Houze \(2010\)](#).

pattern for moderate threshold WCCs; the pattern for strong threshold WCCs (not shown) is similar and the same conclusions apply.

[Houze et al. \(2015\)](#) also mapped the occurrence of broad stratiform echo objects over all of the low latitudes. The BSRs and WCCs are both characteristics of MCSs, and [Houze et al. \(2015\)](#) found that the occurrence of BSRs maximizes in the same locations as WCCs. [Hartmann et al. \(1984\)](#) and [Schumacher et al. \(2004\)](#) have shown that more realistic representations of the mean general circulation of the tropics are obtained when the heating profile is top-heavy in a way that is consistent with the presence of MCS-generated stratiform precipitation. Figure 17-51 shows that the upper-level circulation across the Indo-Pacific Ocean sector is more robust when the precipitation is assumed to be 40% stratiform (Fig. 17-51b) versus 0% stratiform (Fig. 17-51a). This difference is consistent with the increase in potential vorticity in midlevels accompanying the more top-heavy heating profile associated with 40% of the precipitation being stratiform. However, in reality the stratiform contribution to the heating varies regionally. [Schumacher and Houze \(2003\)](#) showed stratiform rain fractions ranging from $\sim 20\%$ to 70% across the tropics. Confirming the inference from [Liu and Zipser \(2013\)](#), [Houze et al. \(2015\)](#) found that the frequency of stratiform precipitation associated with mesoscale convection in the

tropics is greater over the oceans than over continental regions. [Schumacher et al. \(2004\)](#) showed that taking account of east–west variation in the stratiform rain fraction was important in representing El Niño circulation over the tropical Pacific. These findings indicate the importance of taking account of MCS occurrence in accurately representing the global circulation.

18. Representing MCS dynamics in global climate models

Planning of GATE in the early 1970s was motivated by the need for an observational basis for parameterizing convective clouds in global atmospheric models. The prevailing view (e.g., [Yanai et al. 1973](#); [Arakawa and Schubert 1974](#)) was that the gap of scale between convective updraft plumes from the boundary layer and large-scale motions allowed for such parameterization. GATE then showed that the scale separation did not exist and that MCS were important forms of convective clouds ([Houze and Betts 1981](#)). However, computing technology has improved and many numerical weather prediction models now resolve MCSs. But climate projection over tens to hundreds of years is still not feasible at global cloud-resolving resolution, and some way of representing MCSs in global climate models therefore will remain a need for some years to come.

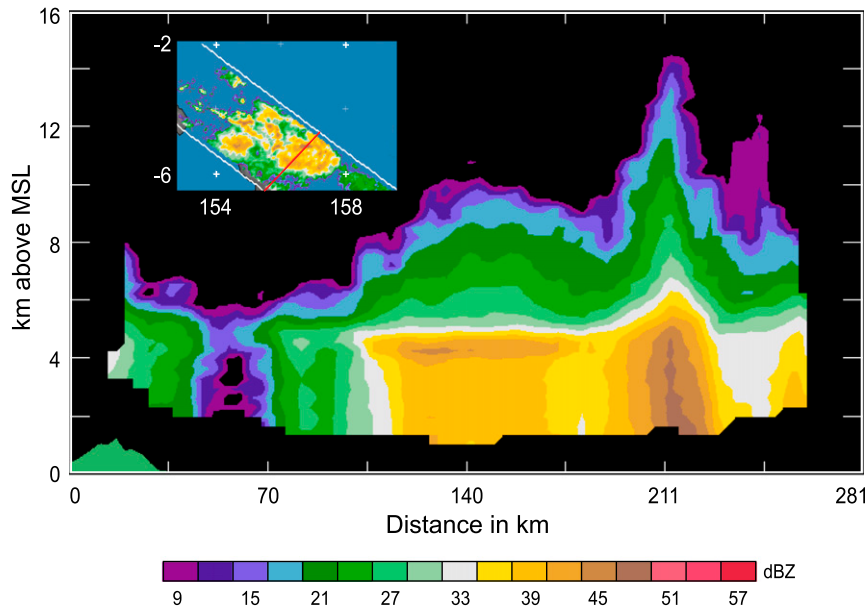


FIG. 17-47. Vertical cross section of radar reflectivity in dBZ seen by the TRMM PR along the red line superimposed on the plan view at 4 shown in the inset. The vertical cross section runs from left to right along the red line. Latitudes -2 to -6 are in the Southern Hemisphere. Longitudes are in the Eastern Hemisphere. From Houze et al. (2015).

The previous section of this review has discussed how patterns of occurrence of MCSs vary over the globe (section 17). We have also seen that large-scale environment dynamics control when and where MCSs form and grow (section 16) and that the MCSs feed back to and influence their parent large-scale circulations (section 12). In climate models running at coarse resolution, the controls and feedbacks between MCSs and the large-scale flow need to be parameterized in a way that is consistent

with the layered overturning flow characterizing MCSs, the potential vorticity generation that occurs in the stratiform regions of longer-lived MCSs, and the ability of MCSs to disconnect from the boundary and occur in elevated form (section 11). Climate models have particular difficulty in representing the diurnal cycle of precipitation in continental regions such as the central United States (Dai 2006; Klein et al. 2006; Van Weverberg et al. 2017), and the inability to include

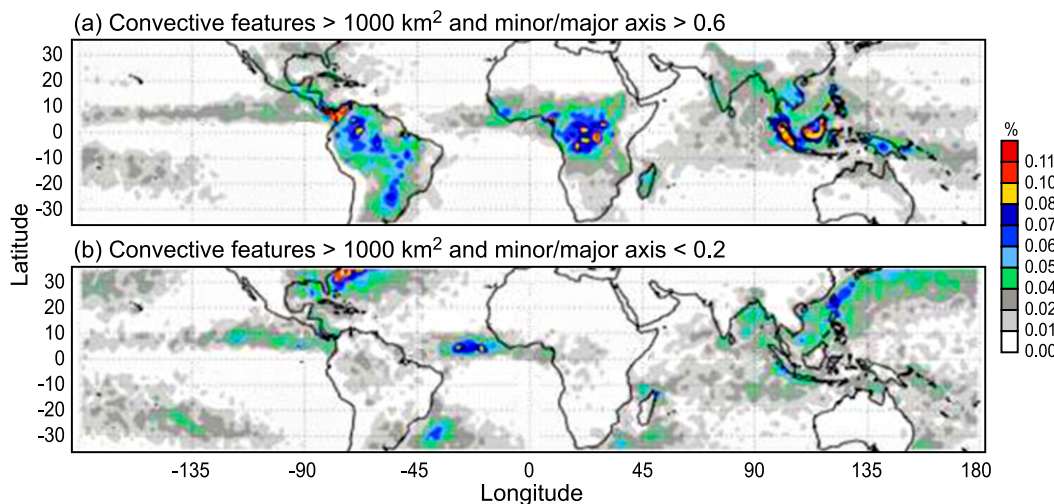


FIG. 17-48. (a) Distribution of the population of large convective echoes (area $> 1000 \text{ km}^2$) and with a near-circular shape (minor/major axis ratio > 0.6). (b) Distribution of the population of large convective lines (convective echoes with minor/major axis ratio < 0.2 and area $> 1000 \text{ km}^2$). From Liu and Zipser (2013).

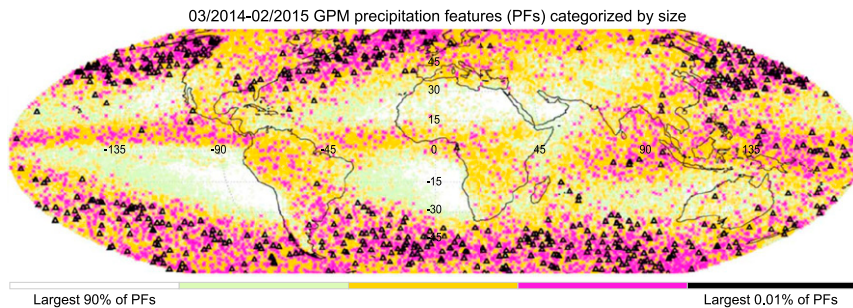


FIG. 17-49. Locations of precipitation features (PFs) seen by the GPM satellite and categorized by size. From [Liu and Zipser \(2015\)](#).

MCSs, especially elevated MCSs ([section 11](#)), and their relationship to diurnally varying low-level jets ([section 16](#)) in coarse-resolution global models is likely to be part of the explanation for this shortcoming.

New approaches are being developed to accommodate MCS characteristics in climate models. One line of work builds on the Mapes et al.'s (2006) building-block concept in which a population of convective clouds consists of three types of cloud: congestus, deep convection, and precipitating stratiform elements ([Fig. 17-38](#)). Khouider et al. (2010) formulated a stochastic model by dividing a coarse grid into a lattice of small-scale sites, each subject to a probability that a congestus, deep, or stratiform element will form. The probabilities for congestus and deep convection are based on convective available potential energy (CAPE)⁵ and dryness is based on large-scale CAPE and midlevel dryness. If midlevels are dry, vertical development is restricted so that congestus can form but deep convection cannot. Once deep convection has formed at a lattice point it may develop over time into stratiform based on specified factors. All the cloud elements have prescribed lifetimes. This approach does not use large-scale shear environmental shear in formulating its probabilities, yet the large-scale shear is important in establishing the layered circulation and associated transport properties of an MCS.

In another approach, Moncrieff et al. (2017) allow a conventional convective parameterization to operate but apply an additional parameterization representing the layered overturning of MCSs. This additional parameterization consists of adding a top-heavy heating profile to the convective heating profile and a corresponding momentum transport profile that is consistent with the momentum transport by the layered flow, as seen in data by Houze et al. (2000) and in cloud-resolving modeling by Mecham et al. (2002, 2006), and inferred from a general

circulation model by Moncrieff and Klinker (1997). The profiles are applied wherever the convective parameterization is activated and are designed to be consistent with the Moncrieff (1992) layered overturning MCS model. The profile magnitudes are controlled by tunable multiplicative coefficients. These coefficients have the potential of being functions of the large-scale shear, thus making this MCS parameterization consistent with the effects of shear in controlling MCS dynamics. This parameterization approach can be visualized conceptually as in [Fig. 17-52](#), where a layered overturning on a larger-than-convective scale is applied where a convective population is occurring in an environment of large-scale shear. A notable feature of this approach is that the overall scale of the overturning may vary with the extent of the field of parameterized convection. Thus, the self-similarity of overturning in dynamic systems of various scales containing convective population ([section 16](#)) is represented in the output of the climate model in which the parameterization is applied. Based on an analysis of data obtained in the Amazon region, Schiro et al. (2018) have found evidence of layered overturning dominating convective mixing and argue that approaches to parameterizing MCSs that emphasize deep-inflow mixing are desirable.

These new approaches to parameterizing MCS effects in climate and general circulation models, which take into account the layered overturning nature of MCSs, are still in their infancy but promise to provide ways of representing MCSs in models that must be run in coarse resolution to project changes in Earth's climate, water cycle, rainfall, and severe weather.

19. Current and future research on MCSs

Since the time of Hamilton and Archbold (1945), details of MCSs have emerged in tandem with developments in observational technology and modeling. They are seen as important elements of the global circulation and climate and producers of precipitation and flooding around the world. MCSs occur in disparate

⁵CAPE is the vertically integrated buoyancy of an undiluted parcel lifted from somewhere in the planetary boundary layer.

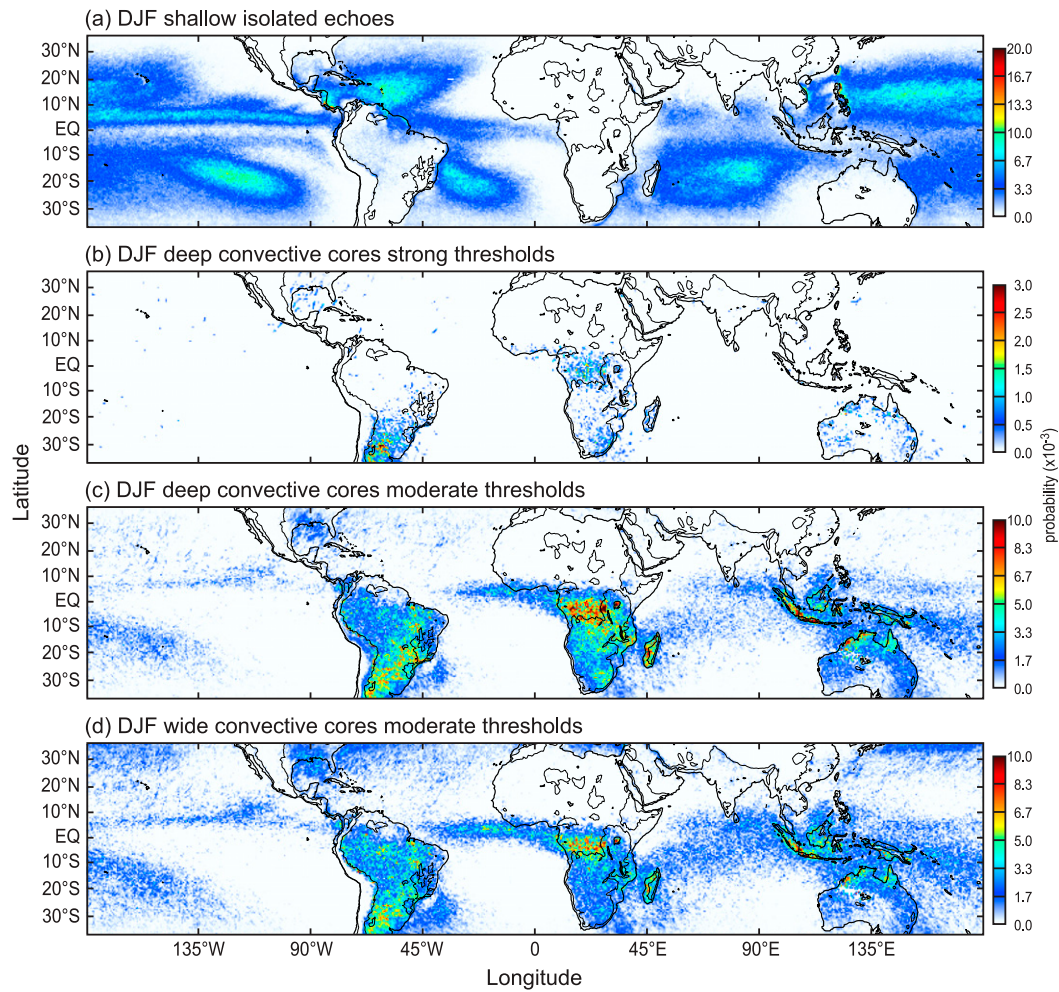


FIG. 17-50. Geographical distribution of the probability of finding various categories of echoes seen by the TRMM PR during December–February: (a) isolated shallow echoes, (b) strong threshold deep convective cores, (c) moderate threshold deep convective cores, and (d) moderate threshold wide convective cores. The black contour inside the continental regions represents the 700-m elevation. The probability is on a scale of 0 to 1 and is computed as the number of pixels identified as belonging to an echo category divided by the total number of pixels sampled by the TRMM PR over the given time period within a $0.5^\circ \times 0.5^\circ$ grid element. From [Houze et al. \(2015\)](#).

climatic regimes and take on a variety of forms, but have the common denominators of mesoscale horizontal scale and the development of stratiform portions that shift latent and radiative heating feedbacks upward into the mid–upper troposphere. Knowledge of these systems and how to represent them in forecasting and climate models remains an area of active and urgent research. The following are some areas of current and future research aimed at advancing knowledge, understanding, and the ability to represent MCSs accurately.

a. Initiation and upscale growth of convection to form MCSs

Forecasting weather from MCSs and representing this form of convection in global climate models depends

critically on determining when and where they will occur. All MCSs arise from an initial outbreak of deep convection, and the environmental factors leading to deep convection are well known. The crucial question is how deep convective elements, which each have a horizontal scale of only ones to tens of kilometers, organize themselves horizontally into a group of elements closely spaced within a zone ~ 100 km. It is this aggregation of deep convective elements that can then induce the mesoscale circulation of an MCS. The idealized “self aggregation” in an oceanic region of convection studied by [Wing and Emanuel \(2014\)](#) and others may be a partial answer to the initiation question. Their work especially highlights feedbacks between moisture convergence and differential radiation between cloudy and less cloudy

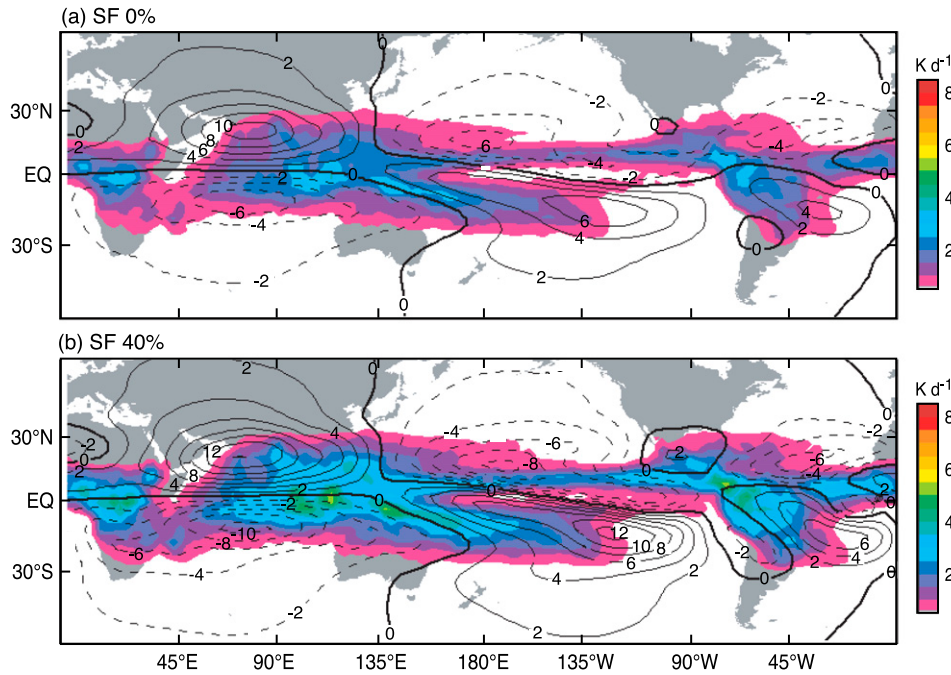


FIG. 17-51. The 400-hPa latent heating (shaded) and the resulting 250-hPa streamfunction anomalies (contours) computed from a simple climate model for the resting basic state and latent heating derived from the PR annually averaged precipitation field and geographically uniform stratiform rain fractions of (a) 0% and (b) 40%. The streamfunction contour interval is $2 \times 10^6 \text{ m}^2 \text{ s}^{-1}$. Negative contours are dashed. From Schumacher et al. (2004).

zones in sweeping convective elements into mesoscale zones. Whether such a process operates over land remains a question. Over land, inhomogeneities in land surface and topography may affect both initiation and early upscale growth. The effect of topography in the upscale growth of MCSs initiated near the Andes has been noted by Rasmussen et al. (2014), and two simultaneous field projects to investigate the upscale growth of these Andes systems [Remote Sensing of Electrification, Lightning, and Mesoscale/Microscale Processes with Adaptive Ground Observations (RELAMPAGO) and Clouds, Aerosols, and Complex Terrain Interactions (CACTI)] will take place in 2018.⁶

b. Forms of MCSs over the globe

As noted in this review, the horizontal patterns of convective elements within an MCS are varied. The canonical leading-line/trailing-stratiform organization is but one spatial arrangement. These variations in patterning are symptoms of different internal dynamics of the MCSs. The variations need to be understood if MCSs are to be predicted accurately either explicitly or in parameterized form. These variations can affect the degree to which the MCSs

influence the potential vorticity of the large-scale environment and how they produce severe weather locally. Parker and Johnson (2000), Schumacher and Johnson (2005), and Peters and Schumacher (2015, 2016) have identified variations on the convective–stratiform structures of MCSs over a large portion of the United States. They find that these variations are sometime related to the baroclinity of the synoptic environment. Rasmussen and Houze (2011) found variations in MCS structure over subtropical Pampas of South America to be similar to those seen over the U.S. Great Plains. However, the various structures and internal dynamics of MCSs seen in other regions such as tropical oceans (Leary and Houze 1979b; Yamada et al. 2010; Barnes and Houze 2014, 2016) and in the Maritime Continent (Houze et al. 1981) need to be unified into a common understanding of MCS internal structure and dynamics. The existence of datasets from past, current, and future satellite-borne radars (Liu and Zipser 2013; Houze et al. 2015) will be important in tying the different structures of MCSs seen around the world into a common unified global understanding of the occurrence of MCSs and their relationship to the large-scale circulation of the atmosphere.

c. MCSs and tropical cyclone genesis

As noted in the early study of Frank (1970), MCSs concentrated in the troughs of synoptic-scale tropical

⁶ <https://publish.illinois.edu/relampago/>.

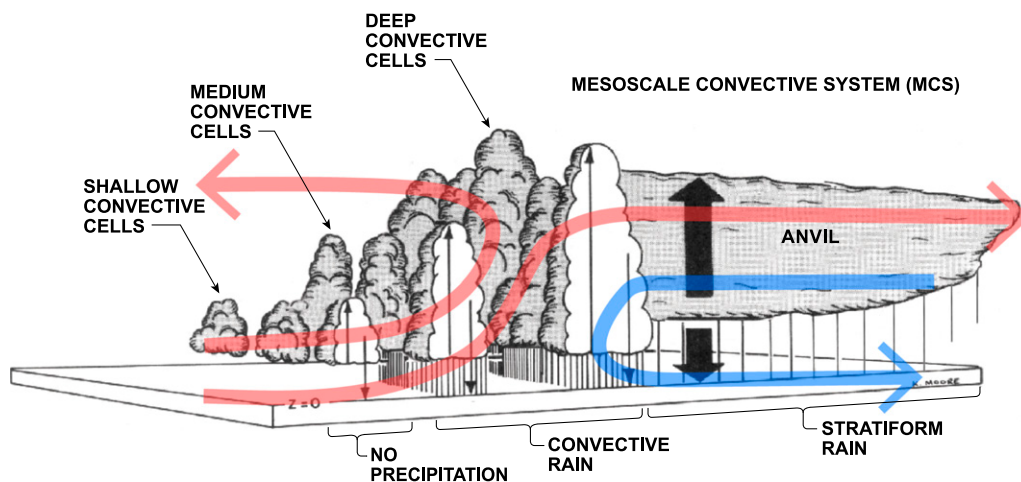


FIG. 17-52. Overlay of a convective cloud population and superimposed layered overturning. Adapted from Houze et al. (1980) and Moncrieff et al. (2017).

waves are precursors of tropical cyclones. In the modern era, Dunkerton et al. (2009) have emphasized how the growth of MCSs in environments of synoptic-scale vorticity can concentrate vorticity and lead to tropical cyclone development. Ritchie et al. (2003) and Houze et al. (2009) have described examples of how MCSs rotate around a common center of larger-scale vorticity just prior to tropical cyclogenesis. Houze et al. (2009) used airborne Doppler radar to show that the convective updrafts in the region prior to the formation of the tropical cyclone were excessively strong and wide and thus capable of concentrating vorticity, as suggested by Montgomery et al. (2006). Figure 17-53 illustrates how the convective population within a preexisting zone of cyclonic vorticity consists of both isolated convective elements and MCSs in different stages of development. The MCSs contain MCVs in mid-levels because of the generation of potential vorticity in their stratiform regions (section 12) while the convective-scale updrafts consist of vortical hot towers. Ritchie and Holland (1997), Simpson et al. (1997), and Ritchie et al. (2003) hypothesized that a tropical cyclone forms when the MCSs spinning around the low center reinforce the larger-scale depression. Bister and Emanuel (1997) suggested further that the stratiform-region vorticity builds downward as the region of MCSs becomes a tropical cyclone. Montgomery et al. (2006) argue on the other hand that the concentration of vorticity in the vortical hot towers (VHTs) is critical to the cyclogenesis. The relative importance of these two hypothesized processes remains a key question in understanding the role of MCSs in tropical cyclogenesis.

d. Extreme precipitation and flooding and societal impacts

MCSs are often implicated in flooding, both of the slow rising and flash flood types. Schumacher and Johnson

(2005) and Peters and Schumacher (2015, 2016) have shown some very specific types of MCS behavior that can inform flood forecasting in the central United States. Rasmussen et al. (2015) have shown how the large-scale conditions favoring floods in the Asian monsoon can be anticipated 7–10 days in advance in global model ensemble forecasts, but that understanding the exact locations and details of the flooding events requires information on topography, soil moisture conditions, river drainage basins, and knowledge of how MCSs form in the specific synoptic conditions dominating at the times of the flood occurrences. Further research seamlessly combining global numerical prediction models, regional cloud-resolving models, and hydrologic models is needed to improve forecasting of floods in regions vulnerable to flooding by MCSs, especially regions such as that of the Asian monsoon, where population and living conditions are highly weather sensitive.

e. Scale interaction and parameterization in global models

Besides forecasting flooding and other severe weather conditions on the time scales of days and weeks, global models are critical to projecting climate changes over longer time periods, for which convection-resolving models are at present still impracticable. As discussed in section 18, it remains necessary to parameterize deep convection in models used for assessing global climate change. No presently used parameterization scheme represents deep convection in the form of MCSs, although several methods, noted in section 18, are under development. Such research on parameterization of MCSs is essential because of the importance of MCSs in determining where rainfall occurs on average and because (as discussed in sections 11–17) the dynamical feedbacks of MCSs to the large-scale are a factor in

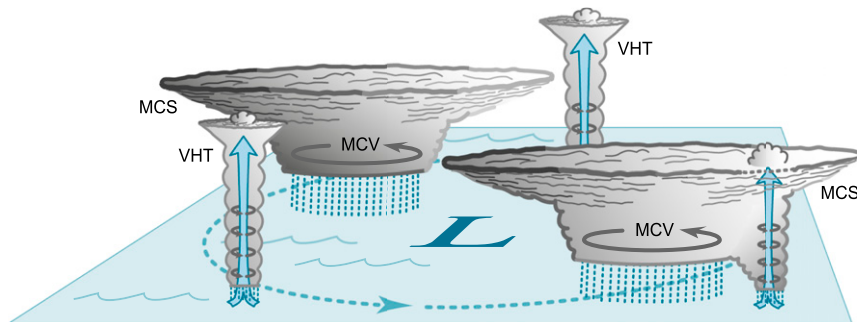


FIG. 17-53. Idealized distribution of convection in a low pressure system (L) in the process of developing into a tropical cyclone. The distribution contains isolated convective cells and MCSs in various stages of development. The convective updrafts stretch the environmental vorticity and advect positive vorticity upward. These updrafts with concentrated positive vorticity are referred to as vertical hot towers (VHT). The larger and longer-lived MCS contain VHTs in early MCS stages. The MCSs also contain stratiform regions with midlevel MCVs. Both the VHTs and MCVs are thought to contribute to cyclogenesis. From Houze et al. (2009).

determining the evolving large-scale circulation. The parameterization methods in section 18 will therefore remain an important and urgent area of research over the coming years.

The underlying difficulty in establishing these parameterization methods is the interplay of different scales in MCSs. The primary characteristic of MCSs is the layered overturning that occurs on horizontal scales of approximately hundreds of kilometers (section 8). However, deep, narrow columns of buoyant convective updrafts $\sim 1\text{--}10\text{ km}$ are embedded within the general overturning. In the boundary layer, cold pools $<1\text{ km}$ in depth spread forward and rearward for hundreds of kilometers. In addition, liquid- and ice-phase microphysics and associated radiative processes must be parameterized on all of these scales. The propagation of MCSs is affected not only by spreading of cold pools but also by the movements of gravity waves or fronts with which the MCSs are entangled. When elevated MCSs occur, cold pools in the boundary layer become irrelevant, so that parameterizations based on cold pool dynamics do not apply. Until further research establishes how all of these processes interact, parameterization cannot be based on firm understanding. Further field campaigns designed to elucidate these processes may be necessary. Virtual field programs involving only modeling and existing datasets (Moncrieff et al. 2012; Waliser et al. 2012) offer additional opportunities to test parameterization concepts. Much research in the area of overlapping and interacting scales within and connected with MCSs thus remains.

f. Aerosol, global warming, and MCSs in a changing climate

At the same time that understanding of MCSs and their importance has been increasing, the environment

in which they occur has been changing in ways that can affect their dynamics and microphysics, as well as where and when they occur. In an environment of global warming, circulation patterns may change such that the favorable locations for MCSs in relation to land, sea, and mountains may shift. In particular, the changing juxtaposition of the general circulation and mountain ranges may affect the occurrence of flooding in the monsoon regions of South Asia (Rasmusson et al. 2015). It is therefore important to continue to monitor MCS occurrence by satellite, as examined in the studies of Liu and Zipser (2013) and Houze et al. (2015), and to use global modeling to project future seasonal and geographic patterns of occurrence of MCSs.

In addition, the environmental conditions affecting the nature and intensity of individual MCSs are changing. In studies such as those of Moncrieff and Zipser, described in previous sections of this review, the structure and dynamics of MCSs have been determined as functions of the temperature, water vapor, wind shear of the larger-scale environment. Because of increased anthropogenic pollution of the atmosphere, the aerosol content of the surroundings has become an additional important environmental determinant of MCS structure. Research on this topic is still in its infancy; however, certain factors are beginning to emerge, and the results are showing that changes in the nature of MCSs as a result of aerosol in the environment are nonlinear and subtle. When considering ensembles of convective clouds, as occur over tropical oceans, some results indicate that aerosol indirect effects associated with shallow cumulus may offset or partially compensate for the aerosol indirect effects associated with congestus and deep convective clouds (van den Heever et al. 2011). It is therefore important to consider MCSs as a specific cloud

type when evaluating aerosol environmental effects. Fan et al. (2013) found that a primary effect of aerosol in deeper convective systems is to alter the nature of the stratiform anvil. Their study indicates that increased environmental aerosol leads to smaller but more numerous ice particles in the anvil clouds. The anvils become broader and thicker under these conditions. Because of the importance of stratiform regions in the feedback of MCSs to the large-scale flow (section 12), this finding has important implications for projecting circulation and climate changes. Saleeby et al. (2016) found that in highly polluted environments, riming of ice crystals in an MCS is greater, leading to less lofted cloud water and lower mixing ratios of ice in the anvils but nevertheless more numerous small ice crystals in the anvil and wider anvil areal coverage, with correspondingly significant effects on radiative transfer through the anvil, which, according to the discussion of section 12, has implications for the heating profiles within MCSs. Clavner et al. (2018a,b) have found in the modeling study of one case of an MCS that a more polluted environment led to greater area of convective precipitation and a smaller area of stratiform rain. Marinescu et al. (2017) have shown that the vertical profile of aerosol concentration in the environment is especially important in determining how aerosols affect MCSs (e.g., Fig. 17-54). Most aerosol observations are near Earth's surface, and Marinescu et al.'s (2017) study indicates how it may be ill advised in modeling studies to extrapolate surface measurements to higher altitudes. In a review of studies of aerosol and convective clouds, Fan et al. (2016) argued that there is an urgent need for observations of vertical profiles of aerosol in the environments of convective clouds. In a world of increasingly polluted environments, further examination of MCS response to the aerosol environment is one of the most urgent needs for future research. Areas such as India and China, where MCSs occur with severe consequences, the degree of pollution is some of the greatest in the world, and forecasting and projecting MCS occurrence cannot be accomplished without taking account of the aerosol environment.

20. Conclusions: The characteristics and importance of MCSs

This review has chronicled the history of the study of mesoscale convection. The MCS is the largest of the convective cloud phenomena. With its horizontal dimension of hundreds of kilometers, it exists near the energy-spectrum boundary between two- and three-dimensional atmospheric turbulence. An MCS occurs when deep convective clouds congregate in a region

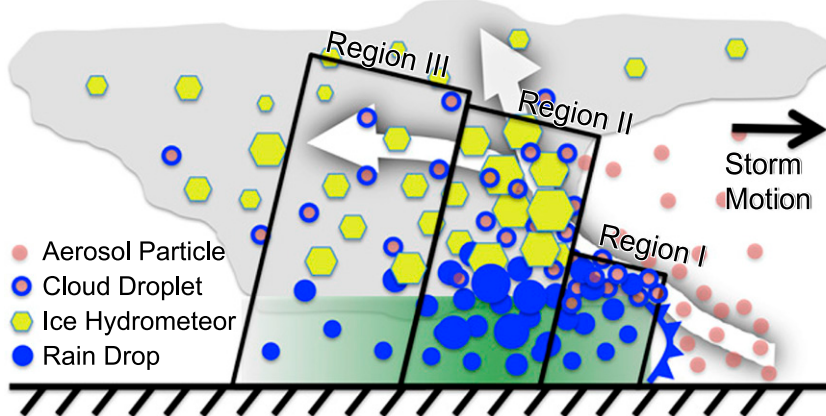
~500–1000 km². As the congregated clouds heat the troposphere by latent and radiative process, they induce a larger circulation, which is mesoscale in dimension and consists of layers of the atmosphere overturning: the rising layer emanates from the lower troposphere, while the subsiding layer is drawn from midlevels. The lower-tropospheric layer feeding the ascending branch of the circulation can be several kilometers deep; that is, the rising air is not necessarily rooted in the boundary layer. Sometimes the entire mesoscale overturning circulation lies above a layer of stable air, completely uncoupled from the boundary layer. This mesoscale, layered circulation sets the MCS apart as a distinct phenomenon with its own set of dynamics.

MCSs are familiar to weather forecasters and other students of severe weather. They account for a large portion of midlatitude and tropical rainfall (Fritsch et al. 1986, Yuan and Houze 2010), they produce severe weather and flooding (Houze et al. 1990; Rasmussen and Houze 2011), and they affect the larger-scale circulation of the atmosphere (Hartmann et al. 1984, Schumacher et al. 2004). It has taken the meteorological community over 70 years—since the time of Hamilton and Archbold (1945)—with ever-improving observational methods and increasing sophisticated models, to reach this level of understanding.

Satellite observations have shown the ubiquity of MCSs. Studies of spaceborne radar observations on board the *CloudSat*, TRMM, and GPM satellites have shown how MCSs (or their proxy radar echo signatures) are distributed over the globe (Liu and Zipser 2013; Houze et al. 2015). These studies further show that MCSs are not all alike. MCSs may or may not contain convection arranged in lines or bands. Over oceans, MCSs have somewhat less intense convective elements but larger and more robust stratiform regions than do MCSs over continents. Some regions, such as Amazonia, have MCSs whose characteristics lie between those of purely oceanic or dry continental MCSs.

Despite such morphological differences from one climatological regime to another, MCSs always contain stratiform as well as convective precipitation. The stratiform may be in the form of a stratiform zone following a propagating squall line, but often the stratiform precipitation forms more or less in place where active convection weakens while new convection forms nearby. The presence of a robust stratiform region implies that the net heating profile of the MCS (latent and radiative heating combined) is top-heavy in proportion to its stratiform rain fraction. This top-heavy profile generates potential vorticity in midlevels. Sometimes this potential vorticity is manifested in a mesoscale

(a) High concentrations of lower tropospheric aerosol particles



(b) High concentrations of middle tropospheric aerosol particles

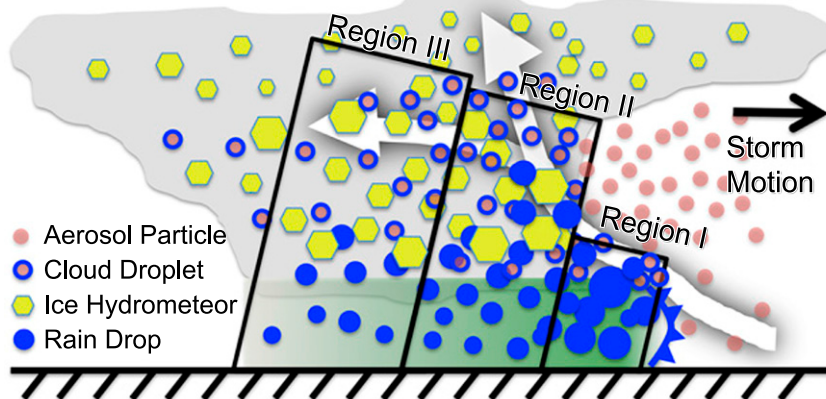


FIG. 17-54. Schematic of an MCS under high concentrations of (a) lower-tropospheric and (b) midtropospheric aerosol particles. The gray area represents cloudy regions, while the green shading represents rainfall with darker shading depicting heavier rain. The blue frontal symbols represent the leading cold pool boundary, and the white arrows represent the primary front-to-rear ascending flow. The three boxes represent three different precipitation regions of the MCS where different microphysical processes are governing the precipitation. Particle types are specified in the legends, with the amounts and sizes of hydrometeors representative of the relative concentrations and mean diameters of particles within those regions. From [Marinescu et al. \(2017\)](#).

convective vortex in midlevels of the stratiform region. Whether or not such a vortex is manifest, the net effect on the large-scale circulation of an MCS is to inject potential vorticity at midlevels and thus affect the future course of the large-scale circulation in which it is embedded. This heating profile of MCSs is one of the most crucial features of MCSs to be captured in a large-scale model, especially if that model aims to understand the role of MCSs in further changes of the global climate. Models with high resolution capture MCSs fairly accurately and, as cloud microphysical parameterizations improve these simulations, will become even more accurate. Such models now being run over limited regions

of Earth are showing aspects of the role of MCSs in climate change ([Prein et al. 2015; Yang et al. 2017](#)).

Models with coarser resolution, such as climate models used to project changes over the entire globe over long periods, must either wait for computing technology to advance sufficiently to accommodate global high-resolution models running over centuries of model time, or develop appropriate parameterizations of MCSs. Convective parameterizations based on a separation of scales between convective and synoptic scales will not suffice because of the horizontal dimension of MCSs. Several methods of parameterizing the heating and momentum transport profiles of MCSs

in climate models are under development. Successful development of climate models that include MCSs, whether by cloud-resolving modeling or parameterization, is critical because MCSs remain an important societal problem. They are implicated in flooding and severe weather around the world. For example, floods in India and Pakistan, which result in massive casualties and human suffering, often involve MCSs (e.g., Houze et al. 2011; Rasmussen et al. 2015). MCS characteristics are affected by the increasingly polluted aerosol environment in many locations of the world, and as Earth warms the patterns of MCS occurrence will likely shift so that the areas affected by MCSs will change. Forecasting MCSs both in real time and projecting their future occurrence in a changing climate therefore remains a grand challenge for meteorology and climate.

Acknowledgments. The author appreciates the invitation to write this article and his long association with the American Meteorological Society. Samson Hagos, Richard Johnson, Ruby Leung, Mitch Moncrieff, and Russ Schumacher provided comments that greatly improved the manuscript. Robert Fovell kindly provided the model results presented in Fig. 17-33. Beth Tully edited the text and refined the graphics for this article. The author was supported by the National Science Foundation under Grant AGS-1355567, the National Aeronautics and Space Administration under Grant NNX16AD75G, and the Pacific Northwest National Laboratory under Master Agreement 243766. PNNL is operated for the Department of Energy by Battelle Memorial Institute under Contract DE-AC05-76RL01830.

REFERENCES

- Abercromby, R., 1887: Suggestions for an international nomenclature of clouds. *Quart. J. Roy. Meteor. Soc.*, **13**, 154–166, <https://doi.org/10.1002/qj.4970136212>.
- Adams-Selin, R. D., and R. H. Johnson, 2010: Mesoscale surface pressure and temperature features associated with bow echoes. *Mon. Wea. Rev.*, **138**, 212–227, <https://doi.org/10.1175/2009MWR2892.1>.
- Anderson, C. J., and R. W. Arritt, 1998: Mesoscale convective complexes and persistent elongated convective systems over the United States during 1992 and 1993. *Mon. Wea. Rev.*, **126**, 578–599, [https://doi.org/10.1175/1520-0493\(1998\)126<0578:MCCAPE>2.0.CO;2](https://doi.org/10.1175/1520-0493(1998)126<0578:MCCAPE>2.0.CO;2).
- Anderson, G. D., 2010: The first weather satellite picture. *Weather*, **65**, 87–87, <https://doi.org/10.1002/wea.550>.
- Arakawa, A., and W. H. Schubert, 1974: Interaction of a cumulus ensemble with the large-scale environment: Part I. *J. Atmos. Sci.*, **31**, 674–701, [https://doi.org/10.1175/1520-0469\(1974\)031<0674:IOACCE>2.0.CO;2](https://doi.org/10.1175/1520-0469(1974)031<0674:IOACCE>2.0.CO;2).
- Austin, P. M., and S. G. Geotis, 1979: Raindrop sizes and related parameters for GATE. *J. Appl. Meteor.*, **18**, 569–575, [https://doi.org/10.1175/1520-0450\(1979\)018<0569:RSARPF>2.0.CO;2](https://doi.org/10.1175/1520-0450(1979)018<0569:RSARPF>2.0.CO;2).
- Awaka, J., T. Iguchi, H. Kumagai, and K. Okamoto, 1997: Rain type classification algorithm for TRMM precipitation radar. *Proc. 1997 Int. Geoscience and Remote Sensing Symp., Remote Sensing—A Scientific Vision for Sustainable Development*, Vol. 4, 1633–1635, Singapore, IEEE, <https://doi.org/10.1109/IGARSS.1997.608993>.
- Barnes, G. M., and M. Garstang, 1982: Subcloud layer energetics of precipitating convection. *Mon. Wea. Rev.*, **110**, 102–117, [https://doi.org/10.1175/1520-0493\(1982\)110<0102:SLEOPC>2.0.CO;2](https://doi.org/10.1175/1520-0493(1982)110<0102:SLEOPC>2.0.CO;2).
- Barnes, H. C., and R. A. Houze Jr., 2013: The precipitating cloud population of the Madden–Julian Oscillation over the Indian and west Pacific Oceans. *J. Geophys. Res. Atmos.*, **118**, 6996–7023, <https://doi.org/10.1002/jgrd.50375>.
- , and —, 2014: Precipitation hydrometeor type relative to the mesoscale airflow in oceanic deep convection of the Madden–Julian Oscillation. *J. Geophys. Res. Atmos.*, **119**, 13 990–14 014, <https://doi.org/10.1002/2014JD022241>.
- , and —, 2016: Comparison of observed and simulated spatial patterns of ice microphysical processes in tropical oceanic mesoscale convective systems. *J. Geophys. Res. Atmos.*, **121**, 8269–8296, <https://doi.org/10.1002/2016JD025074>.
- , M. D. Zuluaga, and R. A. Houze Jr., 2015: Latent heating characteristics of the MJO computed from TRMM observations. *J. Geophys. Res. Atmos.*, **120**, 1322–1334, <https://doi.org/10.1002/2014JD022530>.
- Bartels, D. L., and R. A. Maddox, 1991: Midlevel cyclonic vortices generated by mesoscale convective systems. *Mon. Wea. Rev.*, **119**, 104–118, [https://doi.org/10.1175/1520-0493\(1991\)119<0104:MCVGBM>2.0.CO;2](https://doi.org/10.1175/1520-0493(1991)119<0104:MCVGBM>2.0.CO;2).
- Bister, M., and K. A. Emanuel, 1997: The genesis of Hurricane Guillermo: TEXMEX analysis and a modeling study. *Mon. Wea. Rev.*, **125**, 2662–2682, [https://doi.org/10.1175/1520-0493\(1997\)125<2662:TGOHGT>2.0.CO;2](https://doi.org/10.1175/1520-0493(1997)125<2662:TGOHGT>2.0.CO;2).
- Bluestein, H. B., and M. H. Jain, 1985: Formation of mesoscale lines of precipitation: Severe squall lines in Oklahoma during the spring. *J. Atmos. Sci.*, **42**, 1711–1732, [https://doi.org/10.1175/1520-0469\(1985\)042<1711:FOMLOP>2.0.CO;2](https://doi.org/10.1175/1520-0469(1985)042<1711:FOMLOP>2.0.CO;2).
- Bonner, W. D., 1968: Climatology of the low-level jet. *Mon. Wea. Rev.*, **96**, 833–850, [https://doi.org/10.1175/1520-0493\(1968\)096<0833:COTLLJ>2.0.CO;2](https://doi.org/10.1175/1520-0493(1968)096<0833:COTLLJ>2.0.CO;2).
- Braun, S. A., and R. A. Houze Jr., 1995: Melting and freezing in a mesoscale convective system. *Quart. J. Roy. Meteor. Soc.*, **121**, 55–77, <https://doi.org/10.1002/qj.49712152104>.
- , and —, 1997: The evolution of the 10–11 June 1985 PRE-STORM squall line: Initiation, development of rear inflow, and dissipation. *Mon. Wea. Rev.*, **125**, 478–504, [https://doi.org/10.1175/1520-0493\(1997\)125<0478:TEOTJP>2.0.CO;2](https://doi.org/10.1175/1520-0493(1997)125<0478:TEOTJP>2.0.CO;2).
- Brown, J. M., 1979: Mesoscale unsaturated downdrafts driven by rainfall evaporation: A numerical study. *J. Atmos. Sci.*, **36**, 313–338, [https://doi.org/10.1175/1520-0469\(1979\)036<0313:MUDDBR>2.0.CO;2](https://doi.org/10.1175/1520-0469(1979)036<0313:MUDDBR>2.0.CO;2).
- Browning, K. A., and F. Ludlam, 1962: Airflow within convective storms. *Quart. J. Roy. Meteor. Soc.*, **88**, 117–135, <https://doi.org/10.1002/qj.49708837602>.
- Bryan, G. H., and J. M. Fritsch, 2000: Moist absolute instability: The sixth static stability state. *Bull. Amer. Meteor. Soc.*, **81**, 1207–1230, [https://doi.org/10.1175/1520-0477\(2000\)081<1207:MAITSS>2.3.CO;2](https://doi.org/10.1175/1520-0477(2000)081<1207:MAITSS>2.3.CO;2).
- , and —, 2003: On the existence of convective rolls in the convective region of squall lines. *10th Conf. on Mesoscale Processes*, Portland, OR, Amer. Meteor. Soc., 4.2, <https://ams.confex.com/ams/pdfpapers/62556.pdf>.

- Byers, H. R., and R. R. Braham Jr., 1949: *The Thunderstorm*. U.S. Government Printing Office, 287 pp.
- Carbone, R. E., J. D. Tuttle, D. A. Ahijevych, and S. B. Trier, 2002: Inferences of predictability associated with warm season precipitation episodes. *J. Atmos. Sci.*, **59**, 2033–2056, [https://doi.org/10.1175/1520-0469\(2002\)059<2033:IOPAWW>2.0.CO;2](https://doi.org/10.1175/1520-0469(2002)059<2033:IOPAWW>2.0.CO;2).
- Cetrone, J., and R. A. Houze Jr., 2011: Leading and trailing anvil clouds of West African squall lines. *J. Atmos. Sci.*, **68**, 1114–1123, <https://doi.org/10.1175/2011JAS3580.1>.
- Chang, C.-P., 1970: Westward propagating cloud patterns in the tropical Pacific as seen from time-composite satellite photographs. *J. Atmos. Sci.*, **27**, 133–138, [https://doi.org/10.1175/1520-0469\(1970\)027<0133:WPCPIT>2.0.CO;2](https://doi.org/10.1175/1520-0469(1970)027<0133:WPCPIT>2.0.CO;2).
- , V. F. Morris, and J. M. Wallace, 1970: A statistical study of easterly waves in the western Pacific: July–December 1964. *J. Atmos. Sci.*, **27**, 195–201, [https://doi.org/10.1175/1520-0469\(1970\)027<0195:ASSEOW>2.0.CO;2](https://doi.org/10.1175/1520-0469(1970)027<0195:ASSEOW>2.0.CO;2).
- Charney, J. G., and A. Eliassen, 1964: On the growth of the hurricane depression. *J. Atmos. Sci.*, **21**, 68–75, [https://doi.org/10.1175/1520-0469\(1964\)021<0068:OTGOTH>2.0.CO;2](https://doi.org/10.1175/1520-0469(1964)021<0068:OTGOTH>2.0.CO;2).
- Chen, S. S., and Coauthors, 2016: Aircraft observations of dry air, the ITCZ, convective cloud systems, and cold pools in MJO during DYNAMO. *Bull. Amer. Meteor. Soc.*, **97**, 405–423, <https://doi.org/10.1175/BAMS-D-13-00196.1>.
- Cheng, C.-P., and R. A. Houze Jr., 1979: The distribution of convective and mesoscale precipitation in GATE radar echo patterns. *Mon. Wea. Rev.*, **107**, 1370–1381, [https://doi.org/10.1175/1520-0493\(1979\)107<1370:TDOCAM>2.0.CO;2](https://doi.org/10.1175/1520-0493(1979)107<1370:TDOCAM>2.0.CO;2).
- Churchill, D. D., and R. A. Houze Jr., 1984: Development and structure of winter monsoon cloud clusters on 10 December 1978. *J. Atmos. Sci.*, **41**, 933–960, [https://doi.org/10.1175/1520-0469\(1984\)041<0933:DASOWM>2.0.CO;2](https://doi.org/10.1175/1520-0469(1984)041<0933:DASOWM>2.0.CO;2).
- Clavner, M., W. R. Cotton, S. C. van den Heever, S. M. Saleeby, and J. R. Pierce, 2018a: The response of a simulated mesoscale convective system to increased aerosol pollution: Part I: Precipitation intensity, distribution, and efficiency. *Atmos. Res.*, **199**, 193–208, <https://doi.org/10.1016/j.atmosres.2017.08.010>.
- , L. D. Grasso, W. R. Cotton, and S. C. van den Heever, 2018b: The response of a simulated mesoscale convective system to increased aerosol pollution: Part II: Derecho characteristics and intensity in response to increased pollution. *Atmos. Res.*, **199**, 209–223, <https://doi.org/10.1016/j.atmosres.2017.06.002>.
- Cotton, W. R., and R. A. Anthes, 1989: *Storm and Cloud Dynamics*. Academic Press, 883 pp.
- Crook, N. A., and M. W. Moncrieff, 1988: The effect of large-scale convergence on the generation and maintenance of deep moist convection. *J. Atmos. Sci.*, **45**, 3606–3624, [https://doi.org/10.1175/1520-0469\(1988\)045<3606:TEOLSC>2.0.CO;2](https://doi.org/10.1175/1520-0469(1988)045<3606:TEOLSC>2.0.CO;2).
- Cunning, J. B., 1986: The Oklahoma-Kansas Preliminary Regional Experiment for STORM-Central. *Bull. Amer. Meteor. Soc.*, **67**, 1478–1486, [https://doi.org/10.1175/1520-0477\(1986\)067<1478:TOKPRE>2.0.CO;2](https://doi.org/10.1175/1520-0477(1986)067<1478:TOKPRE>2.0.CO;2).
- , and R. I. Sax, 1977: A Z–R relationship for the GATE B-scale array. *Mon. Wea. Rev.*, **105**, 1330–1336, [https://doi.org/10.1175/1520-0493\(1977\)105<1330:ARFTGB>2.0.CO;2](https://doi.org/10.1175/1520-0493(1977)105<1330:ARFTGB>2.0.CO;2).
- Dai, A., 2006: Precipitation characteristics in eighteen coupled climate models. *J. Climate*, **19**, 4605–4630, <https://doi.org/10.1175/JCLI3884.1>.
- , F. Giorgi, and K. E. Trenberth, 1999: Observed and model-simulated diurnal cycles of precipitation over the contiguous United States. *J. Geophys. Res.*, **104**, 6377–6402, <https://doi.org/10.1029/98JD02720>.
- Davis, C., and Coauthors, 2004: The Bow Echo and MCV Experiment. *Bull. Amer. Meteor. Soc.*, **85**, 1075–1093, <https://doi.org/10.1175/BAMS-85-8-1075>.
- Didlake, A. C., Jr., and R. A. Houze Jr., 2013: Dynamics of the stratiform sector of a tropical cyclone rainband. *J. Atmos. Sci.*, **70**, 1891–1911, <https://doi.org/10.1175/JAS-D-12-0245.1>.
- Dorst, N. M., 2007: The National Hurricane Research Project: 50 years of research, rough rides, and name changes. *Bull. Amer. Meteor. Soc.*, **88**, 1566–1588, <https://doi.org/10.1175/BAMS-88-10-1566>.
- Douglas, M. W., M. Nicolini, and C. A. Saulo, 1998: Observational evidences of a low level jet east of the Andes during January–March 1998. *Meteorologica*, **23**, 63–72.
- Drager, A. J., and S. C. van den Heever, 2017: Characterizing convective cold pools. *J. Adv. Model. Earth Syst.*, **9**, 1091–1115, <https://doi.org/10.1002/2016MS000788>.
- Dunkerton, T. J., M. T. Montgomery, and Z. Wang, 2009: Tropical cyclogenesis in a tropical wave critical layer: Easterly waves. *Atmos. Chem. Phys.*, **9**, 5587–5646, <https://doi.org/10.5194/acp-9-5587-2009>.
- Emanuel, K., A. A. Wing, and E. M. Vincent, 2014: Radiative–convective instability. *J. Adv. Model. Earth Syst.*, **6**, 75–90, <https://doi.org/10.1002/2013MS000270>.
- Esbensen, S. K., and M. J. McPhaden, 1996: Enhancement of tropical ocean evaporation and sensible heat flux by atmospheric mesoscale systems. *J. Climate*, **9**, 2307–2325, [https://doi.org/10.1175/1520-0442\(1996\)009<2307:EOTOEA>2.0.CO;2](https://doi.org/10.1175/1520-0442(1996)009<2307:EOTOEA>2.0.CO;2).
- Fan, J., L. R. Leung, D. Rosenfeld, Q. Chen, Z. Li, J. Zhang, and H. Yan, 2013: Microphysical effects determine macrophysical response for aerosol impact on deep convective clouds. *Proc. Natl. Acad. Sci. USA*, **110**, E4581–E4590, <https://doi.org/10.1073/pnas.1316830110>.
- , Y. Wang, D. Rosenfeld, and X. Liu, 2016: Review of aerosol–cloud interactions: Mechanisms, significance, and challenges. *J. Atmos. Sci.*, **73**, 4221–4252, <https://doi.org/10.1175/JAS-D-16-0037.1>.
- Feng, Z., S. Hagos, A. K. Rowe, C. D. Burleyson, M. N. Martini, and S. P. de Szoeke, 2015: Mechanisms of convective cloud organization by cold pools over tropical warm ocean during the AMIE/DYNAMO field campaign. *J. Adv. Model. Earth Syst.*, **7**, 357–381, <https://doi.org/10.1002/2014MS000384>.
- , L.-Y. Leung, S. Hagos, R. A. Houze Jr., C. Burleyson, and K. Balaguru, 2016: More frequent intense and long-lived storms dominate the springtime trend in central U.S. rainfall. *Nat. Commun.*, **7**, 13429, <https://doi.org/10.1038/ncomms13429>.
- Fink, A. H., and A. Reiner, 2003: Spatiotemporal variability of the relation between African easterly waves and West African squall lines in 1998 and 1999. *J. Geophys. Res.*, **108**, 4332, <https://doi.org/10.1029/2002JD002816>.
- Fortune, M., 1980: Properties of African squall lines inferred from time-lapse satellite imagery. *Mon. Wea. Rev.*, **108**, 153–168, [https://doi.org/10.1175/1520-0493\(1980\)108<0153:POASLI>2.0.CO;2](https://doi.org/10.1175/1520-0493(1980)108<0153:POASLI>2.0.CO;2).
- Fovell, R. G., and Y. Ogura, 1988: Numerical simulation of a midlatitude squall line in two dimensions. *J. Atmos. Sci.*, **45**, 3846–3879, [https://doi.org/10.1175/1520-0469\(1988\)045<3846:NSOAMS>2.0.CO;2](https://doi.org/10.1175/1520-0469(1988)045<3846:NSOAMS>2.0.CO;2).
- Frank, N. L., 1970: Atlantic tropical systems of 1969. *Mon. Wea. Rev.*, **98**, 307–314, [https://doi.org/10.1175/1520-0493\(1970\)098<0307:ATSO>2.3.CO;2](https://doi.org/10.1175/1520-0493(1970)098<0307:ATSO>2.3.CO;2).
- Fritsch, J. M., and G. S. Forbes, 2001: Mesoscale convective systems. *Severe Convective Storms, Meteor. Monogr.*, No. 50, Amer. Meteor. Soc., 323–357, <https://doi.org/10.1175/0065-9401-28.50.323>.

- , R. J. Kane, and C. R. Chelius, 1986: The contribution of mesoscale convective weather systems to the warm-season precipitation in the United States. *J. Climate Appl. Meteor.*, **25**, 1333–1345, [https://doi.org/10.1175/1520-0450\(1986\)025<1333:TCOMCW>2.0.CO;2](https://doi.org/10.1175/1520-0450(1986)025<1333:TCOMCW>2.0.CO;2).
- , J. D. Murphy, and J. S. Kain, 1994: Warm core vortex amplification over land. *J. Atmos. Sci.*, **51**, 1780–1807, [https://doi.org/10.1175/1520-0469\(1994\)051<1780:WCVAOL>2.0.CO;2](https://doi.org/10.1175/1520-0469(1994)051<1780:WCVAOL>2.0.CO;2).
- Fujita, T. T., 1955: Results of detailed synoptic studies of squall lines. *Tellus*, **7**, 405–436, <https://doi.org/10.3402/tellusa.v7i4.8920>.
- Funk, A., C. Schumacher, and J. Awaka, 2013: Analysis of rain classifications over the tropics by Version 7 of the TRMM PR 2A23 algorithm. *J. Meteor. Soc. Japan*, **91**, 257–272, <https://doi.org/10.2151/jmsj.2013-302>.
- Futyan, J., and A. Del Genio, 2007: Deep convective system evolution over Africa and the tropical Atlantic. *J. Climate*, **20**, 5041–5060, <https://doi.org/10.1175/JCLI4297.1>.
- Gaynor, J. E., and P. A. Mandics, 1978: Analysis of the tropical marine boundary layer during GATE using acoustic sounder data. *Mon. Wea. Rev.*, **106**, 223–232, [https://doi.org/10.1175/1520-0493\(1978\)106<0223:AOTTMB>2.0.CO;2](https://doi.org/10.1175/1520-0493(1978)106<0223:AOTTMB>2.0.CO;2).
- Geerts, B., and Coauthors, 2017: The 2015 Plains Elevated Convection at Night field project. *Bull. Amer. Meteor. Soc.*, **98**, 767–786, <https://doi.org/10.1175/BAMS-D-15-00257.1>.
- Gentine, P., A. Garelli, S.-B. Park, J. Nie, G. Torri, and Z. Kuang, 2016: Role of surface heat fluxes underneath cold pools. *Geophys. Res. Lett.*, **43**, 874–883, <https://doi.org/10.1002/2015GL067262>.
- Godfrey, J. S., R. A. Houze Jr., R. H. Johnson, R. Lukas, J.-L. Redelsperger, A. Sumi, and R. Weller, 1998: Coupled Ocean–Atmosphere Response Experiment (COARE): An interim report. *J. Geophys. Res.*, **103**, 14 395–14 450, <https://doi.org/10.1029/97JC03120>.
- Grant, L. D., and S. C. van den Heever, 2016: Cold pool dissipation. *J. Geophys. Res. Atmos.*, **121**, 1138–1155, <https://doi.org/10.1002/2015JD023813>.
- Hamilton, R. A., and J. W. Archbold, 1945: Meteorology of Nigeria and adjacent territory. *Quart. J. Roy. Meteor. Soc.*, **71**, 231–262, <https://doi.org/10.1002/qj.49707130905>.
- Hartmann, D. L., 2016: Tropical anvil clouds and climate sensitivity. *Proc. Natl. Acad. Sci. USA*, **113**, 8897–8899, <https://doi.org/10.1073/pnas.1610455113>.
- , H. H. Hendon, and R. A. Houze Jr., 1984: Some implications of the mesoscale circulations in tropical cloud clusters for large-scale dynamics and climate. *J. Atmos. Sci.*, **41**, 113–121, [https://doi.org/10.1175/1520-0469\(1984\)041<0113:SIOTMC>2.0.CO;2](https://doi.org/10.1175/1520-0469(1984)041<0113:SIOTMC>2.0.CO;2).
- Hence, D. A., and R. A. Houze Jr., 2008: Kinematic structure of convective-scale elements in the rainbands of Hurricanes Katrina and Rita (2005). *J. Geophys. Res.*, **113**, D15108, <https://doi.org/10.1029/2007JD009429>.
- Hildebrandsson, H. H., 1887: Remarks concerning the nomenclature of clouds for ordinary use. *Quart. J. Roy. Meteor. Soc.*, **13**, 148–154, <https://doi.org/10.1002/qj.4970136211>.
- Hinrichs, G., 1888a: Tornadoes and derechos. *Amer. Meteor. J.*, **5**, 306–317.
- , 1888b: Tornadoes and derechos (continued). *Amer. Meteor. J.*, **5**, 341–349.
- Holland, J. Z., 1970: Preliminary report on the BOMEX Sea–Air Interaction Program. *Bull. Amer. Meteor. Soc.*, **51**, 809–820, [https://doi.org/10.1175/1520-0477\(1970\)051<0809:PROTBS>2.0.CO;2](https://doi.org/10.1175/1520-0477(1970)051<0809:PROTBS>2.0.CO;2).
- Houze, R. A., Jr., 1973: A climatological study of vertical transports by cumulus-scale convection. *J. Atmos. Sci.*, **30**, 1112–1123, [https://doi.org/10.1175/1520-0469\(1973\)030<1112:ACSOVT>2.0.CO;2](https://doi.org/10.1175/1520-0469(1973)030<1112:ACSOVT>2.0.CO;2).
- , 1977: Structure and dynamics of a tropical squall-line system. *Mon. Wea. Rev.*, **105**, 1540–1567, [https://doi.org/10.1175/1520-0493\(1977\)105<1540:SADOAT>2.0.CO;2](https://doi.org/10.1175/1520-0493(1977)105<1540:SADOAT>2.0.CO;2).
- , 1982: Cloud clusters and large-scale vertical motions in the tropics. *J. Meteor. Soc. Japan*, **60**, 396–410, https://doi.org/10.2151/jmsj1965.60.1_396.
- , 1989: Observed structure of mesoscale convective systems and implications for large-scale heating. *Quart. J. Roy. Meteor. Soc.*, **115**, 425–461, <https://doi.org/10.1002/qj.49711548702>.
- , 1997: Stratiform precipitation in regions of convection: A meteorological paradox? *Bull. Amer. Meteor. Soc.*, **78**, 2179–2196, [https://doi.org/10.1175/1520-0477\(1997\)078<2179:SPIROC>2.0.CO;2](https://doi.org/10.1175/1520-0477(1997)078<2179:SPIROC>2.0.CO;2).
- , 2010: Clouds in tropical cyclones. *Mon. Wea. Rev.*, **138**, 293–344, <https://doi.org/10.1175/2009MWR2989.1>.
- , 2014: *Cloud Dynamics*. 2nd ed. Elsevier/Academic Press, 432 pp.
- , and A. K. Betts, 1981: Convection in GATE. *Rev. Geophys.*, **19**, 541–576, <https://doi.org/10.1029/RG019i004p00541>.
- , and D. D. Churchill, 1987: Mesoscale organization and cloud microphysics in a Bay of Bengal depression. *J. Atmos. Sci.*, **44**, 1845–1867, [https://doi.org/10.1175/1520-0469\(1987\)044<1845:MOACMI>2.0.CO;2](https://doi.org/10.1175/1520-0469(1987)044<1845:MOACMI>2.0.CO;2).
- , C.-P. Cheng, C. A. Leary, and J. F. Gamache, 1980: Diagnosis of cloud mass and heat fluxes from radar and synoptic data. *J. Atmos. Sci.*, **37**, 754–773, [https://doi.org/10.1175/1520-0469\(1980\)037<0754:DOCMAH>2.0.CO;2](https://doi.org/10.1175/1520-0469(1980)037<0754:DOCMAH>2.0.CO;2).
- , S. G. Geotis, F. D. Marks Jr., and A. K. West, 1981: Winter monsoon convection in the vicinity of north Borneo. Part I: Structure and time variation of the clouds and precipitation. *Mon. Wea. Rev.*, **109**, 1595–1614, [https://doi.org/10.1175/1520-0493\(1981\)109<1595:WMCITV>2.0.CO;2](https://doi.org/10.1175/1520-0493(1981)109<1595:WMCITV>2.0.CO;2).
- , S. A. Rutledge, M. I. Biggerstaff, and B. F. Smull, 1989: Interpretation of Doppler weather radar displays in midlatitude mesoscale convective systems. *Bull. Amer. Meteor. Soc.*, **70**, 608–619, [https://doi.org/10.1175/1520-0477\(1989\)070<0608:IODWRD>2.0.CO;2](https://doi.org/10.1175/1520-0477(1989)070<0608:IODWRD>2.0.CO;2).
- , B. F. Smull, and P. Dodge, 1990: Mesoscale organization of springtime rainstorms in Oklahoma. *Mon. Wea. Rev.*, **118**, 613–654, [https://doi.org/10.1175/1520-0493\(1990\)118<0613:MOOSRI>2.0.CO;2](https://doi.org/10.1175/1520-0493(1990)118<0613:MOOSRI>2.0.CO;2).
- , S. S. Chen, D. E. Kingsmill, Y. Serra, and S. E. Yuter, 2000: Convection over the Pacific warm pool in relation to the atmospheric Kelvin–Rossby wave. *J. Atmos. Sci.*, **57**, 3058–3089, [https://doi.org/10.1175/1520-0469\(2000\)057<3058:COTPWP>2.0.CO;2](https://doi.org/10.1175/1520-0469(2000)057<3058:COTPWP>2.0.CO;2).
- , W.-C. Lee, and M. M. Bell, 2009: Convective contribution to the genesis of Hurricane Ophelia (2005). *Mon. Wea. Rev.*, **137**, 2778–2800, <https://doi.org/10.1175/2009MWR2727.1>.
- , K. L. Rasmussen, S. Medina, S. R. Brodzik, and U. Romatschke, 2011: Anomalous atmospheric events leading to the summer 2010 floods in Pakistan. *Bull. Amer. Meteor. Soc.*, **92**, 291–298, <https://doi.org/10.1175/2010BAMS3173.1>.
- , —, M. D. Zuluaga, and S. R. Brodzik, 2015: The variable nature of convection in the tropics and subtropics: A legacy of 16 years of the Tropical Rainfall Measuring Mission (TRMM) satellite. *Rev. Geophys.*, **53**, <https://doi.org/10.1002/2015RG000488>.
- Howard, L., 1865: Essay on the modifications of clouds. 3rd ed. John Churchill & Sons, 37 pp.
- Hudlow, M. D., 1979: Mean rainfall patterns for the three phases of GATE. *J. Appl. Meteor.*, **18**, 1656–1669, [https://doi.org/10.1175/1520-0450\(1979\)018<1656:MRPFTT>2.0.CO;2](https://doi.org/10.1175/1520-0450(1979)018<1656:MRPFTT>2.0.CO;2).

- Humphreys, W. J., 1914: The thunderstorm and its phenomena. *Mon. Wea. Rev.*, **42**, 348–380, [https://doi.org/10.1175/1520-0493\(1914\)42<348:TTAIP>2.0.CO;2](https://doi.org/10.1175/1520-0493(1914)42<348:TTAIP>2.0.CO;2).
- Jirak, I. L., W. R. Cotton, and R. L. McAnelly, 2003: Satellite and radar survey of mesoscale convective system development. *Mon. Wea. Rev.*, **131**, 2428–2449, [https://doi.org/10.1175/1520-0493\(2003\)131<2428:SARSON>2.0.CO;2](https://doi.org/10.1175/1520-0493(2003)131<2428:SARSON>2.0.CO;2).
- Johnson, R. H., and M. E. Nicholls, 1983: A composite analysis of the boundary layer accompanying a tropical squall line. *Mon. Wea. Rev.*, **111**, 308–319, [https://doi.org/10.1175/1520-0493\(1983\)111<0308:ACAOBT>2.0.CO;2](https://doi.org/10.1175/1520-0493(1983)111<0308:ACAOBT>2.0.CO;2).
- , S. L. Aves, P. E. Ciesielski, and T. D. Keenan, 2005: Organization of oceanic convection during the onset of the 1998 East Asian summer monsoon. *Mon. Wea. Rev.*, **133**, 131–148, <https://doi.org/10.1175/MWR-2843.1>.
- Jorgensen, D. P., H. V. Murphrey, and R. M. Wakimoto, 2004: Rear-inflow evolution in a non-severe bow-echo observed by airborne Doppler radar during BAMEX. *22nd Conf. on Severe Local Storms*, Hyannis, MA, Amer. Meteor. Soc., 4.6, <https://ams.confex.com/ams/pdfpapers/81428.pdf>.
- Khouider, B., J. Biello, and A. J. Majda, 2010: A stochastic multicloud model for tropical convection. *Commun. Math. Sci.*, **8**, 187–216, <https://doi.org/10.4310/CMS.2010.v8.n1.a10>.
- Kingsmill, D. E., and R. A. Houze Jr., 1999: Kinematic characteristics of air flowing into and out of precipitating convection over the west Pacific warm pool: An airborne Doppler radar survey. *Quart. J. Roy. Meteor. Soc.*, **125**, 1165–1207, <https://doi.org/10.1002/qj.1999.4971255605>.
- Klein, S. A., X. Jiang, J. Boyle, S. Malyshev, and S. Xie, 2006: Diagnosis of the summertime warm and dry bias over the U.S. southern Great Plains in the GFDL climate model using a weather forecasting approach. *Geophys. Res. Lett.*, **33**, L18805, <https://doi.org/10.1029/2006GL027567>.
- Kuettner, J. P., and D. E. Parker, 1976: GATE: Report of the field phase. *Bull. Amer. Meteor. Soc.*, **57**, 11–27, <https://doi.org/10.1175/1520-0477-57.1.11>.
- Lafore, J.-P., and M. W. Moncrieff, 1989: A numerical investigation of the organization and interaction of the convective and stratiform regions of tropical squall lines. *J. Atmos. Sci.*, **46**, 521–544, [https://doi.org/10.1175/1520-0469\(1989\)046<0521:ANIOTO>2.0.CO;2](https://doi.org/10.1175/1520-0469(1989)046<0521:ANIOTO>2.0.CO;2).
- Laing, A. G., and J. M. Fritsch, 1997: The global population of mesoscale convective complexes. *Quart. J. Roy. Meteor. Soc.*, **123**, 389–405, <https://doi.org/10.1002/qj.49712353807>.
- Leary, C. A., and R. A. Houze Jr., 1979a: Melting and evaporation of hydrometeors in precipitation from the anvil clouds of deep tropical convection. *J. Atmos. Sci.*, **36**, 669–679, [https://doi.org/10.1175/1520-0469\(1979\)036<0669:MAEOH>2.0.CO;2](https://doi.org/10.1175/1520-0469(1979)036<0669:MAEOH>2.0.CO;2).
- , and —, 1979b: The structure and evolution of convection in a tropical cloud cluster. *J. Atmos. Sci.*, **36**, 437–457, [https://doi.org/10.1175/1520-0469\(1979\)036<0437:TSAEOC>2.0.CO;2](https://doi.org/10.1175/1520-0469(1979)036<0437:TSAEOC>2.0.CO;2).
- LeMone, M. A., and E. J. Zipser, 1980: Cumulonimbus vertical velocity events in GATE. Part I: Diameter, intensity, and mass flux. *J. Atmos. Sci.*, **37**, 2444–2457, [https://doi.org/10.1175/1520-0469\(1980\)037<2444:CVVEIG>2.0.CO;2](https://doi.org/10.1175/1520-0469(1980)037<2444:CVVEIG>2.0.CO;2).
- , —, and S. B. Trier, 1998: The role of environmental shear and thermodynamic conditions in determining the structure and evolution of mesoscale convective systems during TOGA COARE. *J. Atmos. Sci.*, **55**, 3493–3518, [https://doi.org/10.1175/1520-0469\(1998\)055<3493:TROESA>2.0.CO;2](https://doi.org/10.1175/1520-0469(1998)055<3493:TROESA>2.0.CO;2).
- Ligda, M. G. H., 1956: The radar observations of mature prefrontal squall lines in the midwestern United States. *Sixth OSTIV Congress*, Publ. IV, Fédération Aéronautique Internationale, St-Yan, France, <http://journals.sfu.ca/ts/index.php/op/article/download/1364/1297>.
- Lindzen, R. S., 1974: Wave-CISK in the tropics. *J. Atmos. Sci.*, **31**, 156–179, [https://doi.org/10.1175/1520-0469\(1974\)031<0156:WCITT>2.0.CO;2](https://doi.org/10.1175/1520-0469(1974)031<0156:WCITT>2.0.CO;2).
- Liu, C., and E. Zipser, 2013: Regional variation of morphology of organized convection in the tropics and subtropics. *J. Geophys. Res. Atmos.*, **118**, 453–466, <https://doi.org/10.1029/2012JD018409>.
- , and —, 2015: The global distribution of largest, deepest, and most intense precipitation systems. *Geophys. Res. Lett.*, **42**, 3591–3595, <https://doi.org/10.1002/2015GL063776>.
- Loehrer, S. M., and R. H. Johnson, 1995: Surface pressure and precipitation life cycle characteristics of PRE-STORM mesoscale convective systems. *Mon. Wea. Rev.*, **123**, 600–621, [https://doi.org/10.1175/1520-0493\(1995\)123<0600:SPAPLC>2.0.CO;2](https://doi.org/10.1175/1520-0493(1995)123<0600:SPAPLC>2.0.CO;2).
- Lorenz, E. N., 1963: Deterministic nonperiodic flow. *J. Atmos. Sci.*, **20**, 130–141, [https://doi.org/10.1175/1520-0469\(1963\)020<0130:DNF>2.0.CO;2](https://doi.org/10.1175/1520-0469(1963)020<0130:DNF>2.0.CO;2).
- Madden, R. A., and P. R. Julian, 1971: Detection of a 40–50 day oscillation in the zonal wind in the tropical Pacific. *J. Atmos. Sci.*, **28**, 702–708, [https://doi.org/10.1175/1520-0469\(1971\)028<0702:DOADOI>2.0.CO;2](https://doi.org/10.1175/1520-0469(1971)028<0702:DOADOI>2.0.CO;2).
- , and —, 1972: Description of global scale circulation cells in the tropics with a 40–50 day period. *J. Atmos. Sci.*, **29**, 1109–1123, [https://doi.org/10.1175/1520-0469\(1972\)029<1109:DOGSCC>2.0.CO;2](https://doi.org/10.1175/1520-0469(1972)029<1109:DOGSCC>2.0.CO;2).
- Maddox, R. A., 1980: Mesoscale convective complexes. *Bull. Amer. Meteor. Soc.*, **61**, 1374–1387, [https://doi.org/10.1175/1520-0477\(1980\)061<1374:MCC>2.0.CO;2](https://doi.org/10.1175/1520-0477(1980)061<1374:MCC>2.0.CO;2).
- , 1983: Large-scale meteorological conditions associated with midlatitude, mesoscale convective complexes. *Mon. Wea. Rev.*, **111**, 1475–1493, [https://doi.org/10.1175/1520-0493\(1983\)111<1475:LSMCAW>2.0.CO;2](https://doi.org/10.1175/1520-0493(1983)111<1475:LSMCAW>2.0.CO;2).
- Mandics, P. A., and F. F. Hall Jr., 1976: Preliminary results from the GATE acoustic echo sounder. *Bull. Amer. Meteor. Soc.*, **57**, 1142–1147, <https://doi.org/10.1175/1520-0477-57.9.1142>.
- Mapes, B. E., S. Tulich, J.-L. Lin, and P. Zuidema, 2006: The mesoscale convection life cycle: Building block or prototype for large-scale tropical waves? *Dyn. Atmos. Oceans*, **42**, 3–29, <https://doi.org/10.1016/j.dynatmoce.2006.03.003>.
- Marengo, J., W. Soares, C. Saulo, and M. Nicolini, 2004: Climatology of the LLJ east of the Andes as derived from the NCEP reanalyses. *J. Climate*, **17**, 2261–2280, [https://doi.org/10.1175/1520-0442\(2004\)017<2261:COTLJE>2.0.CO;2](https://doi.org/10.1175/1520-0442(2004)017<2261:COTLJE>2.0.CO;2).
- Marinescu, P. J., S. C. van den Heever, S. M. Saleeby, S. M. Kreidenweis, and P. J. DeMott, 2017: The microphysical roles of lower-tropospheric versus midtropospheric aerosol particles in mature-stage MCS precipitation. *J. Atmos. Sci.*, **74**, 3657–3678, <https://doi.org/10.1175/JAS-D-16-0361.1>.
- Marks, F. D., Jr., and R. A. Houze Jr., 1983: Three-dimensional wind field in the developing inner core of Hurricane Debby. *Preprints, 21st Conf. on Radar Meteorology*, Edmonton, AB, Canada, Amer. Meteor. Soc., 298–304.
- Marsham, J. H., K. A. Browning, J. C. Nicol, D. J. Parker, E. G. Norton, A. M. Blyth, U. Corsmeier, and F. M. Perry, 2010: Multisensor observations of a wave beneath an impacting rear-inflow jet in an elevated mesoscale convective system. *Quart. J. Roy. Meteor. Soc.*, **136**, 1788–1812, <https://doi.org/10.1002/qj.669>.
- , S. B. Trier, T. M. Weckwerth, and J. W. Wilson, 2011: Observations of elevated convection initiation leading to a surface-based squall line during 13 June IHOP_2002. *Mon. Wea. Rev.*, **108**, 322–336, <https://doi.org/10.1175/2010MWR3422.1>.

- Martin, D. W., and O. Karst, 1969: A census of cloud systems over the tropical Pacific. *Studies in Atmospheric Energetics Based on Aerospace Probing Annual Rep. 1968*, Space Science and Engineering Center, University of Wisconsin, 37–50.
- , and V. E. Suomi, 1972: A satellite study of cloud clusters over the tropical north Atlantic ocean. *Bull. Amer. Meteor. Soc.*, **53**, 135–156, <https://doi.org/10.1175/1520-0477-53.2.135>.
- Mecham, D. B., R. A. Houze Jr., and S. S. Chen, 2002: Layer inflow into precipitating convection over the western tropical Pacific. *Quart. J. Roy. Meteor. Soc.*, **128**, 1997–2030, <https://doi.org/10.1256/003590002320603502>.
- , S. S. Chen, and R. A. Houze Jr., 2006: Momentum transport processes in the stratiform regions of mesoscale convective systems over the western Pacific warm pool. *Quart. J. Roy. Meteor. Soc.*, **132**, 709–736, <https://doi.org/10.1256/qj.04.141>.
- Mohr, K. I., and E. J. Zipser, 1996: Defining mesoscale convective systems by their 85-GHz ice-scattering signatures. *Bull. Amer. Meteor. Soc.*, **77**, 1179–1189, [https://doi.org/10.1175/1520-0477\(1996\)077<1179:DMCSBT>2.0.CO;2](https://doi.org/10.1175/1520-0477(1996)077<1179:DMCSBT>2.0.CO;2).
- Moncrieff, M. W., 1978: The dynamical structure of two-dimensional steady convection in constant vertical shear. *Quart. J. Roy. Meteor. Soc.*, **104**, 543–568, <https://doi.org/10.1002/qj.49710444102>.
- , 1981: A theory of organised steady convection and its transport properties. *Quart. J. Roy. Meteor. Soc.*, **107**, 29–50, <https://doi.org/10.1002/qj.49710745103>.
- , 1992: Organized convective systems: Archetypical dynamical models, mass and momentum flux theory, and parametrization. *Quart. J. Roy. Meteor. Soc.*, **118**, 819–850, <https://doi.org/10.1002/qj.49711850703>.
- , 2004: Analytic representation of the large-scale organization of tropical convection. *J. Atmos. Sci.*, **61**, 1521–1538, [https://doi.org/10.1175/1520-0469\(2004\)061<1521:AROTLO>2.0.CO;2](https://doi.org/10.1175/1520-0469(2004)061<1521:AROTLO>2.0.CO;2).
- , and M. J. Miller, 1976: The dynamics and simulation of tropical squall lines. *Quart. J. Roy. Meteor. Soc.*, **102**, 373–394, <https://doi.org/10.1002/qj.49710243208>.
- , and E. Klinker, 1997: Mesoscale cloud systems in the tropical Western Pacific as a process in general circulation models. *Quart. J. Roy. Meteor. Soc.*, **123**, 805–827, <https://doi.org/10.1002/qj.49712354002>.
- , D. E. Waliser, M. J. Miller, M. E. Shapiro, G. Asrar, and J. Caughey, 2012: Multiscale convective organization and the YOTC Virtual Global Field Campaign. *Bull. Amer. Meteor. Soc.*, **93**, 1171–1187, <https://doi.org/10.1175/BAMS-D-11-00233.1>.
- , C. Liu, and P. Bogenschutz, 2017: Simulation, modeling, and dynamically based parameterization of organized tropical convection for global climate models. *J. Atmos. Sci.*, **74**, 1363–1380, <https://doi.org/10.1175/JAS-D-16-0166.1>.
- Montgomery, M. T., M. E. Nicholls, T. A. Cram, and A. B. Saunders, 2006: A vortical hot tower route to tropical cyclogenesis. *J. Atmos. Sci.*, **63**, 355–386, <https://doi.org/10.1175/JAS3604.1>.
- Morrison, H., G. Thompson, and V. Tatarskii, 2009: Impact of cloud microphysics on the development of trailing stratiform precipitation in a simulated squall line: Comparison of one- and two-moment schemes. *Mon. Wea. Rev.*, **137**, 991–1007, <https://doi.org/10.1175/2008MWR2556.1>.
- Nakazawa, T., 1988: Tropical super clusters within intraseasonal variations over the western Pacific. *J. Meteor. Soc. Japan*, **66**, 823–839, https://doi.org/10.2151/jmsj1965.66.6_823.
- Nesbitt, S. W., E. J. Zipser, and D. J. Cecil, 2000: A census of precipitation features in the tropics using TRMM: Radar, ice scattering, and lightning observations. *J. Climate*, **13**, 4087–4106, [https://doi.org/10.1175/1520-0442\(2000\)013<4087:ACOPFI>2.0.CO;2](https://doi.org/10.1175/1520-0442(2000)013<4087:ACOPFI>2.0.CO;2).
- Newton, C. W., 1950: Structure and mechanisms of the pre-frontal squall line. *J. Meteor.*, **7**, 210–222, [https://doi.org/10.1175/1520-0469\(1950\)007<0210:SAMOTP>2.0.CO;2](https://doi.org/10.1175/1520-0469(1950)007<0210:SAMOTP>2.0.CO;2).
- Nogués-Paegle, J., and K. C. Mo, 1997: Alternating wet and dry conditions over South America during summer. *Mon. Wea. Rev.*, **125**, 279–291, [https://doi.org/10.1175/1520-0493\(1997\)125<0279:AWADCO>2.0.CO;2](https://doi.org/10.1175/1520-0493(1997)125<0279:AWADCO>2.0.CO;2).
- Pandya, R., and D. Durran, 1996: The influence of convectively generated thermal forcing on the mesoscale circulation around squall lines. *J. Atmos. Sci.*, **53**, 2924–2951, [https://doi.org/10.1175/1520-0469\(1996\)053<2924:TIOCGT>2.0.CO;2](https://doi.org/10.1175/1520-0469(1996)053<2924:TIOCGT>2.0.CO;2).
- Parker, M. D., 2008: Response of simulated squall lines to low-level cooling. *J. Atmos. Sci.*, **65**, 1323–1341, <https://doi.org/10.1175/2007JAS2507.1>.
- , and R. H. Johnson, 2000: Organizational modes of mid-latitude mesoscale convective systems. *Mon. Wea. Rev.*, **128**, 3413–3436, [https://doi.org/10.1175/1520-0493\(2001\)129<3413:OMOMMC>2.0.CO;2](https://doi.org/10.1175/1520-0493(2001)129<3413:OMOMMC>2.0.CO;2).
- Payne, S. W., and M. M. McGarry, 1977: The relationship of satellite infrared convective activity to easterly waves over West Africa and the adjacent ocean during Phase II of GATE. *Mon. Wea. Rev.*, **105**, 413–420, [https://doi.org/10.1175/1520-0493\(1977\)105<0413:TROSIC>2.0.CO;2](https://doi.org/10.1175/1520-0493(1977)105<0413:TROSIC>2.0.CO;2).
- Peters, J. M., and R. S. Schumacher, 2015: Mechanisms for organization and echo training in a flash-flood-producing mesoscale convective system. *Mon. Wea. Rev.*, **143**, 1058–1085, <https://doi.org/10.1175/MWR-D-14-00070.1>.
- , and —, 2016: Dynamics governing a simulated mesoscale convective system with a training convective line. *J. Atmos. Sci.*, **73**, 2643–2664, <https://doi.org/10.1175/JAS-D-15-0199.1>.
- Petersen, W. A., R. C. Cifelli, S. A. Rutledge, B. S. Ferrier, and B. F. Smull, 1999: Shipborne dual-Doppler operations during TOGA COARE: Integrated observations of storm kinematics and electrification. *Bull. Amer. Meteor. Soc.*, **80**, 81–97, [https://doi.org/10.1175/1520-0477\(1999\)080<0081:SDDODT>2.0.CO;2](https://doi.org/10.1175/1520-0477(1999)080<0081:SDDODT>2.0.CO;2).
- Powell, S. W., R. A. Houze Jr., A. Kumar, and S. A. McFarlane, 2012: Comparison of simulated and observed continental tropical anvil clouds and their radiative heating profiles. *J. Atmos. Sci.*, **69**, 2662–2681, <https://doi.org/10.1175/JAS-D-11-0251.1>.
- Prein, A. F., and Coauthors, 2015: A review on regional convection-permitting climate modeling: Demonstrations, prospects, and challenges. *Rev. Geophys.*, **53**, 323–361, <https://doi.org/10.1002/2014RG000475>.
- Rasmussen, K. L., and R. A. Houze Jr., 2011: Orogenic convection in South America as seen by the TRMM satellite. *Mon. Wea. Rev.*, **139**, 2399–2420, <https://doi.org/10.1175/MWR-D-10-05006.1>.
- , and —, 2016: Convective initiation near the Andes in subtropical South America. *Mon. Wea. Rev.*, **144**, 2351–2374, <https://doi.org/10.1175/MWR-D-15-0058.1>.
- , M. D. Zuluaga, and R. A. Houze Jr., 2014: Severe convection and lightning in subtropical South America. *Geophys. Res. Lett.*, **41**, 7359–7366, <https://doi.org/10.1002/2014GL061767>.
- , A. J. Hill, V. E. Toma, M. D. Zuluaga, P. J. Webster, and R. A. Houze Jr., 2015: Multiscale analysis of three consecutive years of anomalous flooding in Pakistan. *Quart. J. Roy. Meteor. Soc.*, **141**, 1259–1276, <https://doi.org/10.1002/qj.2433>.
- Raymond, D. J., 1984: A wave-CISK model of squall lines. *J. Atmos. Sci.*, **41**, 1946–1958, [https://doi.org/10.1175/1520-0469\(1984\)041<1946:AWCMS>2.0.CO;2](https://doi.org/10.1175/1520-0469(1984)041<1946:AWCMS>2.0.CO;2).

- , and H. Jiang, 1990: A theory for long-lived mesoscale convective systems. *J. Atmos. Sci.*, **47**, 3067–3077, [https://doi.org/10.1175/1520-0469\(1990\)047<3067:ATFLLM>2.0.CO;2](https://doi.org/10.1175/1520-0469(1990)047<3067:ATFLLM>2.0.CO;2).
- Reed, R. J., and E. E. Recker, 1971: Structure and properties of synoptic-scale wave disturbances in the equatorial western Pacific. *J. Atmos. Sci.*, **28**, 1117–1133, [https://doi.org/10.1175/1520-0469\(1971\)028<1117:SAPOSS>2.0.CO;2](https://doi.org/10.1175/1520-0469(1971)028<1117:SAPOSS>2.0.CO;2).
- Ritchie, E. A., and G. J. Holland, 1997: Scale interactions during the formation of Typhoon Irving. *Mon. Wea. Rev.*, **125**, 1377–1396, [https://doi.org/10.1175/1520-0493\(1997\)125<1377:SIDTFO>2.0.CO;2](https://doi.org/10.1175/1520-0493(1997)125<1377:SIDTFO>2.0.CO;2).
- , J. Simpson, W. T. Liu, J. Halverson, C. Velden, K. F. Brueske, and H. Pierce, 2003: Present day satellite technology for hurricane research: A closer look at formation and intensification. *Hurricane! Coping with Disaster*, R. Simpson, Ed., Amer. Geophys. Union, 249–289.
- Robe, F. R., and K. A. Emanuel, 2001: The effect of vertical wind shear on radiative-convective equilibrium states. *J. Atmos. Sci.*, **58**, 1427–1445, [https://doi.org/10.1175/1520-0469\(2001\)058<1427:TEOVWS>2.0.CO;2](https://doi.org/10.1175/1520-0469(2001)058<1427:TEOVWS>2.0.CO;2).
- Rotunno, R., J. B. Klemp, and M. L. Weisman, 1988: A theory for strong, long-lived squall lines. *J. Atmos. Sci.*, **45**, 463–485, [https://doi.org/10.1175/1520-0469\(1988\)045<0463:ATFSLL>2.0.CO;2](https://doi.org/10.1175/1520-0469(1988)045<0463:ATFSLL>2.0.CO;2).
- Roux, F., 1988: The West African squall line observed on 23 June 1981 during COPT 81: Kinematics and thermodynamics of the convective region. *J. Atmos. Sci.*, **45**, 406–426, [https://doi.org/10.1175/1520-0469\(1988\)045<0406:TWASLO>2.0.CO;2](https://doi.org/10.1175/1520-0469(1988)045<0406:TWASLO>2.0.CO;2).
- Rowe, A. K., and R. A. Houze Jr., 2015: Cloud organization and growth during the transition from suppressed to active MJO conditions. *J. Geophys. Res. Atmos.*, **120**, 10 324–10 350, <https://doi.org/10.1002/2014JD022948>.
- Saleeby, S. M., S. C. van den Heever, P. J. Marinescu, S. M. Kreidenweis, and P. J. DeMott, 2016: Aerosol effects on the anvil characteristics of mesoscale convective systems. *J. Geophys. Res. Atmos.*, **121**, 10 880–10 901, <https://doi.org/10.1002/2016JD025082>.
- Salio, P., M. Nicolini, and E. J. Zipser, 2007: Mesoscale convective systems over southeastern South America and their relationship with the South American low-level jet. *Mon. Wea. Rev.*, **135**, 1290–1309, <https://doi.org/10.1175/MWR3305.1>.
- Saulo, A. C., M. Nicolini, and S. C. Chou, 2000: Model characterization of the South American low-level flow during the 1997–1998 spring–summer season. *Climate Dyn.*, **16**, 867–881, <https://doi.org/10.1007/s003820000085>.
- Saxen, T. R., and S. A. Rutledge, 1998: Surface fluxes and boundary layer recovery in TOGA COARE: Sensitivity to convective organization. *J. Atmos. Sci.*, **55**, 2763–2781, [https://doi.org/10.1175/1520-0469\(1998\)055<2763:SFABL>2.0.CO;2](https://doi.org/10.1175/1520-0469(1998)055<2763:SFABL>2.0.CO;2).
- Schiro, K. A., F. Ahmed, and D. J. Neelin, 2018: GoAmazon2014/5 campaign points to deep-inflow approach to mesoscale-organized and unorganized deep convection. *Proc. Natl. Acad. Sci. USA*, **115**, 4577–4582, <https://doi.org/10.1073/pnas.1719842115>.
- Schmidt, J. M., and W. R. Cotton, 1990: Interactions between upper and lower tropospheric gravity waves on squall line structure and maintenance. *J. Atmos. Sci.*, **47**, 1205–1222, [https://doi.org/10.1175/1520-0469\(1990\)047<1205:IBUALT>2.0.CO;2](https://doi.org/10.1175/1520-0469(1990)047<1205:IBUALT>2.0.CO;2).
- Schumacher, C., and R. A. Houze Jr., 2003: Stratiform rain in the tropics as seen by the TRMM Precipitation Radar. *J. Climate*, **16**, 1739–1756, [https://doi.org/10.1175/1520-0442\(2003\)016<1739:SRITTA>2.0.CO;2](https://doi.org/10.1175/1520-0442(2003)016<1739:SRITTA>2.0.CO;2).
- , and —, 2006: Stratiform precipitation production over sub-Saharan Africa and the tropical East Atlantic as observed by TRMM. *Quart. J. Roy. Meteor. Soc.*, **132**, 2235–2255, <https://doi.org/10.1256/qj.05.121>.
- , —, and I. Kraucunas, 2004: The tropical dynamical response to latent heating estimates derived from the TRMM Precipitation Radar. *J. Atmos. Sci.*, **61**, 1341–1358, [https://doi.org/10.1175/1520-0469\(2004\)061<1341:TTDRTL>2.0.CO;2](https://doi.org/10.1175/1520-0469(2004)061<1341:TTDRTL>2.0.CO;2).
- Schumacher, R. S., and R. H. Johnson, 2005: Organization and environmental properties of extreme-rain-producing mesoscale convective systems. *Mon. Wea. Rev.*, **133**, 961–976, <https://doi.org/10.1175/MWR2899.1>.
- , A. J. Clark, M. Xue, and F. Kong, 2013: Factors influencing the development and maintenance of nocturnal heavy-rain-producing convective systems in a storm-scale ensemble. *Mon. Wea. Rev.*, **141**, 2778–2801, <https://doi.org/10.1175/MWR-D-12-00239.1>.
- Shupiatsky, A. B., A. I. Korotov, and R. S. Pastushkov, 1976a: Radar investigations of the evolution of clouds in the east Atlantic, in *TROPEX-74. Atmosphere* (in Russian), Vol. 1, Gidrometeoizdat, 508–514.
- , G. N. Evseonok, and A. I. Korotov, 1976b: Complex investigations of clouds in the ITCZ with the help of satellite and ship radar equipment, in *TROPEX-74. Atmosphere* (in Russian), Vol. 1, Gidrometeoizdat, 515–520.
- Simpson, J. S., and G. van Helvoort, 1980: GATE cloud-subcloud interactions examined using a three-dimensional cumulus model. *Contrib. Atmos. Phys.*, **53**, 106–134.
- , E. Ritchie, G. J. Holland, J. Halverson, and S. Stewart, 1997: Mesoscale interactions in tropical cyclone genesis. *Mon. Wea. Rev.*, **125**, 2643–2661, [https://doi.org/10.1175/1520-0493\(1997\)125<2643:MIITCG>2.0.CO;2](https://doi.org/10.1175/1520-0493(1997)125<2643:MIITCG>2.0.CO;2).
- Skamarock, W. C., M. L. Weisman, and J. B. Klemp, 1994: Three-dimensional evolution of simulated long-lived squall lines. *J. Atmos. Sci.*, **51**, 2563–2584, [https://doi.org/10.1175/1520-0469\(1994\)051<2563:TDEOSL>2.0.CO;2](https://doi.org/10.1175/1520-0469(1994)051<2563:TDEOSL>2.0.CO;2).
- Smull, B. F., and R. A. Houze Jr., 1987: Rear inflow in squall lines with trailing stratiform precipitation. *Mon. Wea. Rev.*, **115**, 2869–2889, [https://doi.org/10.1175/1520-0493\(1987\)115<2869:RIISLW>2.0.CO;2](https://doi.org/10.1175/1520-0493(1987)115<2869:RIISLW>2.0.CO;2).
- Sommeria, G., and J. Testud, 1984: COPT81: A field experiment designed for the study of dynamics and electrical activity of deep convection in continental tropical regions. *Bull. Amer. Meteor. Soc.*, **65**, 4–10, [https://doi.org/10.1175/1520-0477\(1984\)065<0004:CAFEDF>2.0.CO;2](https://doi.org/10.1175/1520-0477(1984)065<0004:CAFEDF>2.0.CO;2).
- Steiner, M., R. A. Houze Jr., and S. E. Yuter, 1995: Climatological characterization of three-dimensional storm structure from operational radar and rain gauge data. *J. Appl. Meteor.*, **34**, 1978–2007, [https://doi.org/10.1175/1520-0450\(1995\)034<1978:CCOTDS>2.0.CO;2](https://doi.org/10.1175/1520-0450(1995)034<1978:CCOTDS>2.0.CO;2).
- Stensrud, D. J., 1996: Effects of persistent, midlatitude mesoscale regions of convection on the large-scale environment during the warm season. *J. Atmos. Sci.*, **53**, 3503–3527, [https://doi.org/10.1175/1520-0469\(1996\)053<3503:EOPMMR>2.0.CO;2](https://doi.org/10.1175/1520-0469(1996)053<3503:EOPMMR>2.0.CO;2).
- Tepper, M., 1950: A proposed mechanism of squall lines: The pressure jump line. *J. Meteor.*, **7**, 21–29, [https://doi.org/10.1175/1520-0469\(1950\)007<0021:APMSOL>2.0.CO;2](https://doi.org/10.1175/1520-0469(1950)007<0021:APMSOL>2.0.CO;2).
- Thompson, G., P. R. Field, R. M. Rasmussen, and W. D. Hall, 2008: Explicit forecasts of winter precipitation using an improved bulk microphysics scheme. Part II: Implementation of a new snow parameterization. *Mon. Wea. Rev.*, **136**, 5095–5115, <https://doi.org/10.1175/2008MWR2387.1>.
- Thompson, R. M., S. W. Payne, E. E. Recker, and R. J. Reed, 1979: Structure and properties of synoptic-scale wave disturbances in the intertropical convergence zone of the

- eastern Atlantic. *J. Atmos. Sci.*, **36**, 53–72, [https://doi.org/10.1175/1520-0469\(1979\)036<0053:SAPOSS>2.0.CO;2](https://doi.org/10.1175/1520-0469(1979)036<0053:SAPOSS>2.0.CO;2).
- Thorpe, A. J., M. J. Miller, and M. W. Moncrieff, 1982: Two-dimensional convection in a non-constant shear: A model of midlatitude squall lines. *Quart. J. Roy. Meteor. Soc.*, **108**, 739–762, <https://doi.org/10.1002/qj.49710845802>.
- Trier, S. B., and D. B. Parsons, 1993: Evolution of environmental conditions preceding the development of a nocturnal mesoscale convective complex. *Mon. Wea. Rev.*, **121**, 1078–1098, [https://doi.org/10.1175/1520-0493\(1993\)121<1078:EOECPT>2.0.CO;2](https://doi.org/10.1175/1520-0493(1993)121<1078:EOECPT>2.0.CO;2).
- , and C. A. Davis, 2002: Influence of balanced motions on heavy precipitation within a long-lived convectively generated vortex. *Mon. Wea. Rev.*, **130**, 877–899, [https://doi.org/10.1175/1520-0493\(2002\)130<0877:IBMOH>2.0.CO;2](https://doi.org/10.1175/1520-0493(2002)130<0877:IBMOH>2.0.CO;2).
- Tulloch, R., and K. S. Smith, 2006: A theory for the atmospheric energy spectrum: Depth-limited temperature anomalies at the tropopause. *Proc. Natl. Acad. Sci. USA*, **103**, 14 690–14 694, <https://doi.org/10.1073/pnas.0605494103>.
- van den Heever, S. C., G. L. Stephens, and N. B. Wood, 2011: Aerosol indirect effects on tropical convection characteristics under conditions of radiative–convective equilibrium. *J. Atmos. Sci.*, **68**, 699–718, <https://doi.org/10.1175/2010JAS3603.1>.
- Van Weverberg, K., and Coauthors, 2013: The role of cloud microphysics parametrization in the simulation of mesoscale convective system clouds and precipitation in the tropical western Pacific. *J. Atmos. Sci.*, **70**, 1104–1128, <https://doi.org/10.1175/JAS-D-12-0104.1>.
- , and Coauthors, 2017: CAUSES: Attribution of surface radiation biases in NWP and climate models near the U.S. southern Great Plains. *J. Geophys. Res. Atmos.*, **123**, 3612–3644, <https://doi.org/10.1002/2017JD027188>.
- Vera, C., and Coauthors, 2006: The South American Low-Level Jet Experiment. *Bull. Amer. Meteor. Soc.*, **87**, 63–77, <https://doi.org/10.1175/BAMS-87-1-63>.
- Virts, K. S., and R. A. Houze Jr., 2015: Variation of lightning in mesoscale convective systems within the MJO. *J. Atmos. Sci.*, **72**, 1932–1944, <https://doi.org/10.1175/JAS-D-14-0201.1>.
- Wakimoto, R. M., 1982: The life cycle of the thunderstorm gust fronts as viewed with Doppler radar and rawinsonde data. *Mon. Wea. Rev.*, **110**, 1060–1082, [https://doi.org/10.1175/1520-0493\(1982\)110<1060:TLGOTG>2.0.CO;2](https://doi.org/10.1175/1520-0493(1982)110<1060:TLGOTG>2.0.CO;2).
- Waliser, D. E., and Coauthors, 2012: The “Year” of Tropical Convection (May 2008–April 2010): Climate variability and weather highlights. *Bull. Amer. Meteor. Soc.*, **93**, 1189–1218, <https://doi.org/10.1175/2011BAMS3095.1>.
- Webster, P. J., and R. Lukas, 1992: TOGA COARE: The Coupled Ocean–Atmosphere Response Experiment. *Bull. Amer. Meteor. Soc.*, **73**, 1377–1416, [https://doi.org/10.1175/1520-0477\(1992\)073<1377:TCTCOR>2.0.CO;2](https://doi.org/10.1175/1520-0477(1992)073<1377:TCTCOR>2.0.CO;2).
- Weisman, M. L., 1992: The genesis of severe long-lived bow echoes. *J. Atmos. Sci.*, **49**, 1826–1847, [https://doi.org/10.1175/1520-0469\(1992\)049<1826:TGBE>2.0.CO;2](https://doi.org/10.1175/1520-0469(1992)049<1826:TGBE>2.0.CO;2).
- , and R. Rotunno, 2004: “A theory for strong long-lived squall lines” revisited. *J. Atmos. Sci.*, **61**, 361–382, [https://doi.org/10.1175/1520-0469\(2004\)061<0361:ATFSLS>2.0.CO;2](https://doi.org/10.1175/1520-0469(2004)061<0361:ATFSLS>2.0.CO;2).
- Wilheit, T. T., 1986: Some comments on passive microwave measurement of rain. *Bull. Amer. Meteor. Soc.*, **67**, 1226–1232, [https://doi.org/10.1175/1520-0477\(1986\)067<1226:SCOPMM>2.0.CO;2](https://doi.org/10.1175/1520-0477(1986)067<1226:SCOPMM>2.0.CO;2).
- Wilson, J. W., and R. D. Roberts, 2006: Summary of convective storm initiation and evolution during IHOP: Observational and modeling perspective. *Mon. Wea. Rev.*, **134**, 23–47, <https://doi.org/10.1175/MWR3069.1>.
- Wing, A. A., and K. A. Emanuel, 2014: Physical mechanisms controlling self-aggregation of convection in idealized numerical modeling simulations. *J. Adv. Model. Earth Syst.*, **6**, 59–74, <https://doi.org/10.1002/2013MS000269>.
- Yamada, H., K. Yoneyama, M. Katsumata, and R. Shirooka, 2010: Observations of a super cloud cluster accompanied by synoptic-scale eastward-propagating precipitating systems over the Indian Ocean. *J. Atmos. Sci.*, **67**, 1456–1473, <https://doi.org/10.1175/2009JAS3151.1>.
- Yanai, M., S. Esbensen, and J. H. Chu, 1973: Determination of bulk properties of tropical cloud clusters from large-scale heat and moisture budgets. *J. Atmos. Sci.*, **30**, 611–627, [https://doi.org/10.1175/1520-0469\(1973\)030<0611:DOBPOT>2.0.CO;2](https://doi.org/10.1175/1520-0469(1973)030<0611:DOBPOT>2.0.CO;2).
- Yang, Q., R. A. Houze Jr., L. R. Leung, and Z. Feng, 2017: Environments of long-lived mesoscale convective systems over the central United States in convection permitting climate simulations. *J. Geophys. Res. Atmos.*, **122**, 13 288–13 307, <https://doi.org/10.1002/2017JD027033>.
- Yoneyama, K., C. Zhang, and C. N. Long, 2013: Tracking pulses of the Madden-Julian Oscillation. *Bull. Amer. Meteor. Soc.*, **94**, 1871–1891, <https://doi.org/10.1175/BAMS-D-12-00157.1>.
- Young, G. S., S. M. Perugini, and C. W. Fairall, 1995: Convective wakes in the equatorial western Pacific during TOGA. *Mon. Wea. Rev.*, **123**, 110–123, [https://doi.org/10.1175/1520-0493\(1995\)123<0110:CWITEW>2.0.CO;2](https://doi.org/10.1175/1520-0493(1995)123<0110:CWITEW>2.0.CO;2).
- Yuan, J., and R. A. Houze Jr., 2010: Global variability of mesoscale convective system anvil structure from A-train satellite data. *J. Climate*, **23**, 5864–5888, <https://doi.org/10.1175/2010JCLI3671.1>.
- , —, and A. Heymsfield, 2011: Vertical structures of anvil clouds of tropical mesoscale convective systems observed by CloudSat. *J. Atmos. Sci.*, **68**, 1653–1674, <https://doi.org/10.1175/2011JAS3687.1>.
- Yuter, S. E., and R. A. Houze Jr., 1995: Three-dimensional kinematic and microphysical evolution of Florida cumulonimbus. Part III: Vertical mass transport, mass divergence, and synthesis. *Mon. Wea. Rev.*, **123**, 1964–1983, [https://doi.org/10.1175/1520-0493\(1995\)123<1964:TDKAME>2.0.CO;2](https://doi.org/10.1175/1520-0493(1995)123<1964:TDKAME>2.0.CO;2).
- Zipser, E. J., 1969: The role of organized unsaturated convective downdrafts in the structure and rapid decay of an equatorial disturbance. *J. Appl. Meteor.*, **8**, 799–814, [https://doi.org/10.1175/1520-0450\(1969\)008<0799:TROOUC>2.0.CO;2](https://doi.org/10.1175/1520-0450(1969)008<0799:TROOUC>2.0.CO;2).
- , 1977: Mesoscale and convective-scale downdrafts as distinct components of squall-line circulation. *Mon. Wea. Rev.*, **105**, 1568–1589, [https://doi.org/10.1175/1520-0493\(1977\)105<1568:MACDAD>2.0.CO;2](https://doi.org/10.1175/1520-0493(1977)105<1568:MACDAD>2.0.CO;2).
- , 2003: Some views on “hot towers” after 50 years of tropical field programs and two years of TRMM data. *Cloud Systems, Hurricanes, and the Tropical Rainfall Measuring Mission (TRMM)*, Meteor. Monogr., No. 51, Amer. Meteor. Soc., 49–58, [https://doi.org/10.1175/0065-9401\(2003\)029<0049:CSVOHT>2.0.CO;2](https://doi.org/10.1175/0065-9401(2003)029<0049:CSVOHT>2.0.CO;2).
- , and M. A. LeMone, 1980: Cumulonimbus vertical velocity events in GATE. Part II: Synthesis and model core structure. *J. Atmos. Sci.*, **37**, 2458–2469, [https://doi.org/10.1175/1520-0469\(1980\)037<2458:CVVEIG>2.0.CO;2](https://doi.org/10.1175/1520-0469(1980)037<2458:CVVEIG>2.0.CO;2).
- , D. J. Cecil, C. Liu, S. W. Nesbitt, and D. P. Yorty, 2006: Where are the most intense thunderstorms on Earth? *Bull. Amer. Meteor. Soc.*, **87**, 1057–1071, <https://doi.org/10.1175/BAMS-87-8-1057>.
- Zuluaga, M. D., and R. A. Houze Jr., 2013: Evolution of the population of precipitating convective systems over the equatorial Indian Ocean in active phases of the Madden–Julian oscillation. *J. Atmos. Sci.*, **70**, 2713–2725, <https://doi.org/10.1175/JAS-D-12-0311.1>.